NASA/TM-2001-211019

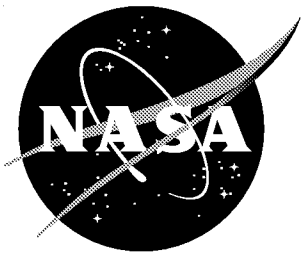

Sidewall Mach Number Distributions for the NASA Langley Transonic Dynamics Tunnel

James R. Florance and José A. Rivera, Jr.
Langley Research Center, Hampton, Virginia

June 2001

The NASA STI Program Office ... in Profile

Since its founding, NASA has been dedicated to the advancement of aeronautics and space science. The NASA Scientific and Technical Information (STI) Program Office plays a key part in helping NASA maintain this important role.

The NASA STI Program Office is operated by Langley Research Center, the lead center for NASA's scientific and technical information. The NASA STI Program Office provides access to the NASA STI Database, the largest collection of aeronautical and space science STI in the world. The Program Office is also NASA's institutional mechanism for disseminating the results of its research and development activities. These results are published by NASA in the NASA STI Report Series, which includes the following report types:

- TECHNICAL PUBLICATION. Reports of completed research or a major significant phase of research that present the results of NASA programs and include extensive data or theoretical analysis. Includes compilations of significant scientific and technical data and information deemed to be of continuing reference value. NASA counterpart of peer-reviewed formal professional papers, but having less stringent limitations on manuscript length and extent of graphic presentations.

- TECHNICAL MEMORANDUM. Scientific and technical findings that are preliminary or of specialized interest, e.g., quick release reports, working papers, and bibliographies that contain minimal annotation. Does not contain extensive analysis.

- CONTRACTOR REPORT. Scientific and technical findings by NASA-sponsored contractors and grantees.

- CONFERENCE PUBLICATION. Collected papers from scientific and technical conferences, symposia, seminars, or other meetings sponsored or co-sponsored by NASA.

- SPECIAL PUBLICATION. Scientific, technical, or historical information from NASA programs, projects, and missions, often concerned with subjects having substantial public interest.

- TECHNICAL TRANSLATION. English-language translations of foreign scientific and technical material pertinent to NASA's mission.

Specialized services that complement the STI Program Office's diverse offerings include creating custom thesauri, building customized databases, organizing and publishing research results ... even providing videos.

For more information about the NASA STI Program Office, see the following:

- Access the NASA STI Program Home Page at ***http://www.sti.nasa.gov***

- E-mail your question via the Internet to help@sti.nasa.gov

- Fax your question to the NASA STI Help Desk at (301) 621-0134

- Phone the NASA STI Help Desk at (301) 621-0390

- Write to:
  NASA STI Help Desk
  NASA Center for AeroSpace Information
  7121 Standard Drive
  Hanover, MD 21076-1320

NASA/TM-2001-211019

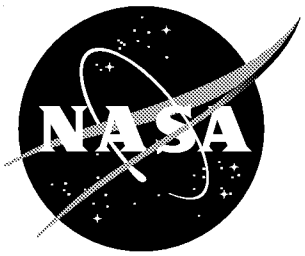

Sidewall Mach Number Distributions for the NASA Langley Transonic Dynamics Tunnel

James R. Florance and José A. Rivera, Jr.
Langley Research Center, Hampton, Virginia

National Aeronautics and
Space Administration

Langley Research Center
Hampton, Virginia 23681-2199

June 2001

Available from:

NASA Center for AeroSpace Information (CASI)
7121 Standard Drive
Hanover, MD 21076-1320
(301) 621-0390

National Technical Information Service (NTIS)
5285 Port Royal Road
Springfield, VA 22161-2171
(703) 605-6000

ABSTRACT

The TDT was recalibrated due to the conversion of the heavy gas test medium from R-12 to R-134a. The objectives of the tests were to determine the relationship between the free-stream Mach number and the measured test section Mach number, and to quantify any necessary corrections. Other tests included the measurement of pressure distributions along the test-section walls, test-section centerline, at certain tunnel stations via a rake apparatus, and in the tunnel settling chamber. Wall boundary layer, turbulence, and flow angularity measurements were also performed. This paper discusses the determination of sidewall Mach number distributions.

SYMBOLS

f_R	flap setting, counts
f_S	flap schedule configuration number
M	Mach Number
P	pressure, psf
q	dynamic pressure, psf
T	temperature, °F
X	distance downstream from origin of tunnel contraction, ft
y_s	slot width, in.
Y	lateral dimension from tunnel centerline (positive using right-hand rule), ft
Z	vertical dimension from tunnel centerline (positive upward), ft
$\alpha_{f,R}$	re-entry flap angle (positive when flap surface is divergent from tunnel centerline), deg.
Δ	difference operator
γ	ratio of specific heats

Subscripts:

local	value at surface pressure measurement orifice
nose	forward (upstream) re-entry flaps
main	aft (downstream) re-entry flaps
t	stagnation condition
tc	test chamber (plenum)
wall	tunnel sidewalls or top and bottom walls
∞	freestream

Abbreviations:

DAS	data acquisition system
ESP	electronically scanned pressure
ID	inside diameter
OD	outside diameter

psf pounds per square foot
psid pounds per square inch differential
TDT Transonic Dynamics Tunnel

INTRODUCTION

A series of calibration tests were conducted in the NASA Langley Transonic Dynamics Tunnel (TDT) to quantify flow properties and flow quality after the completion of the facility test medium conversion from R-12 to R-134a. The objectives of the calibration tests were to determine the relationship between the free-stream Mach number and the measured test section Mach number, and to quantify any necessary corrections. Calibration tests included measurement of pressure distributions along the test-section walls, test-section centerline, at certain tunnel stations using a rake apparatus, and in the tunnel settling chamber. Wall boundary layer, turbulence, and flow angularity measurements were also performed. Reference 1 discusses the calibration of a transonic tunnel and was used as a guide for this report. This report is focused on the determination of the test section sidewall Mach number distribution. The sidewall Mach number distribution is obtained from sidewall measurements of local static pressure along any of the primary wall, ceiling, or floor surfaces of the TDT test section. Four primary streamwise rows of static pressure ports are located in the test section, one row on each of the primary test section wall surfaces. There are approximately 28 static pressure ports along each of these rows. The static ports are spaced more densely at the tunnel station of the sidewall turntable, where sting-, cable-, and sidewall-mounted models are tested. The reentry flap schedule determined from the calibration conducted in 1969 was used.

The objective of this paper is to present the following:

1. A selection of the tunnel sidewall Mach number distributions
2. The effects of total pressure variations on the sidewall Mach number distributions
3. The effects of the reentry flap settings on the sidewall Mach number distribution
4. The effects of covering the sidewall slots on one side of the test section on the sidewall Mach number distributions

FACILITY DESCRIPTION

The TDT is a continuous-flow, variable-pressure wind tunnel with control capability to independently vary Mach number and total pressure and to regulate total temperature. The test section is 16 x 16 feet with cropped corners, making the cross-sectional area approximately 248 ft^2. The floor and ceiling of the test section are axially slotted to allow a continuous variation of test section Mach number up to about 1.2. The tunnel is capable of operating at total pressures from near-vacuum to atmospheric pressure in air or in a heavy gas (1,1,1,2-Tetrafluoroethane, also known as R-134a). An advantage of R-134a as a test medium is its density, which is almost four times that of air. This property of R-134a eases both aeroelastic scaling concerns and energy requirements for the facility. It is this combination of large scale, variable pressure, high speed, and high density that makes the TDT ideally suited for testing aeroelastically scaled models. The TDT operating boundaries for both air and R-134a test mediums are presented in figure 1. In addition to these operating

capabilities, there are unique features that enhance the suitability of the TDT for aeroelastic testing. These features include: 1) a set of four quick-opening bypass valves that rapidly reduce the test-section Mach number and dynamic pressure when an instability is encountered while testing; 2) a set of four oscillating vanes, referred to as the airstream oscillator system for gust load alleviation testing; 3) a control room with a large matrix of observation windows allowing direct visual monitoring of the wind-tunnel model which is essential due to the dynamic nature of aeroelastic testing; 4) the test section and test chamber (plenum) area of the TDT can be isolated from the remainder of the tunnel circuit by a butterfly valve and a gate valve allowing faster model configuration changes; 5) a cooling system that does not actively control the airstream temperature, but consists of cooling coils that maintain a reasonably constant operating temperature, which can affect model instrumentation and material properties; and 6) a model debris catch screen to protect the drive motor fan blades in the event of a model failure. Figure 2 shows several of these features, as well as the general arrangement of the TDT. Figure 2(a) also shows the compass direction of the TDT facility, which can be used to define the names of the test section sidewalls as east or west. Reference 2 describes in greater detail these features of the facility and the various types of tests conducted in the TDT.

An early description of the TDT test section geometry is given in an internal report (NASA LWP-799, Sept. 1969). The section of the tunnel within the plenum shell which is instrumented with static pressure ports begins at tunnel station 32 (X = 32 ft) and ends at tunnel station 80 (X = 80 ft). The geometry of this section can be seen in figure 2(a) and 2(b). The walls of the section diverge slightly with increasing tunnel station, with the side walls diverging at a rate of 0.014 in/ft and the top and bottom sides (ceiling and floor) diverging at a rate of 0.0355 in/ft. The walls of the test section ventilate through ten discrete slots into a 60-foot diameter plenum. The three floor and three ceiling slots run from X = 50 ft to 80 ft and their centerlines are located approximately at Y = -4.90 ft, Y = 0 ft, and Y = 4.90 ft. Their width is given in Table I, within an accuracy of ±0.125 in, and are constant width from X = 65 ft to X = 80 ft. The four sidewall slots (two per side) start at X = 64 ft and end at X = 80 ft. The straight taper to constant width slots have centerlines at Z = -3.81 ft and Z = 3.81 ft; their widths are given in Table II, within an accuracy of ±0.125 in.

The 16-ft.-long diffuser entrance section between X = 80 ft and X = 96 ft contains the diffuser entrance flaps located on the top and bottom sides of the diffuser. These flaps are often called re-entry flaps because the flow that exits the test section through the upstream end of the slots reenters the tunnel circuit over these flaps, permitting continuous operation through transonic speeds. These flaps consist of four, independently variable panels, with the smaller, upstream panels called the upper and lower nose, and the larger, downstream panels called the upper and lower main. The upper and lower nose flaps are hinged at X = 85.5 ft and the upper and lower main flaps are hinged at X = 96 ft. Figure 2(c) is a photograph showing the location of the re-entry flaps and figure 3 is a schematic detailing the flap shapes for various Mach number ranges with a table of the re-entry flap schedule. The re-entry flap position has a large effect on the Mach number distribution in the test section, however no attempt was made to determine an optimum flap schedule during this portion of the TDT calibration effort.

EXPERIMENTAL APPARATUS

The pertinent flow properties (i.e. Mach number, dynamic pressure, etc.) are calculated from four measured tunnel parameters: 1) total pressure, 2) static pressure, 3) total temperature, and 4) R-134a purity. The total pressure is measured in the settling chamber of the TDT by a total pressure probe mounted two feet away from the west wall of the settling chamber at a position slightly below the vertical centerline of the settling chamber. The primary static pressure measurement is made via a tube located between the west wall of the plenum exterior shell and the control room (see figure 2(a)), at a height near the centerline of the test section. This is a reasonable location under the assumption that the test medium in the plenum is relatively still and at nominally uniform pressure except in the immediate vicinity of the sidewall slots in the test section. Both total and static (plenum) pressures are measured with Ruska Series 6000 digital pressure gages, which have a fused-quartz bourdon tube transducer with a digital read-out. Another set of Ruska Series 6000 pressure gages is used as a backup system. Total temperature is measured with a J-type thermocouple located just a few feet downstream of the cooling coils in the tunnel circuit using a J-Type thermocouple. The purity of the R-134a gas with respect to air contamination is based on purity measurements made with gas analyzers. This technique employs a new system of modern gas analyzers for the new heavy gas. Table III shows the accuracy for the primary flow parameter instruments just reviewed.

Data acquisition is done using the TDT open-architecture dynamic data acquisition system (DAS), which allows real-time acquisition and display of measured static and dynamic data as well as online analysis of the acquired data. Reference 3 describes the open-architecture system implementation in the TDT. The DAS hardware is comprised of three subsystems, each switch connectable to a subset of four, 64-channel NEFF-620 signal conditioners, for a total capability of 256 channels. The main computer systems for basic data acquisition, archiving, and continuous buffering are two Motorola quad 88100 25MHz processors with 80MB of RAM. On-line frequency analysis, postpoint time- and frequency-domain data analysis, and controller performance evaluations are performed on SGI-IRIX computer systems. The 8400 Electronically Scanned Pressure (ESP) system consists of the Key Entry Unit, two Scanner Digitizer Units, three Scanner Interface Connector Boxes, seven Pressure Calibration Units, and 21 16-port modules. Four, 1-psid and four, 2.5-psid ESP modules measure the steady state pressure at each of the tunnel sidewall static ports. The frame rate for the ESP system is set to 10 frames per second and the acquisition duration is six seconds.

Static pressure ports are installed in the test section walls. Rather than drilling the orifices directly into the test section walls, orifice inserts were designed and fabricated to control the orifice quality. This eliminated the need for any corrections due to orifice shape as discussed in reference 4. These inserts consist of stainless steel tubing (0.040 in. OD, 0.020 in. ID) brazed into 0.25 in.-diameter steel rod, and the orifice face sanded and polished to minimize imperfections. Figure 4 shows the details of the orifice inserts. These inserts are bonded flush with the test section walls. Several orifices were not installed or were relocated from areas where support structure did not allow orifices to be installed. The floor static ports are midway between the floor centerline slot and the east floor slot, and the ceiling

static ports are midway between the ceiling centerline slot and the west ceiling slot. There are no orifices installed on the test section ceiling from X = 30 ft to X = 46 ft, the waterline for the east wall static ports is three inches below tunnel centerline, and the waterline for the west wall static ports is three inches above centerline. Table IV shows the locations where static pressure ports are installed and figure 2(d) shows the location of ports on the test section east wall.

Sidewall static pressure measurements were obtained for various tunnel configurations and flow conditions. The main parameters investigated were Mach number, re-entry flap settings, wind-off total pressure, test medium, and east wall porosity. Figure 2(d) shows the test section east wall slots covered and open. Conditions in the TDT operating envelope for air and R-134a where data were acquired are shown in figure 5. Tables V and VI contain the values of the tunnel conditions for the acquired points in air and R-134a, respectively. Each data set was obtained by setting an initial wind-off total pressure, and varying tunnel speed to achieve the desired Mach numbers. The initial wind-off total pressures were 200 psf, 400 psf, 700 psf, 1200 psf, and atmospheric pressure in air, and 200 psf, 500 psf, 700 psf, 1000 psf, 1400 psf, and 1800 psf in R-134a. The target Mach numbers were 0.25, 0.5, 0.6, 0.7, 0.75, 0.8, 0.85, 0.9, 0.95, 0.975, 1.0, 1.025, 1.05, 1.1, and tunnel maximum in air, and 0.1, 0.2, 0.3, 0.5, 0.6, 0.7, 0.8, 0.9, 0.95, 0.975, 1.0, 1.025, 1.05, 1.1, and tunnel maximum in R-134a. The time required for the pressure in the module reference lines to equalize to the plenum static pressure varied with initial wind-off total pressures, increasing with decreasing initial pressure.

Mach number from the sidewall static pressure orifices is calculated using the equation (Ref. 5):

$$M_{local} = \sqrt{\left\{ \frac{2}{\gamma - 1} \left[\left(\frac{P_{t,\infty}}{P_{local}} \right)^{\frac{\gamma - 1}{\gamma}} - 1 \right] \right\}}$$

The Ruska accuracy is quoted as ± 0.016% of the reading pressure and ± 0.008% of the full-scale pressure, which provides an accuracy in the calculated Mach number of about ± 0.002 for most Mach numbers and pressures, in air and R-134a. This Mach number accuracy is based on assuming the maximum instrument error range for measured free-stream stagnation pressure $P_{t,\infty}$, and plenum pressure $P_{t,c}$. (See figure 6.) The ESP data acquisition system is calibrated daily and/or whenever the plenum chamber pressure was near atmospheric. Below atmospheric pressure, the pressure calibration units have difficulty attaining negative pressures for calibrating the modules. Figure 7 shows the variation of the error in the Mach number computed from a local static pressure orifice for various Mach numbers and pressures for the worst-case condition of the $P_{t,\infty}$ Ruska having the maximum error at the measured pressure and the pressure data sensor having its maximum 0.36-psf error simultaneously.

DISCUSSION OF RESULTS

Figure 8 presents Mach number distribution plots for each reference Mach number and test section wall. The data are presented for a total pressure, $P_{t,\infty}$, between 200 psf and 300 psf in air. These plots are representative of typical Mach number distributions in air for the test section walls for all $P_{t,\infty}$. For each test section wall and reference Mach number, the Mach number distributions presented are for the re-entry flap position given in the re-entry flap schedule (see figure 3). The vertical scale is somewhat coarse when compared to the resolution of the data system. The symbol size in figure 8 corresponds to about ±0.01 uncertainty in Mach number; whereas figure 7(a) shows that, based on the estimated precision of the instrumentation, most of the local Mach number data in figure 8 have a precision of better than ±0.006. The vertical scale is acceptable since the data clearly have random variations greater than the ±0.006 attributable to the instrumentation precision. These variations in the data can be easily seen with a vertical scale of $M_\infty = 0.1$ per division and are believed to be caused by imperfections in the smoothness of the wall surface at the orifice.

Figure 9 presents Mach number distribution plots with R-134a as the test medium. The data are presented for a total pressure, $P_{t,\infty}$, between 700 psf and 900 psf. As in air, these plots are representative of typical Mach number distributions on the walls for all $P_{t,\infty}$. Again, the vertical scale is somewhat coarse, with the symbol size in figure 10 corresponding to about ±0.01 uncertainty in Mach number; whereas figure 7(b) shows that most of the data in figure 9 have a precision greater than ±0.003. Random variations in the data greater than ±0.003 are clearly visible with the vertical scale of $M_\infty = 0.1$ per division and are believed to be caused by imperfections in the smoothness of the wall surface at the orifice.

Figures 10 through 13 show Mach number distributions for certain M_∞ and each test section wall at various total pressures, $P_{t,\infty}$, with air as the test medium. The purpose of these plots are to illustrate the insensitivity of test section wall Mach number distributions to $P_{t,\infty}$. The range of values for the vertical scale for each plot was held to 0.4 to show overall variations in local Mach number and not accentuate the variations due to wall smoothness or orifice imperfections. The consistent ranges also facilitate comparisons of different M_∞.

Variation in Mach number distribution in R-134a due to changes in $P_{t,\infty}$ are plotted in Figures 14 through 17. The purpose of these plots are to illustrate the insensitivity of test section wall Mach number distributions to $P_{t,\infty}$. The range of values for the vertical scale are consistent with the plots with air as the test medium (Figures 10 through 13) in order to not emphasize local variations in Mach number. The constant ranges also facilitate comparisons of different M_∞. A close examination of the plots with R-134a as the test medium and $M_\infty \approx 1.0$ shows a surprising rise in M_{local} around $X = 44$, peaking near $X = 48$, and subsequent decrease in M_{local} by $X = 52$ for increasing $P_{t,\infty}$ (Figures 14(e), 15(e), 16(e), and 17(e)). This variation did not occur at any other Mach number or with air as the test medium.

Figures 18 and 19 show Mach number distributions, one for each test section wall in air for $M_\infty \approx 0.5$ and 0.9. Figures 20 and 21 are similar plots with R-134a as the test medium and $M_\infty \approx 0.5$ and 0.8. Significant re-entry flap variations could not be tested above these

Mach numbers due to substantial affects on the flow conditions. The range of values for the vertical scale for each plot was held to 0.5 to show overall variations in local Mach number due to re-entry flap setting and de-emphasize the variations due to wall smoothness or orifice imperfections. Variations in the Mach number distributions due to the re-entry flap settings were mostly located just upstream of their location. The Mach number distributions measured along the test section walls should not be used to determine the optimal setting for the re-entry flaps, and were not acquired for that purpose.

Figures 22, 23, and 24 are Mach number distribution plots which show the effect of covering the slots in the east test section wall for $M_\infty \approx 0.49$, 0.9, and 1.17, respectively. The test medium was air and each figure contains plots of the Mach number distributions on each test section wall. Figures 25, 26, and 27 are Mach number distributions illustrating the same effects of covering the east wall slots, but with a test medium of R-134a and $M_\infty \approx 0.5$, 0.9, and 1.2, respectively. Covering the east wall slots did not show any significant effect on the wall Mach number distributions, particularly on the east wall where one might expect some effect. By normalizing the Mach number distributions by the appropriate M_∞, differences in M_{local} between open and covered slot were no larger than 0.5 percent and averaged less than 0.2 percent between $X = 65$ and $X = 80$. Also, the differences did not show identifiable trends which could be attributed to the covered slots, such as M_{local} always being lower or higher with the slots covered.

CONCLUDING REMARKS

One of the objectives of the TDT calibration tests was to determine an empirical relationship between the calculated free-stream Mach number and the nominal Mach number in the test section based on the measured pressures in the tunnel settling chamber and plenum and to quantify any necessary corrections. Calibration tests included measurement of pressure distributions along the test-section walls, test-section centerline, at certain tunnel stations via a rake apparatus, and in the tunnel settling chamber. Wall boundary layer, turbulence, and flow angularity measurements were also performed. The focus of this report is on the measurement and analysis of the test section wall Mach number distributions.

Results from these measurements may be correlated with results from the other tests conducted as part of the TDT calibration effort to determine any necessary correction factors. The most significant result from the wall Mach number distribution measurements was that no significant discrepancies were found. Results from the specific parameter variations showed the following:

1. Small variations in the wall Mach number distributions are suspected to be due to wall and orifice imperfections, most notably at Mach numbers greater than one.
2. Wall Mach number distributions are relatively insensitive to variations in the tunnel total pressure, except at $M_\infty = 1$ in R-134a. At those conditions, a small increase in M_{local} occurs around $X = 44$ to 48 with increasing total pressure.
3. The current TDT re-entry flap schedule was acceptable for the test conditions investigated. Optimal flap positions were not investigated.

4. No effects directly attributable to covering the wall slots on the east side of the test section were found.

REFERENCES

1. Brooks, Cuyler W., Jr.; Harris, Charles D.; and Reagon, Patricia G.: *The NASA Langley 8-Foot Transonic Pressure Tunnel Calibration.* NASA TP- 3437, August 1994.

2. Cole, Stanley C., and Rivera, Jose, A., Jr.: *The New Heavy Gas Testing Capability in the NASA Langley Transonic Dynamics Tunnel.* Paper No. 4, Presented at the Royal Aeronautical Society Wind Tunnels and Wind Tunnel Test Techniques Forum, Churchill College, Cambridge, Cambridge, UK, April 14-16, 1997.

3. Bryant, C.; and Hoadley, S. T.: *Open Architecture Dynamic Data System at Langley's Transonic Dynamics Tunnel.* AAIA Paper 98-0343, Jan. 1998.

4. Pope, Alan: *Wind Tunnel Calibration Techniques.* AGARDograph 54, April, 1961.

5. Anderson, John D.: *Introduction to Flight.* McGraw-Hill, Inc., 1989.

TABLES

Table I. Measured width of expansion slots along test-section floor and ceiling.

***X*, ft.**	**y_s, in.** (±0.125 in.)
50	0.375
51	1.0
52	1.875
53	2.75
54	3.5
55	4.125
56	4.75
57	5.5
58	5.625
59	5.875
60	5.625
61	5.0
62	4.375
63	3.625
64	3.0
65	2.625
80	2.625

Table II. Measured width of test-section sidewall slots.

***X*, ft.**	**y_s, in.** (±0.125 in.)
64	0
67.667	4.0
80	4.0

Table III. Instrument accuracy.

Instrument	**Range**	**Accuracy, %FS**	**Accuracy, EU**
Ruska Series 6000 pressure gages	0 to 2200 psf	±0.016% RDG ± 0.008% FS	±0.016% RDG ± 0.176 psf
J-Type Thermocouple	32 to 1382 °F	±0.4 %	± 2 °F
R-134a purity gage	0 to 100%	±1%	±1%
1.0-psid ESP modules	0 to 1 psid	±0.1%	±0.144 psf
2.5-psid ESP modules	0 to 2.5 psid	±0.1%	±0.36 psf

Table IV. Tunnel station, *X*, buttline, *Y*, and waterline, *Z* locations of the static pressure orifices.

East Wall		West Wall		Ceiling		Floor	
***X*, ft.**	***Z*, ft.**	***X*, ft.**	***Z*, ft.**	***X*, ft.**	***Y*, ft.**	***X*, ft.**	***Y*, ft.**
32.0	-0.25	32.0	0.25	46.0	2.45	32.0	-2.45
37.1	-0.25	37.0	0.25	48.0	2.45	37.0	-2.45
42.0	-0.25	42.0	0.25	50.0	2.45	42.0	-2.45
44.2	-0.25	44.0	0.25	52.0	2.45	44.0	-2.45
46.0	-0.25	46.0	0.25	54.0	2.45	46.0	-2.45
48.0	-0.25	48.0	0.25	56.0	2.45	48.0	-2.45
50.0	-0.25	50.0	0.25	58.0	2.45	50.0	-2.45
52.0	-0.25	52.0	0.25	60.0	2.45	52.0	-2.45
54.0	-0.25	54.0	0.25	61.0	2.45	54.0	-2.45
56.0	-0.25	56.0	0.25	62.0	2.45	56.0	-2.45
58.0	-0.25	58.0	0.25	63.0	2.45	58.0	-2.45
60.0	-0.25	60.0	0.25	64.0	2.45	60.0	-2.45
61.1	-0.25	61.0	0.25	66.0	2.45	61.0	-2.45
64.0	-0.25	62.0	0.25	68.0	2.45	62.0	-2.45
66.0	-0.25	64.0	0.25	70.0	2.45	63.0	-2.45
68.0	-0.25	66.0	0.25	71.0	2.45	64.0	-2.45
70.0	-0.25	68.0	0.25	72.0	2.45	66.0	-2.45
71.0	-0.25	70.8	0.25	73.0	2.45	68.0	-2.45
72.0	-0.25	73.2	0.25	74.0	2.45	70.0	-2.45
73.0	-0.25	76.0	0.25	75.0	2.45	71.0	-2.45
74.0	-0.25	77.0	0.25	76.0	2.45	72.0	-2.45
75.0	-0.25	80.0	0.25	77.0	2.45	73.0	-2.45
76.0	-0.25			78.0	2.45	74.0	-2.45
77.0	-0.25			79.8	2.45	75.0	-2.45
79.9	-0.25					76.0	-2.45
						77.0	-2.45
						78.0	-2.45
						79.8	-2.45

Table V. Tunnel conditions where data were acquired in air.

M_∞	q, psf	$P_{t,\infty}$	P_{tc}	T_t
0.501	30.09	203.12	171.09	114.2
0.601	41.33	208.60	163.40	117.3
0.501	30.91	208.70	175.80	111.6
0.701	53.41	215.40	155.10	121.7
0.951	76.60	216.57	121.07	133.4
0.751	59.60	219.29	150.81	124.0
0.975	79.42	219.49	119.36	135.1
1.001	81.92	221.39	116.85	134.6
0.749	59.97	221.47	152.60	125.2
0.799	65.54	223.40	146.73	126.5
1.027	84.82	224.50	114.90	136.9
0.948	81.59	231.30	129.69	131.8
1.171	95.42	232.22	99.49	115.9
0.850	75.42	239.17	149.13	133.3
0.900	81.76	244.01	144.34	136.3
1.048	98.48	256.59	127.99	112.7
1.100	107.49	270.92	126.84	113.6
0.249	16.61	399.40	382.53	108.0
0.502	60.93	410.88	346.02	98.6
0.501	61.56	416.49	350.98	101.7
0.600	83.36	421.68	330.54	102.7
0.700	107.19	433.90	312.94	107.3
0.750	119.65	441.31	303.87	110.1
0.750	120.21	443.72	305.67	111.7
0.799	131.71	448.74	294.64	113.1
0.850	147.42	467.64	291.65	126.3
0.895	164.39	493.00	292.97	121.3
0.950	189.06	534.76	299.07	128.6
0.975	195.40	539.87	293.48	130.4
0.999	201.35	545.08	288.40	132.5
1.001	202.87	548.16	289.25	134.3
1.024	207.61	550.80	282.93	134.5
0.250	29.16	695.10	665.48	96.2
0.500	108.07	731.49	616.48	107.8
0.500	109.47	741.09	624.59	115.0
0.601	148.87	752.32	589.54	113.9
0.700	191.80	775.85	559.39	120.9
0.749	213.62	789.54	544.28	125.3
0.750	215.42	794.32	546.86	128.4
0.799	235.98	803.95	527.85	129.7
0.250	49.23	1176.30	1126.30	96.7
0.249	49.14	1185.81	1135.90	103.6
0.490	176.00	1235.90	1049.10	107.9
0.501	184.23	1244.35	1048.26	112.3
0.522	198.57	1253.07	1040.59	113.8
0.250	89.79	2142.30	2051.10	96.3
0.494	320.95	2216.97	1875.92	115.6

Table VI. Tunnel conditions where data were acquired in R-134a.

M_∞	q, psf	$P_{t,\infty}$	P_{tc}	T_t	R-134a Purity	γ
0.298	9.99	212.81	202.41	100.1	0.930	1.1119
0.498	26.41	219.59	191.51	102.5	0.930	1.1122
0.696	47.37	229.01	175.35	103.8	0.910	1.1148
0.899	69.69	240.32	154.78	104.9	0.910	1.1161
0.999	80.19	247.47	144.19	107.6	0.900	1.1174
1.196	98.76	266.38	123.46	115.3	0.900	1.1182
0.301	23.98	504.19	479.53	97.0	0.960	1.1105
0.500	62.66	519.39	452.73	99.0	0.960	1.1108
0.700	114.24	550.02	420.52	107.8	0.950	1.1114
0.897	166.28	576.09	371.76	111.5	0.940	1.1129
0.949	179.78	585.76	359.39	113.9	0.940	1.1130
0.973	185.97	590.65	353.77	115.2	0.940	1.1130
1.000	192.61	595.80	347.06	116.4	0.940	1.1130
1.023	198.28	600.34	341.24	117.2	0.930	1.1140
1.048	205.17	608.11	336.16	119.8	0.930	1.1138
1.081	214.26	618.96	329.49	121.7	0.930	1.1138
1.204	241.34	650.40	299.40	131.5	0.930	1.1135
0.104	4.20	709.90	705.79	98.8	0.946	1.1116
0.200	15.39	713.79	698.15	100.1	0.946	1.1115
0.301	34.47	720.89	685.70	101.9	0.946	1.1115
0.501	89.42	740.59	645.50	105.9	0.952	1.1110
0.701	159.94	770.10	588.97	112.3	0.957	1.1106
0.949	243.82	796.26	489.53	118.1	0.967	1.1104
0.975	253.53	804.93	481.55	119.6	0.967	1.1104
0.901	232.97	805.43	518.88	122.5	0.957	1.1103
0.999	261.49	811.44	473.78	120.6	0.967	1.1104
1.026	270.37	818.53	464.57	121.8	0.967	1.1104
1.036	276.62	829.82	465.75	124.1	0.967	1.1102
1.097	295.36	845.34	442.75	128.3	0.957	1.1109
1.207	330.34	890.76	409.37	139.4	0.957	1.1103
0.100	5.48	1002.80	997.21	104.6	0.950	1.1111
0.201	21.93	1010.01	987.95	106.5	0.950	1.1110
0.300	48.17	1022.19	973.20	109.2	0.950	1.1108
0.497	126.14	1061.05	926.47	117.7	0.950	1.1101
0.700	227.96	1099.45	841.22	115.0	0.950	1.1114
0.900	332.74	1152.15	743.21	120.6	0.950	1.1117
0.949	358.92	1171.92	719.85	123.8	0.950	1.1116
0.976	372.67	1182.95	707.23	125.6	0.950	1.1115
1.000	384.87	1193.27	695.72	127.9	0.950	1.1114
1.023	396.78	1203.21	683.85	129.5	0.940	1.1122
1.047	410.28	1219.82	676.26	133.6	0.940	1.1118
1.118	443.73	1253.32	640.68	138.8	0.940	1.1116
0.099	7.48	1381.73	1373.88	100.0	0.950	1.1128
0.199	29.69	1388.35	1357.91	100.6	0.940	1.1136
0.299	66.29	1413.06	1344.93	106.7	0.950	1.1120
1.001	527.69	1634.78	952.08	128.3	0.950	1.1120
0.099	9.58	1789.30	1779.88	94.0	0.950	1.1147
0.199	38.36	1800.14	1761.39	95.2	0.950	1.1147
0.300	85.92	1818.10	1730.92	96.4	0.950	1.1146
0.501	225.77	1874.01	1633.73	99.8	0.950	1.1146
0.700	412.50	1993.55	1525.70	117.6	0.950	1.1127

FIGURES

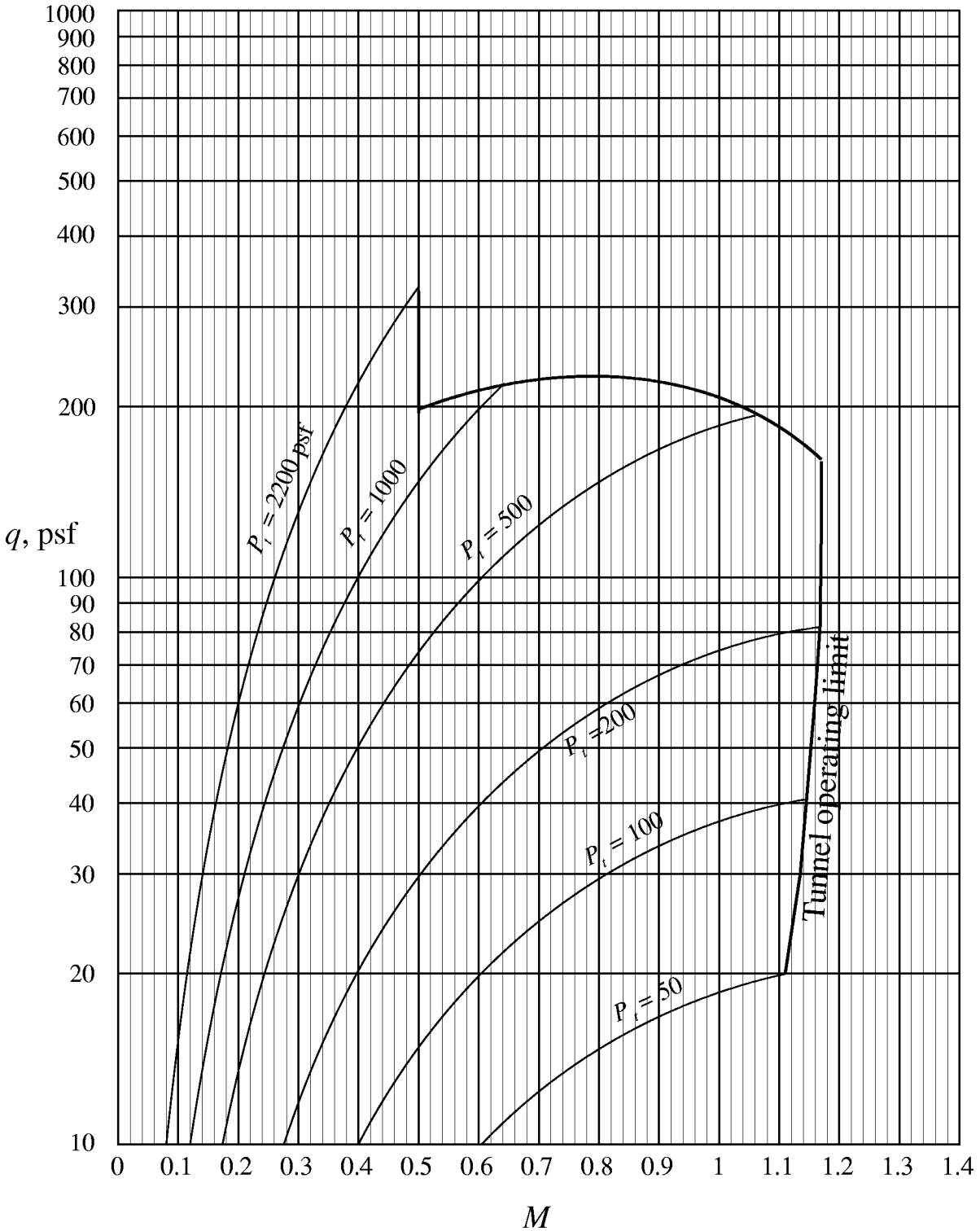

(a) *M-q* curves for air (T_t = 100 °F)

Figure 1. TDT operating envelope.

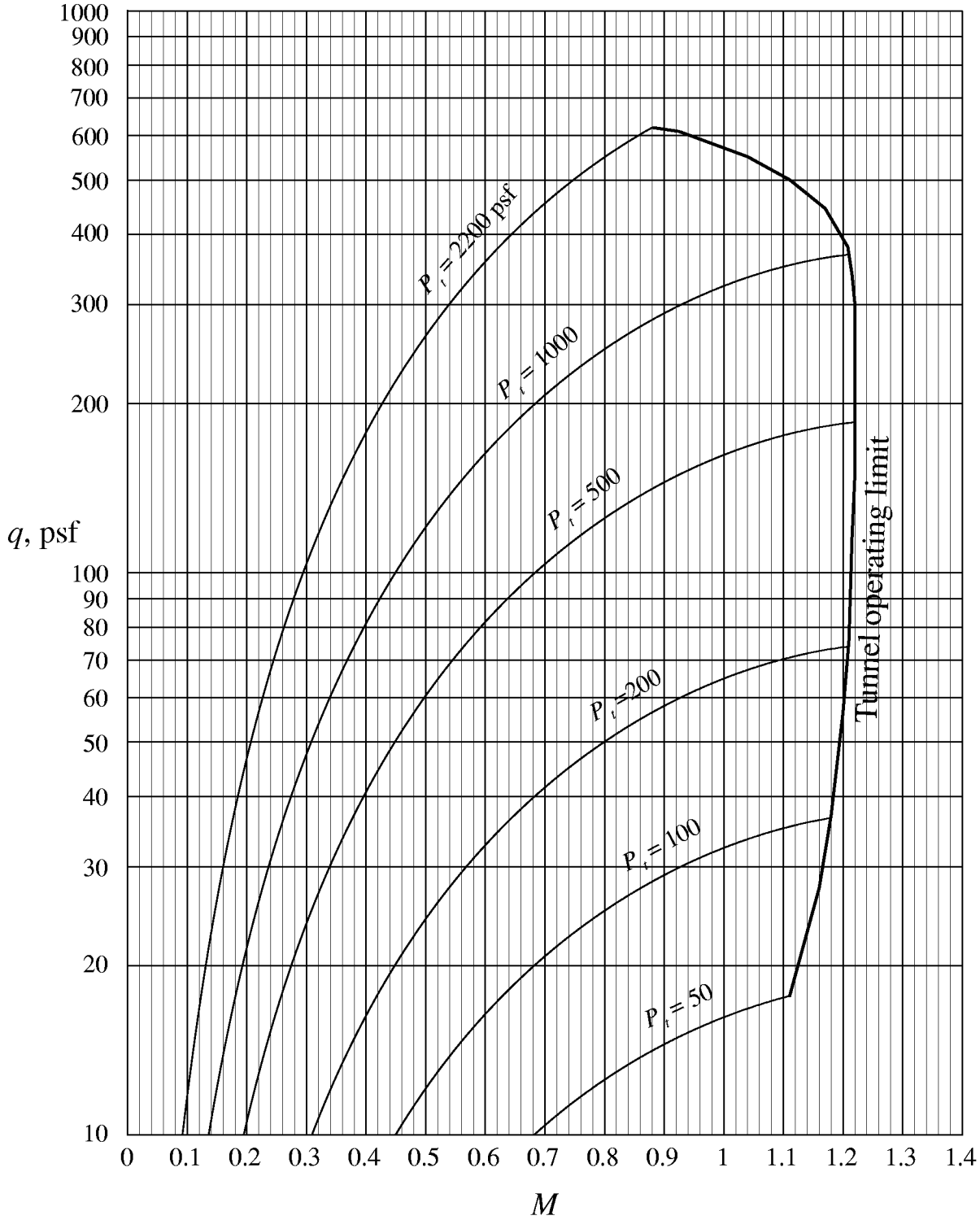

(b) *M*-*q* curves for 95-percent R-134a/air mixture (T_t = 100 °F)

Figure 1. Concluded.

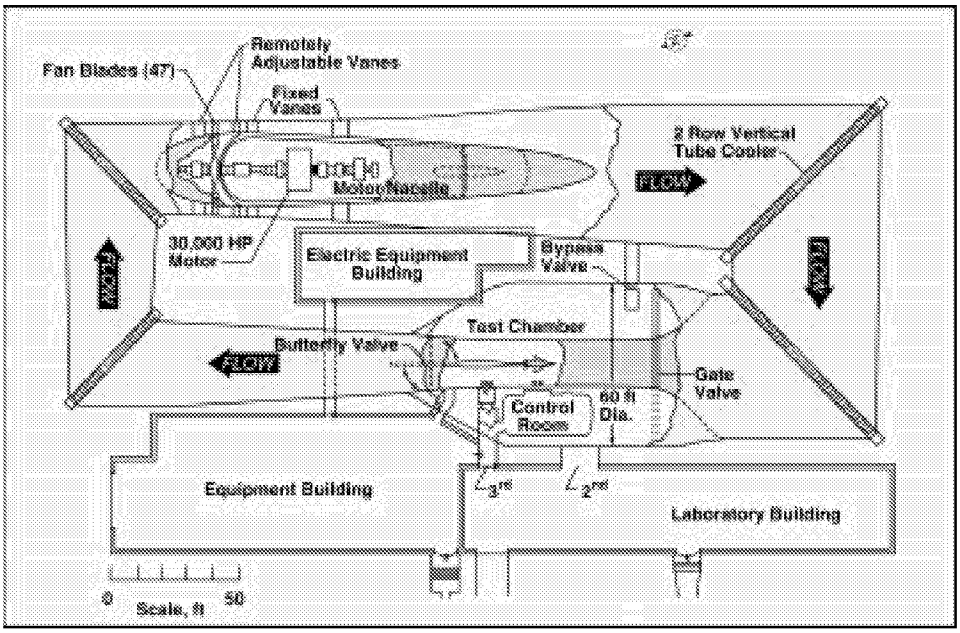

(a) Plan view of the TDT facility.

Figure 2. General arrangement of the Langley Transonic Dynamics Tunnel.

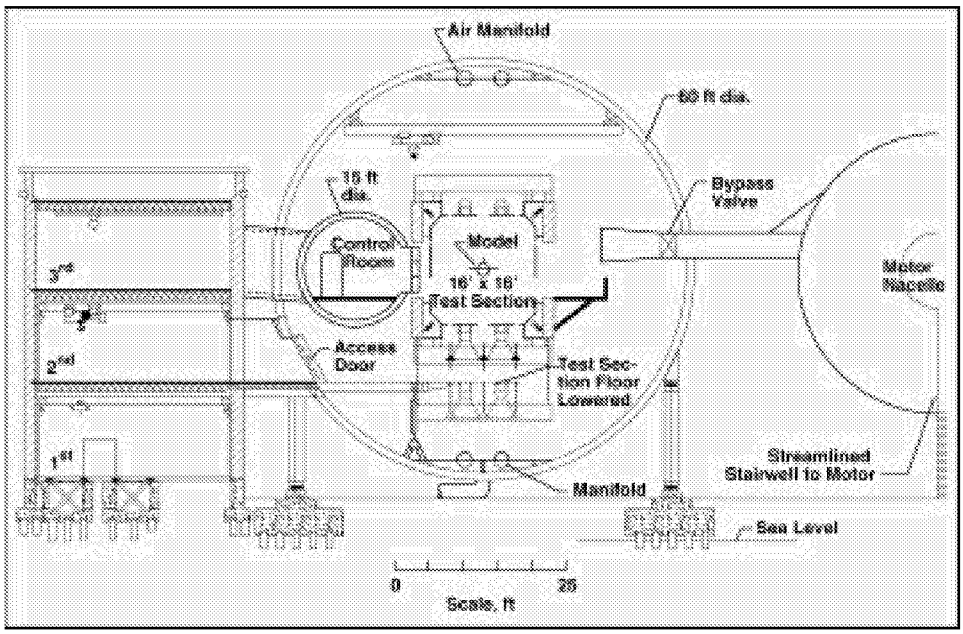

(b) Cutaway view of the test section area of TDT.

Figure 2. Continued.

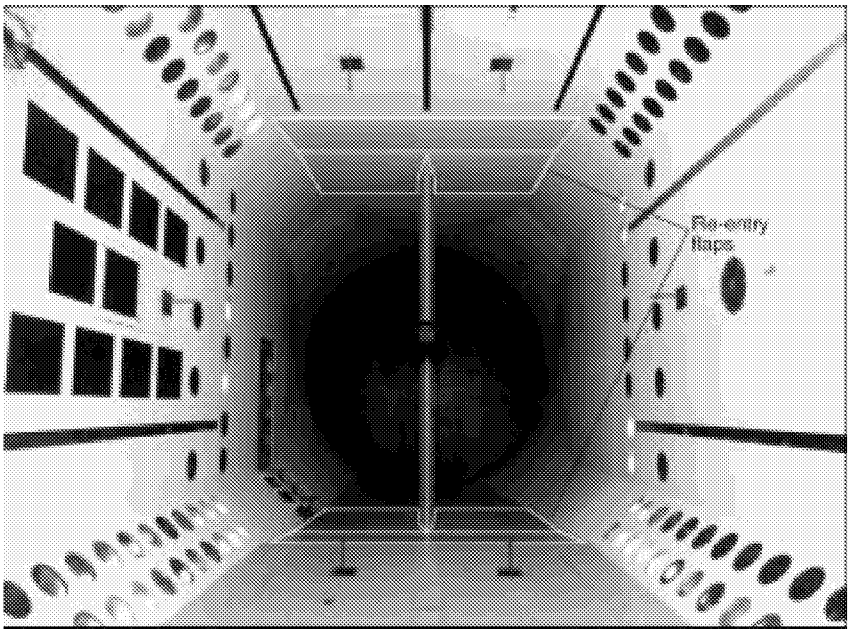

(c) Photograph detailing re-entry flaps

Figure 2. Continued.

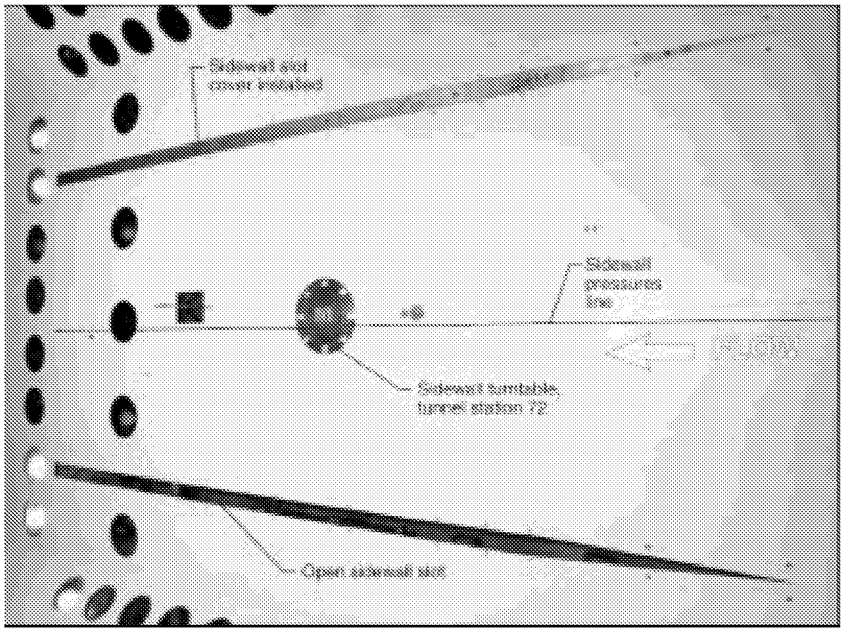

(d) Photograph of east test section wall details.

Figure 2. Concluded.

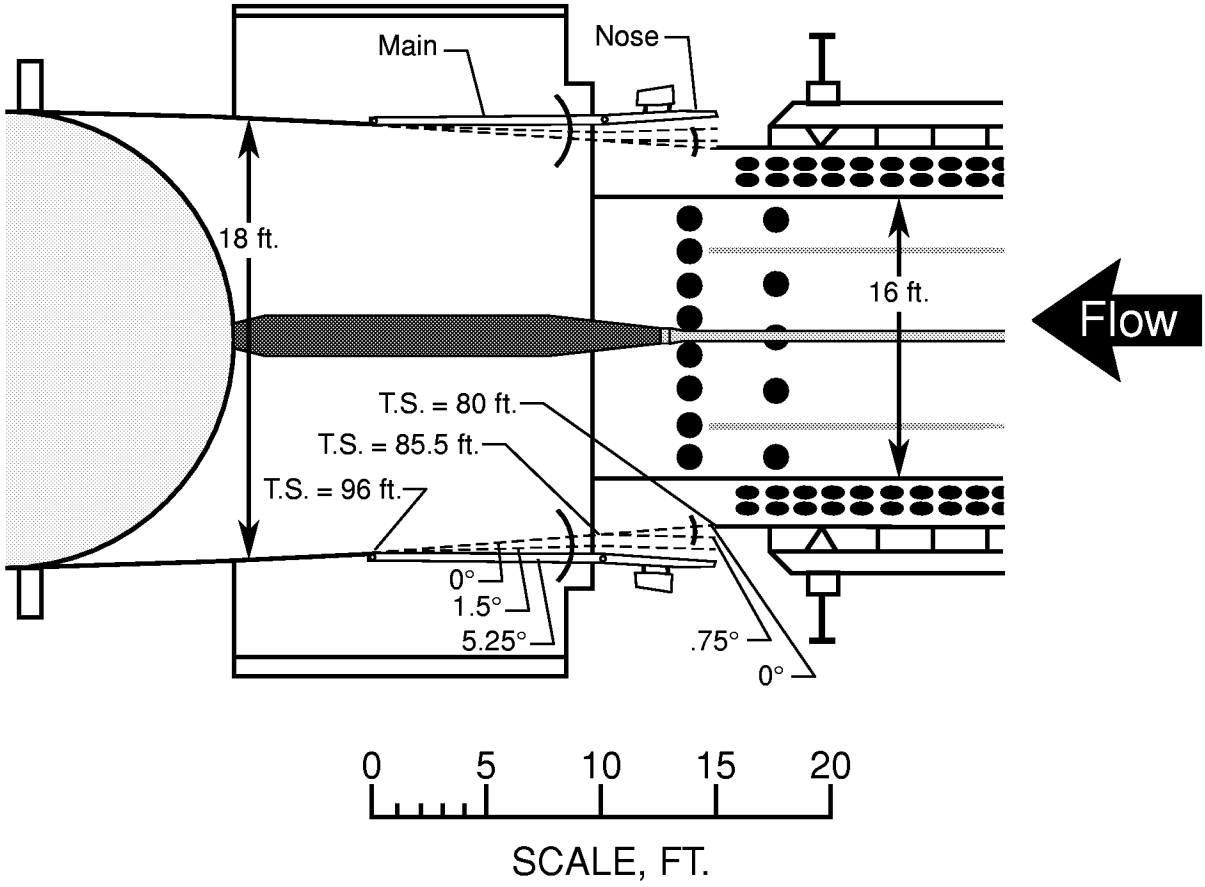

f_S	***M* Range**	$f_{R\text{-}main}$, **counts**	$f_{R\text{-}nose}$, **counts**	$\alpha_{f,R\text{-}main}$, **deg.**	$\alpha_{f,R\text{-}nose}$, **deg.**
1	0.00 to 0.85	470	99460	0.00°	0.00°
2	0.85 to 0.95	470	99550	0.00°	0.75°
3	0.95 to 1.05	900	99550	1.50°	0.75°
4	1.05 to Tunnel Max.	2000	99550	5.25°	0.75°

Figure 3. Diagram of the TDT re-entry flap settings and schedule.

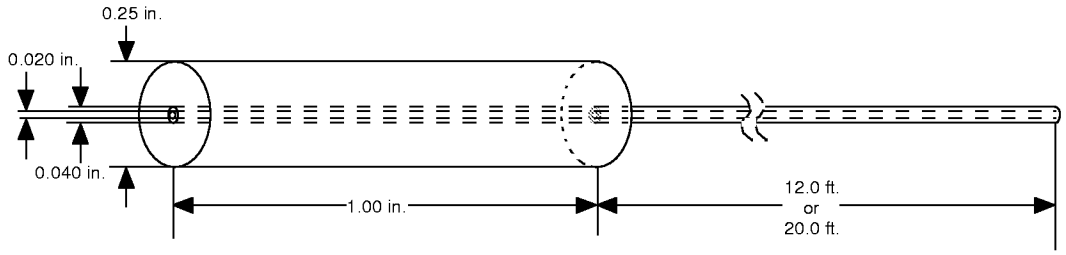

Figure 4. Schematic of sidewall pressure orifice insert.

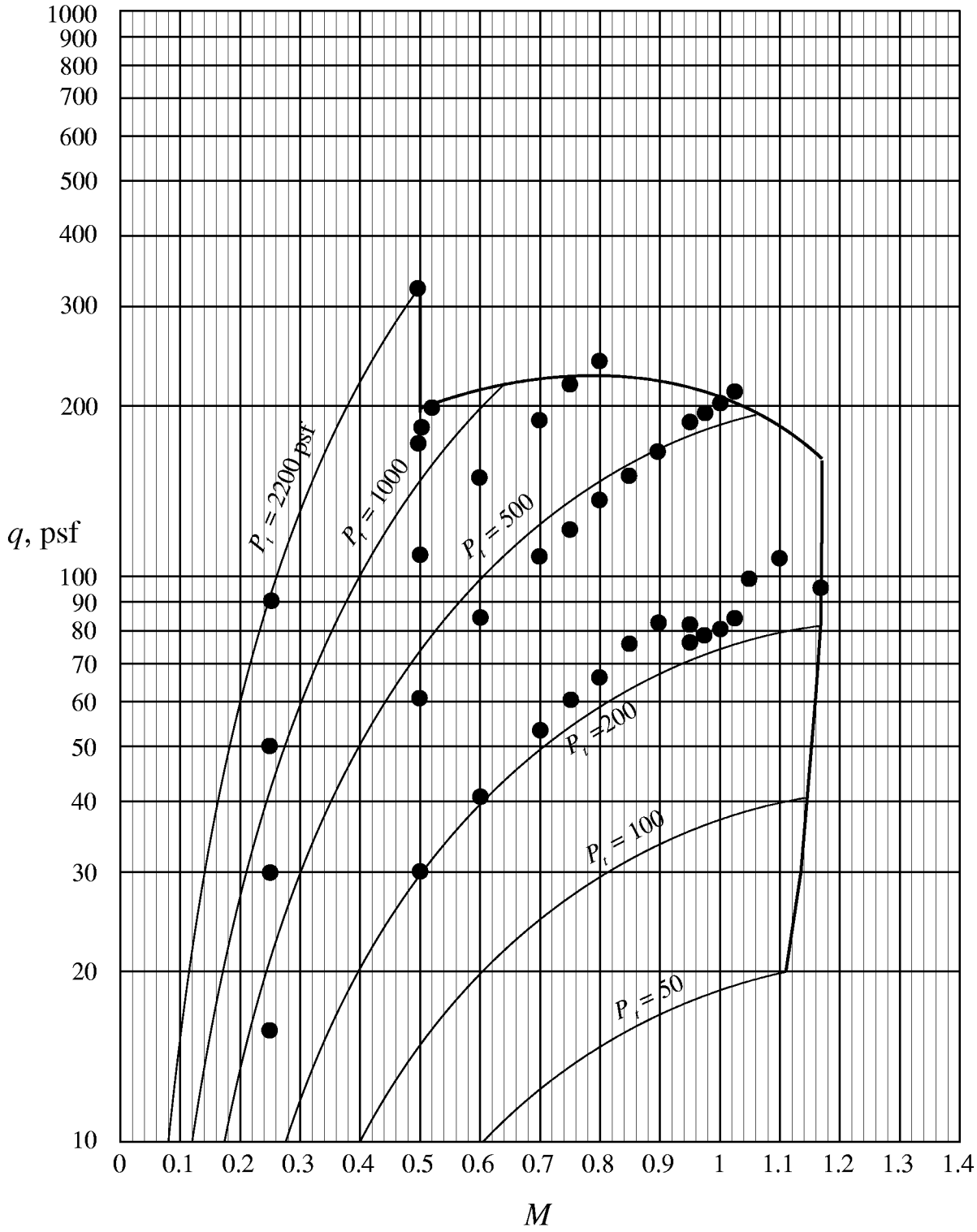

(a) Air

Figure 5. Conditions within the TDT operating boundary where data was acquired.

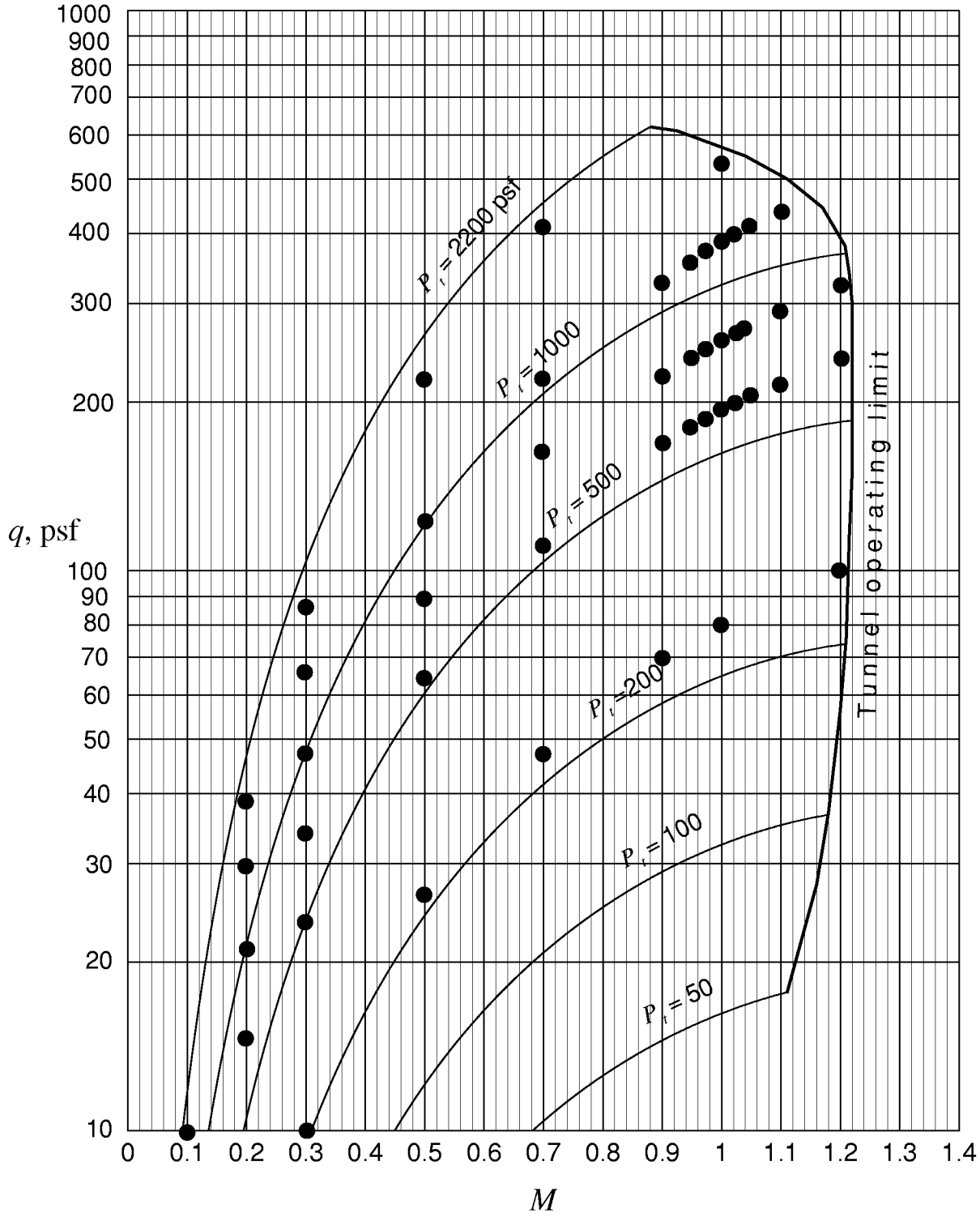

(b) R-134a

Figure 5. Concluded.

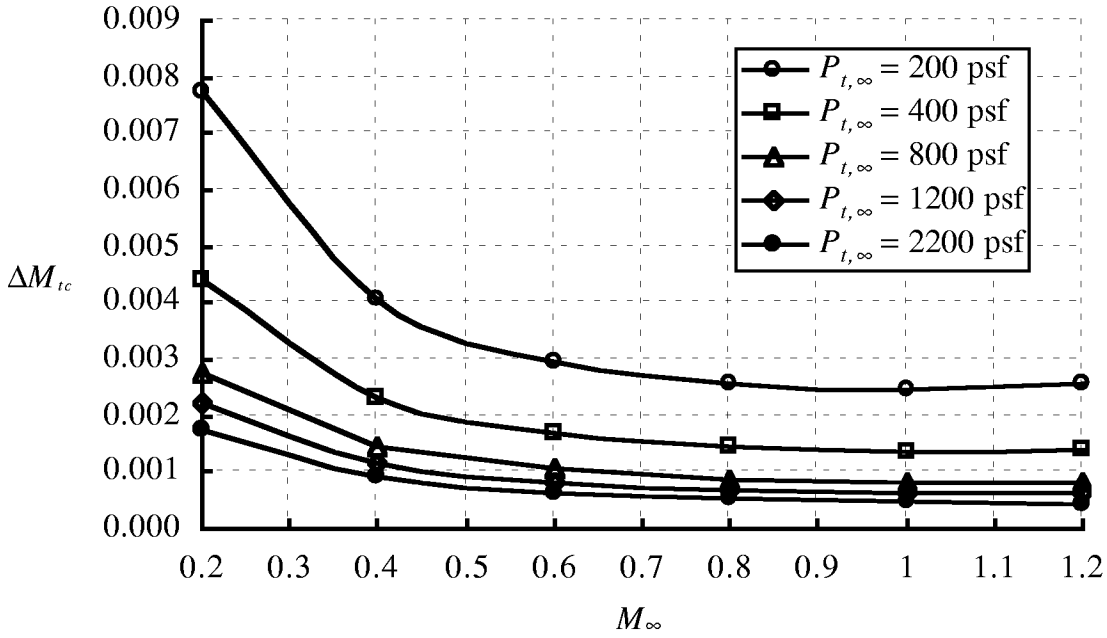

(a) Variation of error in M_{tc} with $P_{t,\infty}$ in air, based on reported Ruska instrument error in P_t and P_{tc}, worst-case combination of errors.

Figure 6. Error in free-stream Mach number as a function of total pressure.

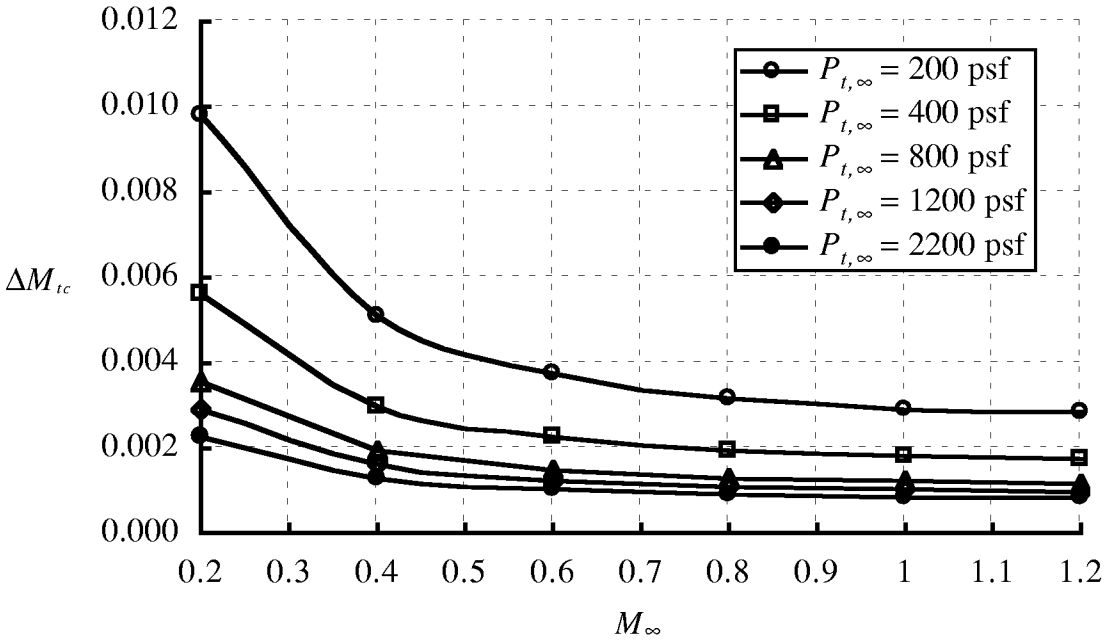

(b) Variation of error in M_{tc} with $P_{t,\infty}$ in R-134a, based on reported Ruska instrument error in P_t and P_{tc}, worst-case combination of errors.

Figure 6. Concluded.

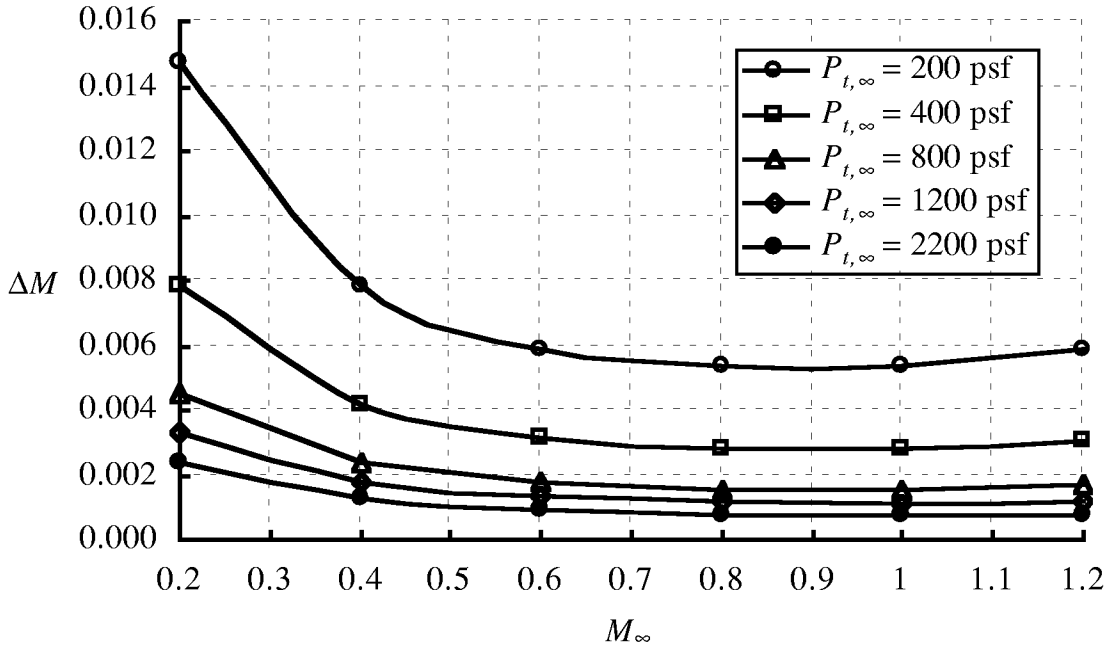

(a) Variation of error in local M with $P_{t,\infty}$ in air, based on 0.36-psf instrument error in P_{local} and reported Ruska instrument error in P_{tc}, worst-case combination of errors.

Figure 7. Error in Mach number as a function of total pressure.

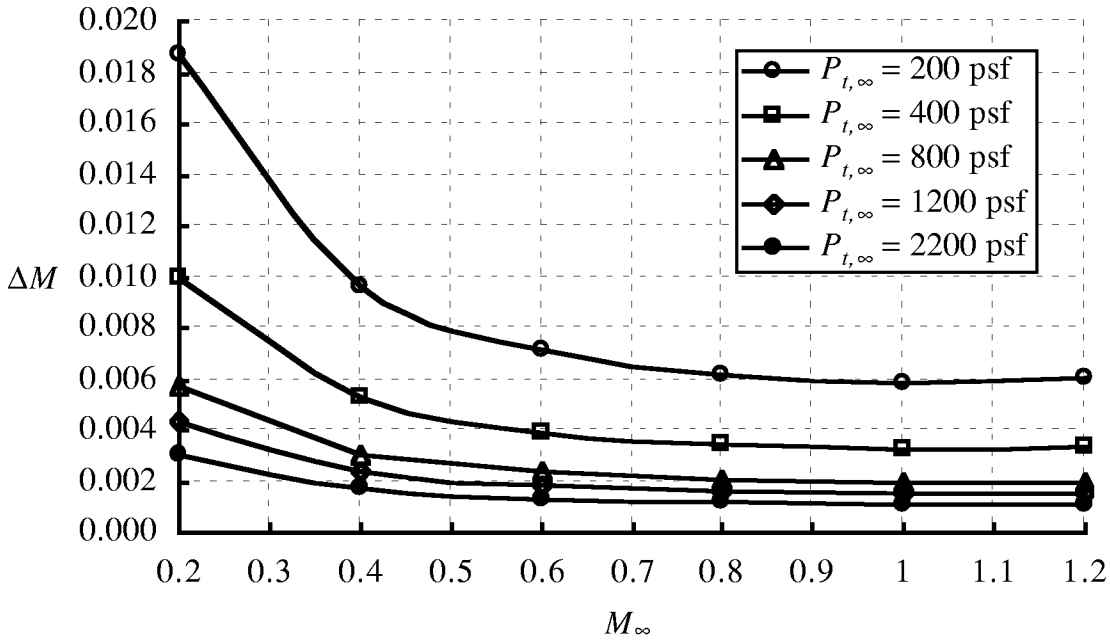

(b) Variation of error in local M with $P_{t,\infty}$ in R-134a, based on 0.36-psf instrument error in P_{local} and reported Ruska instrument error in P_{tc}, worst-case combination of errors.

Figure 7. Concluded.

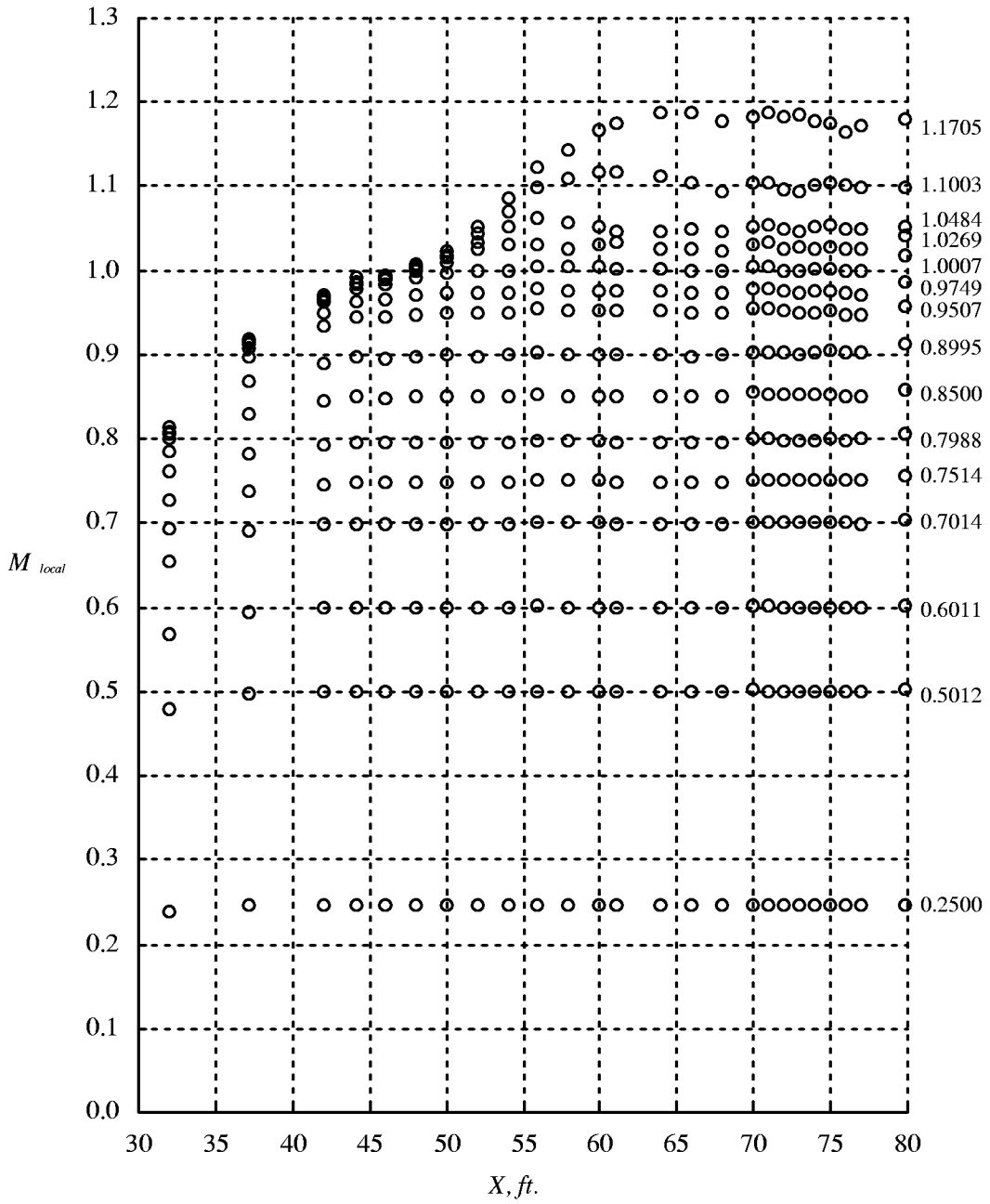

(a) Test section east wall M_{local} distributions.

Figure 8. Mach number distribution of test section in air; 200 psf $\leq P_{t,\infty} \leq$ 300 psf and re-entry flaps set to scheduled position.

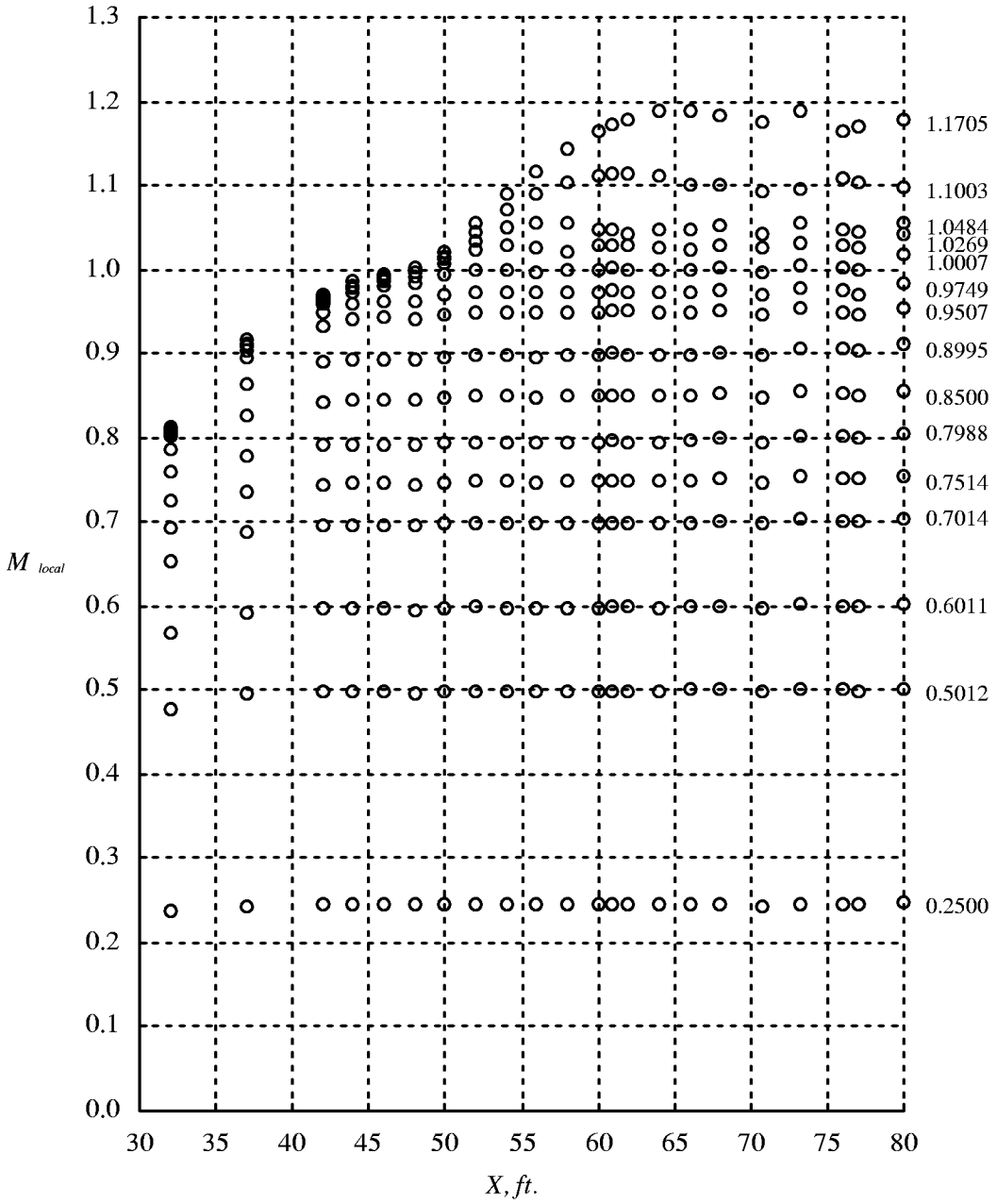

(b) Test section west wall M_{local} distributions.
Figure 8. Continued.

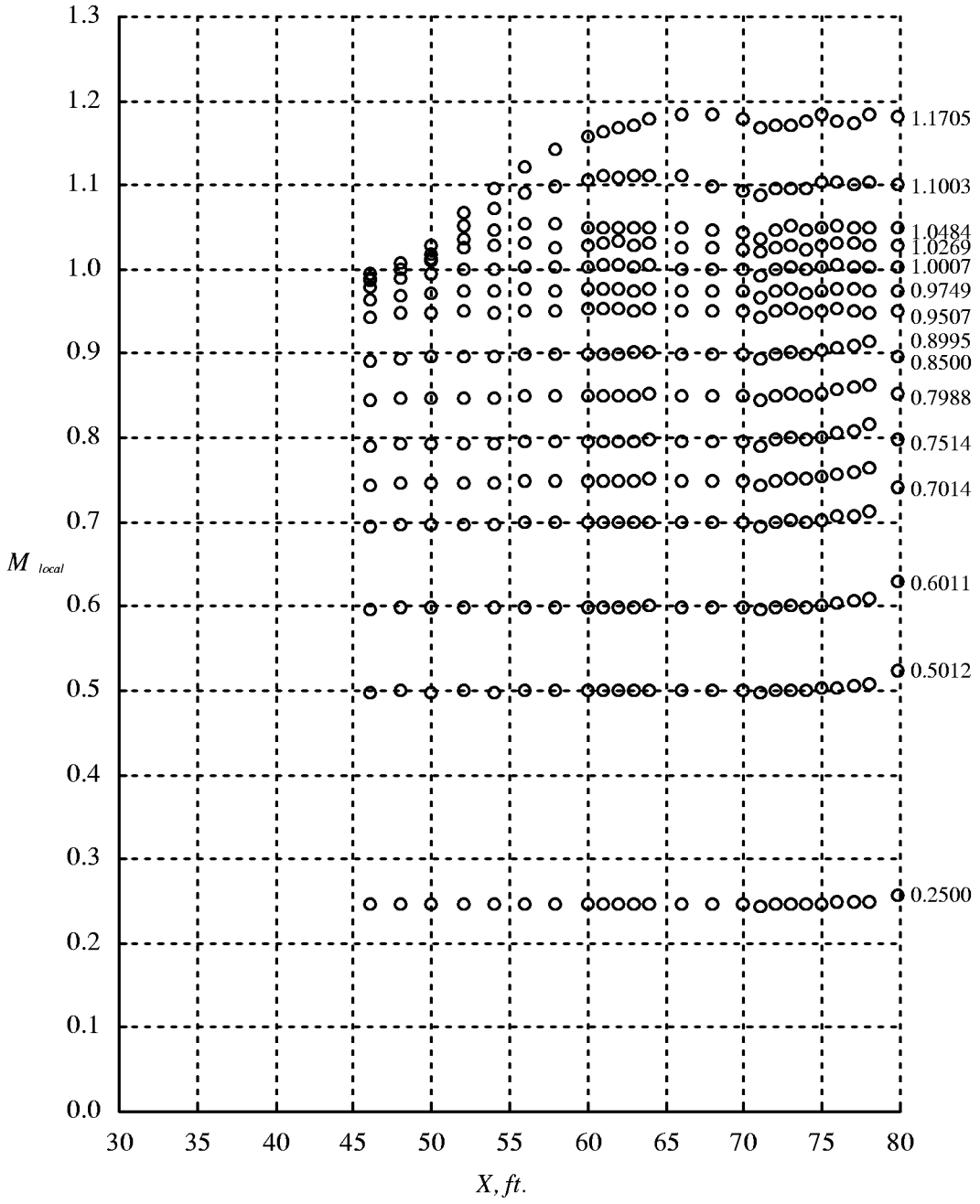

(c) Test section ceiling M_{local} distributions.
Figure 8. Continued.

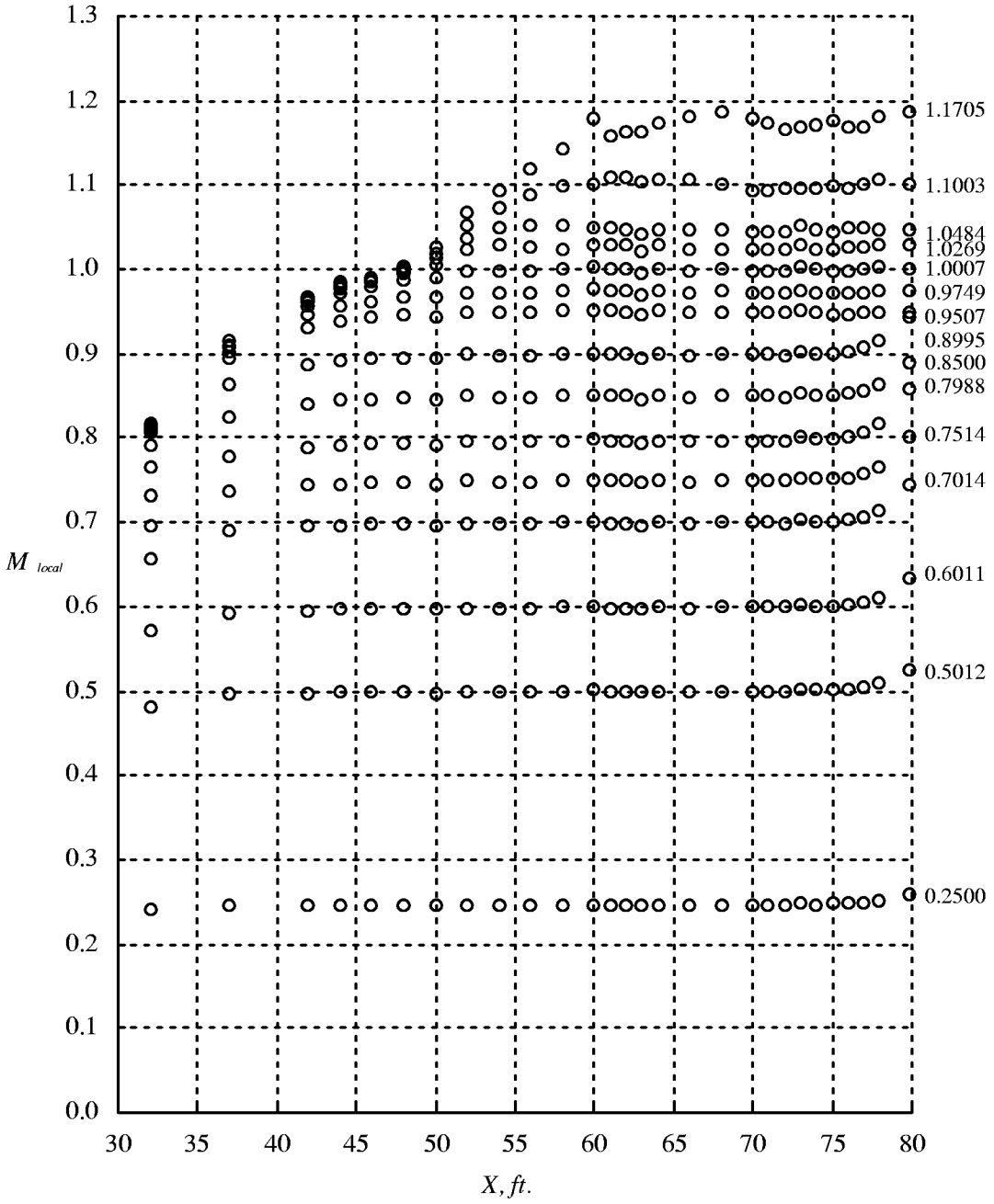

(d) Test section floor M_{local} distributions.

Figure 8. Concluded.

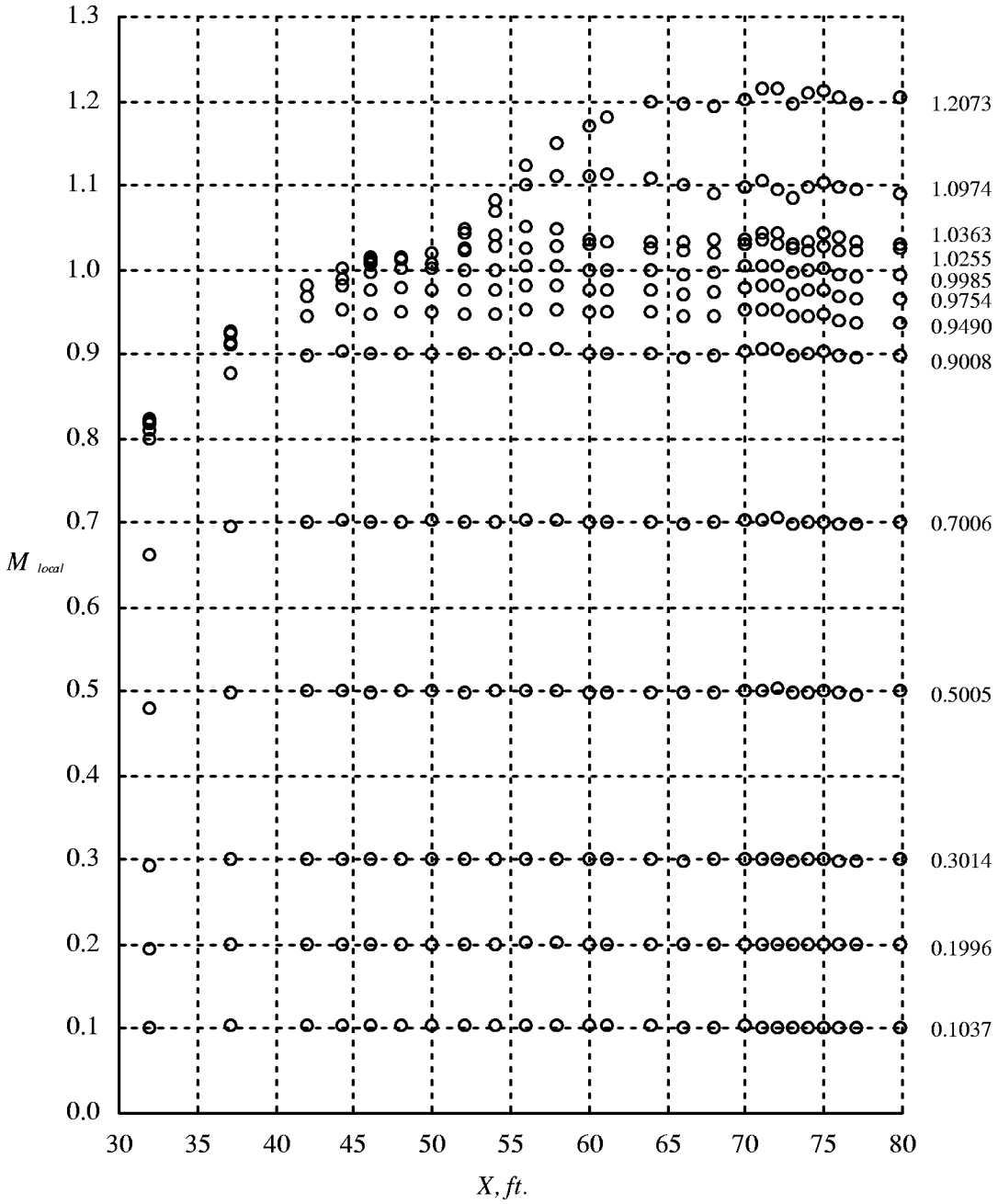

(a) Test section east wall M_{local} distributions.

Figure 9. Mach number distribution of test section in R-134a; 700 psf $\leq P_{t,\infty} \leq$ 900 psf and re-entry flaps set to scheduled position.

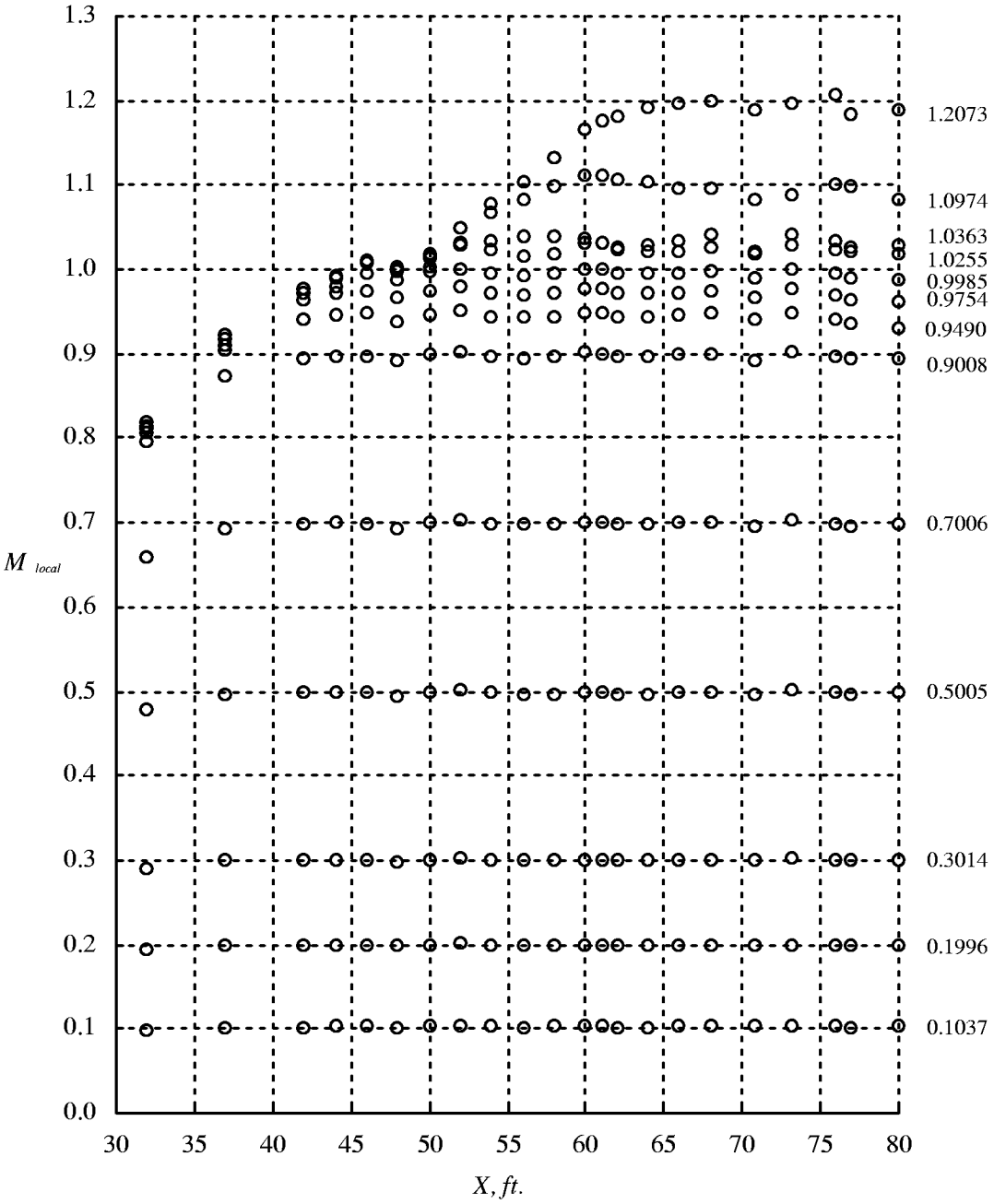

(b) Test section west wall M_{local} distributions.
Figure 9. Continued.

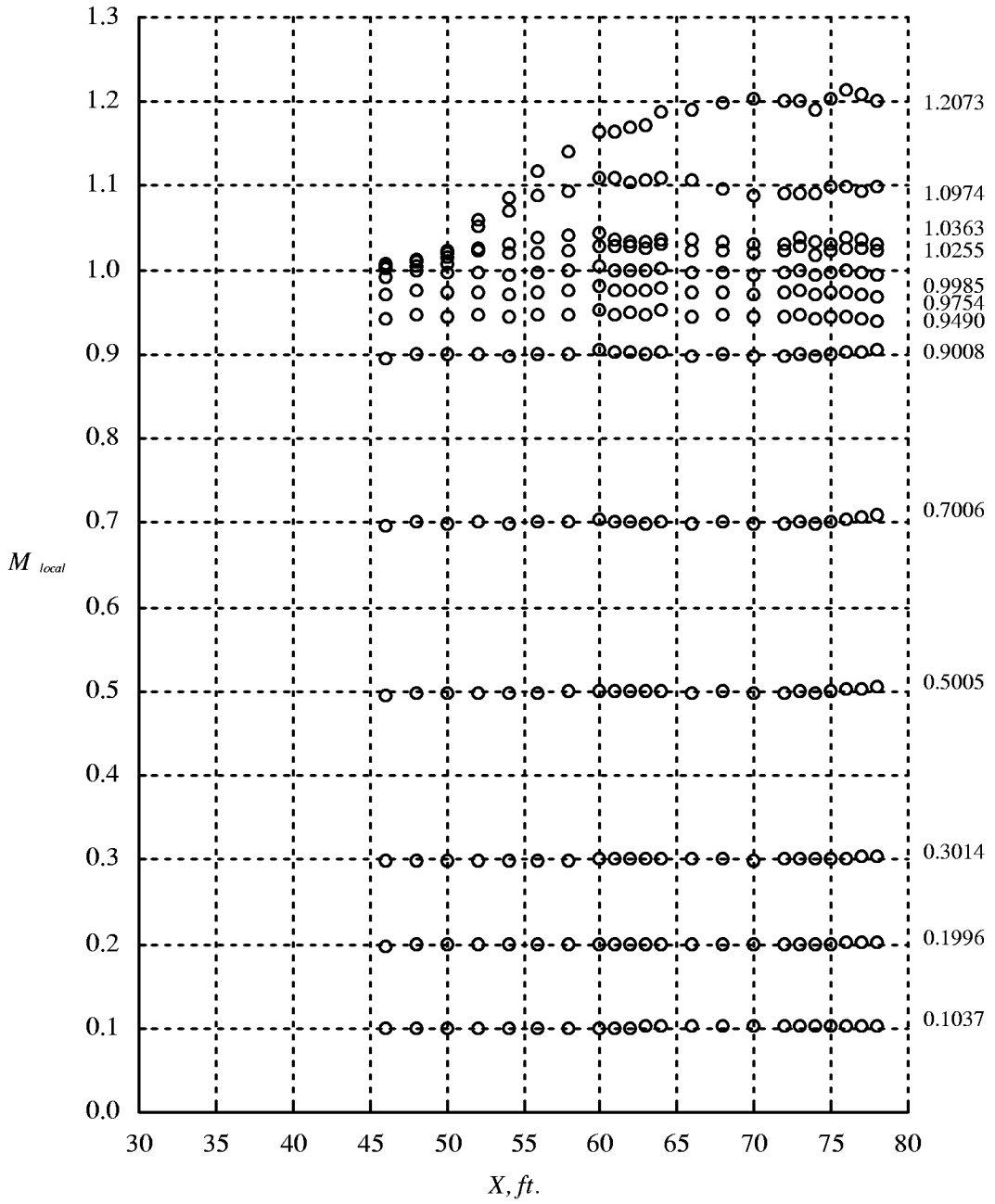

(b) Test section ceiling M_{local} distributions.
Figure 9. Continued.

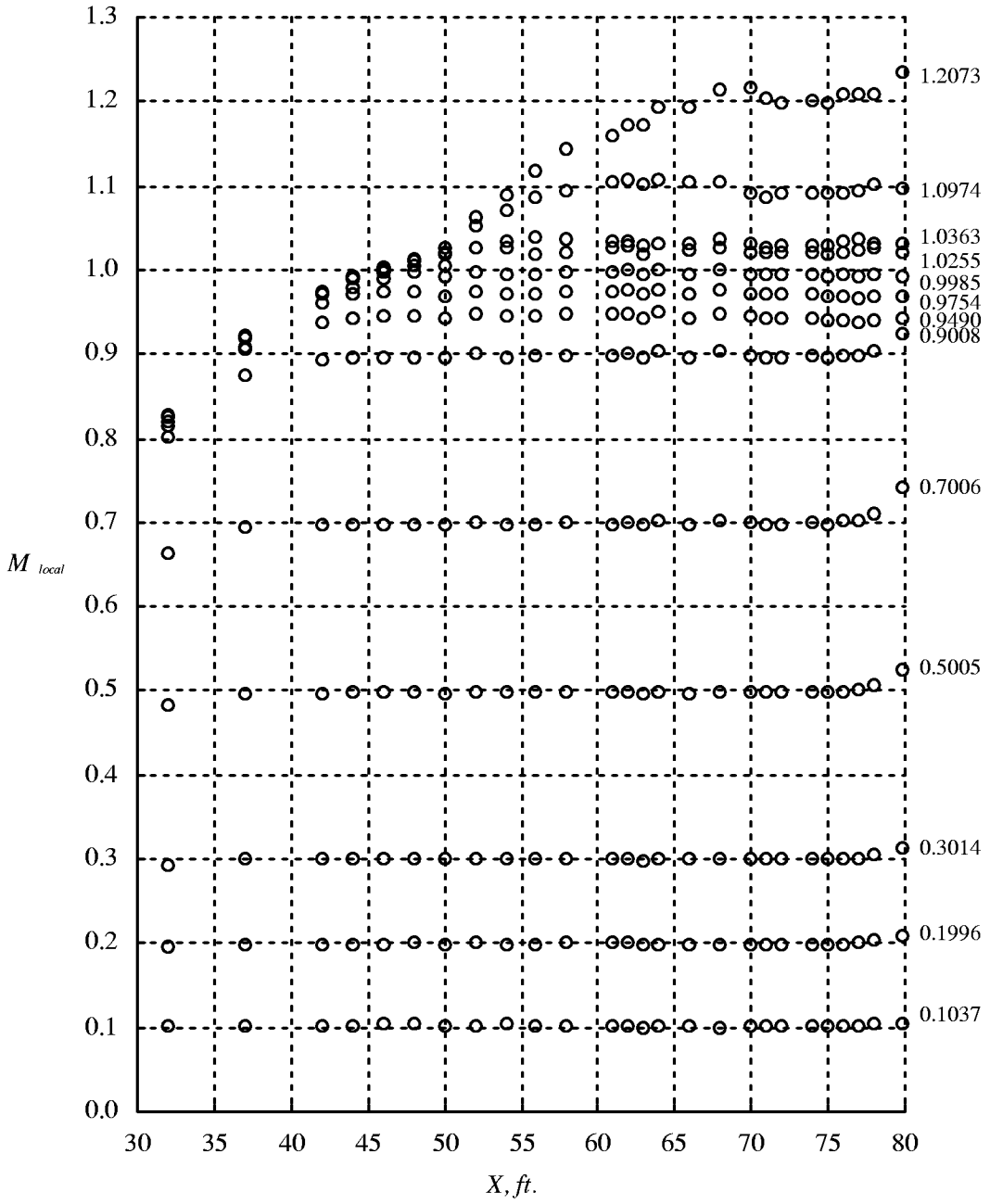

(b) Test section floor M_{local} distributions.
Figure 9. Concluded.

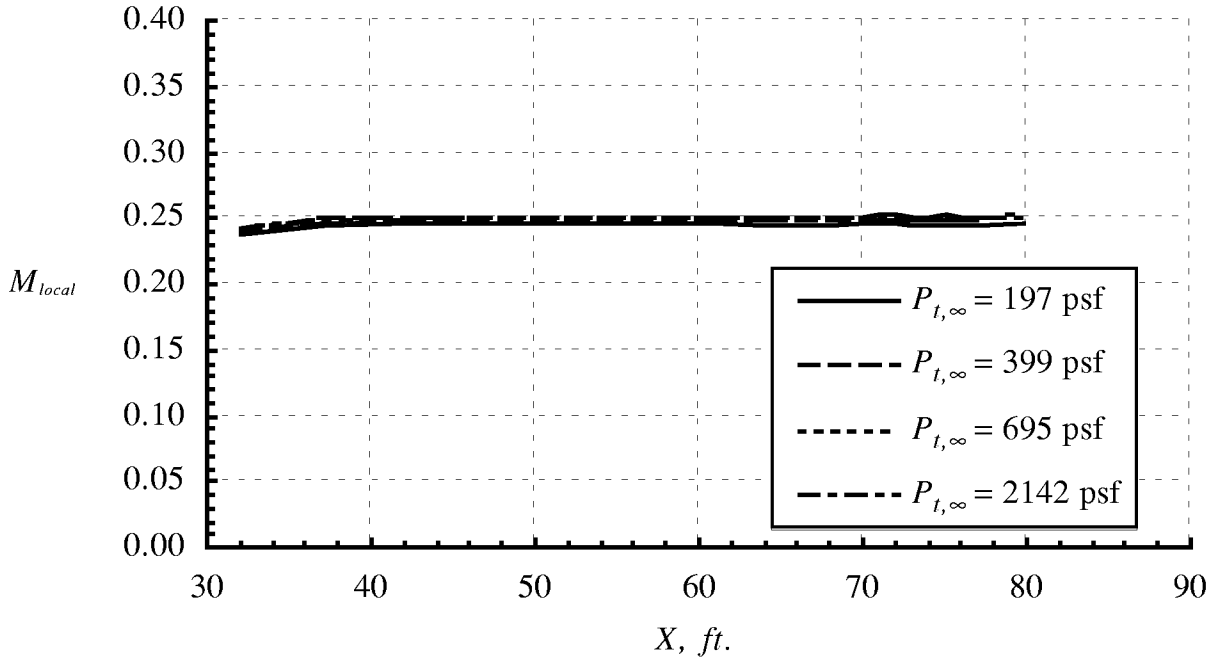

(a) Effect of $P_{t,\infty}$ at $M_\infty \approx 0.25$.

Figure 10. Variation in Mach number distribution on the east wall of the test section in air due to $P_{t,\infty}$; re-entry flaps set to scheduled position.

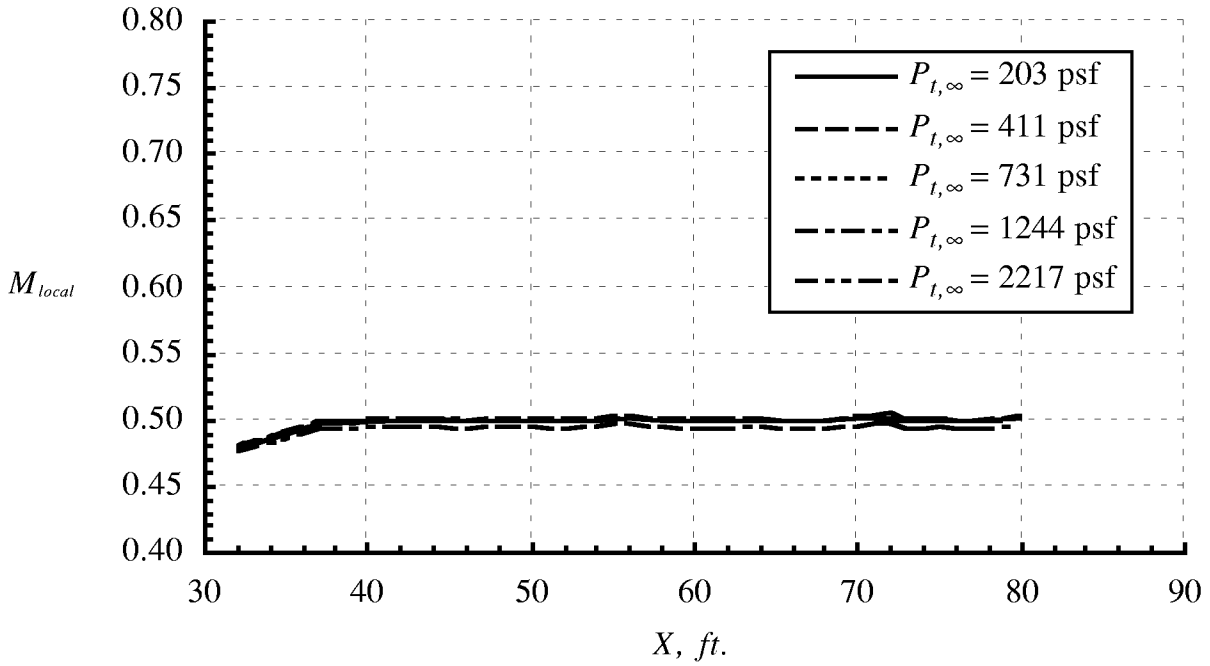

(b) Effect of $P_{t,\infty}$ at $M_\infty \approx 0.50$.

Figure 10. Continued.

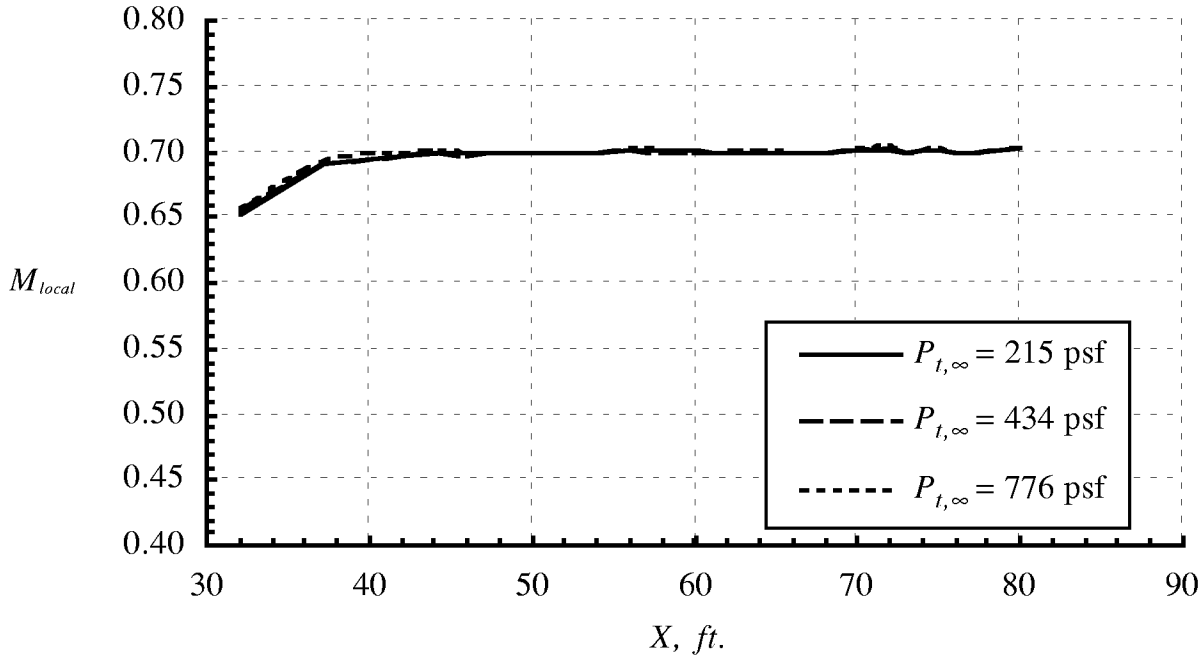

(c) Effect of $P_{t,\infty}$ at $M_\infty \approx 0.70$.
Figure 10. Continued.

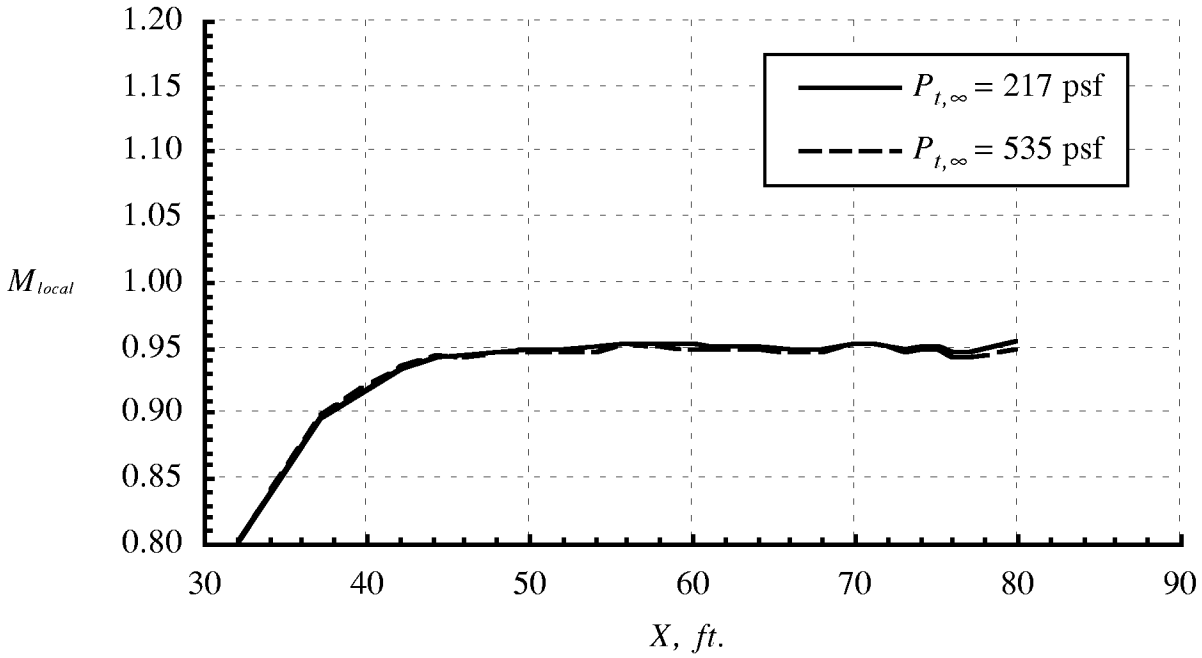

(d) Effect of $P_{t,\infty}$ at $M_\infty \approx 0.95$.
Figure 10. Continued.

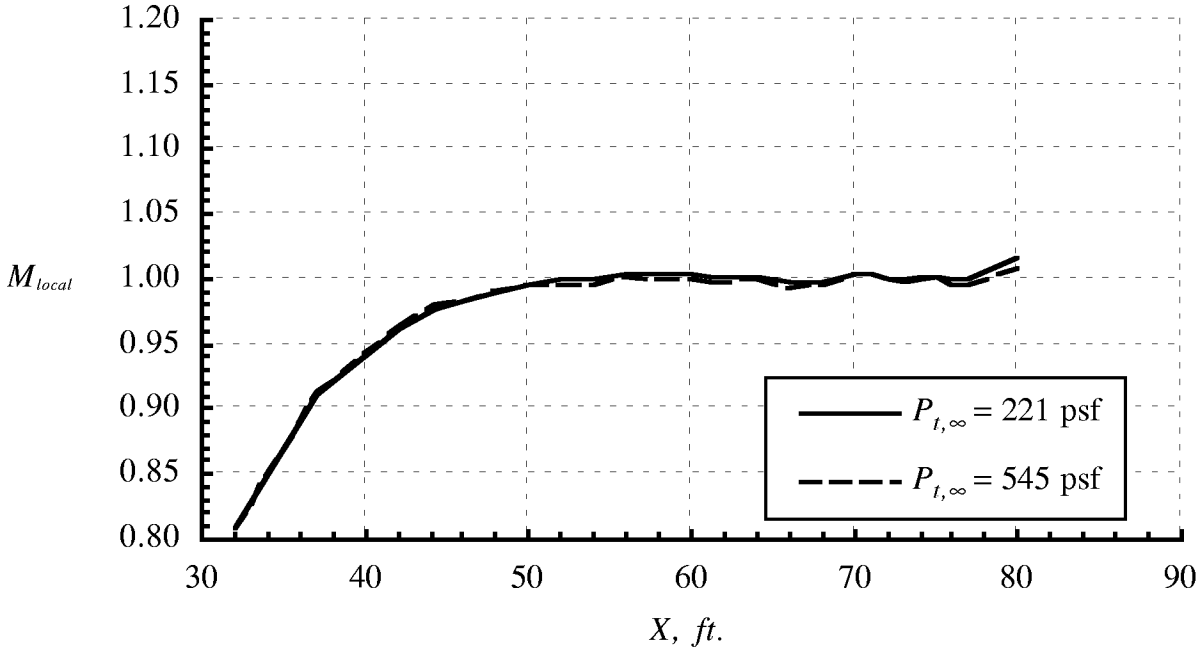

(e) Effect of $P_{t,\infty}$ at $M_\infty \approx 1.00$.

Figure 10. Concluded.

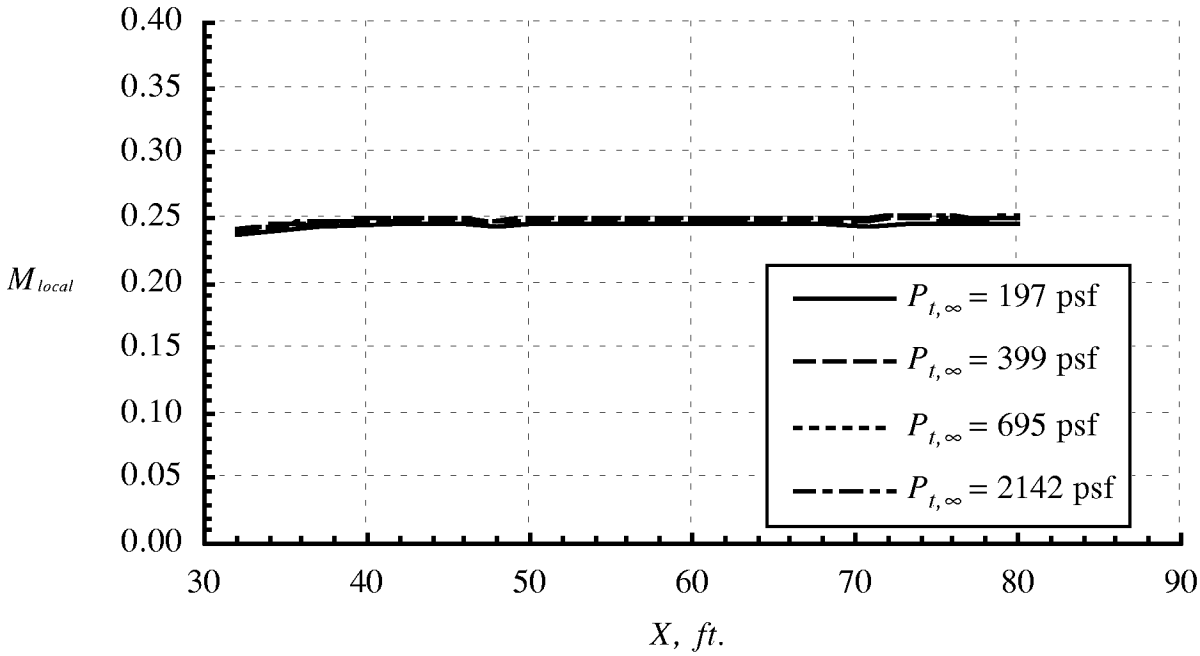

(a) Effect of $P_{t,\infty}$ at $M_\infty \approx 0.25$.

Figure 11. Variation in Mach number distribution on the west wall of the test section in air due to $P_{t,\infty}$; re-entry flaps set to scheduled position.

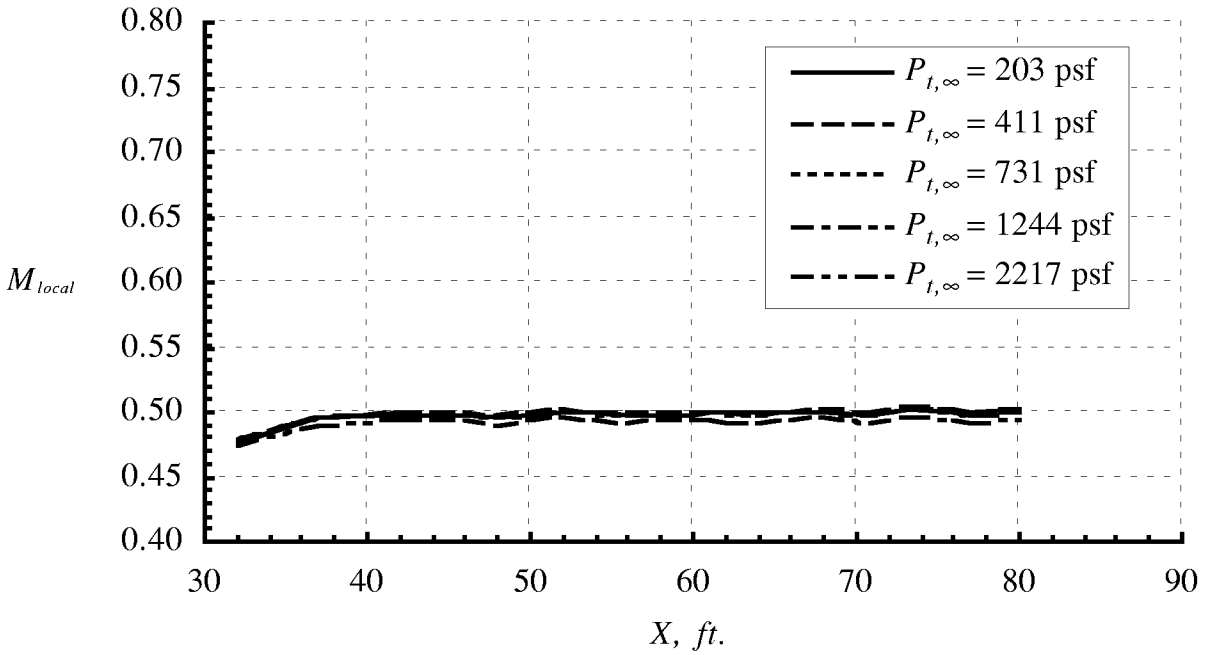

(b) Effect of $P_{t,\infty}$ at $M_\infty \approx 0.50$.
Figure 11. Continued.

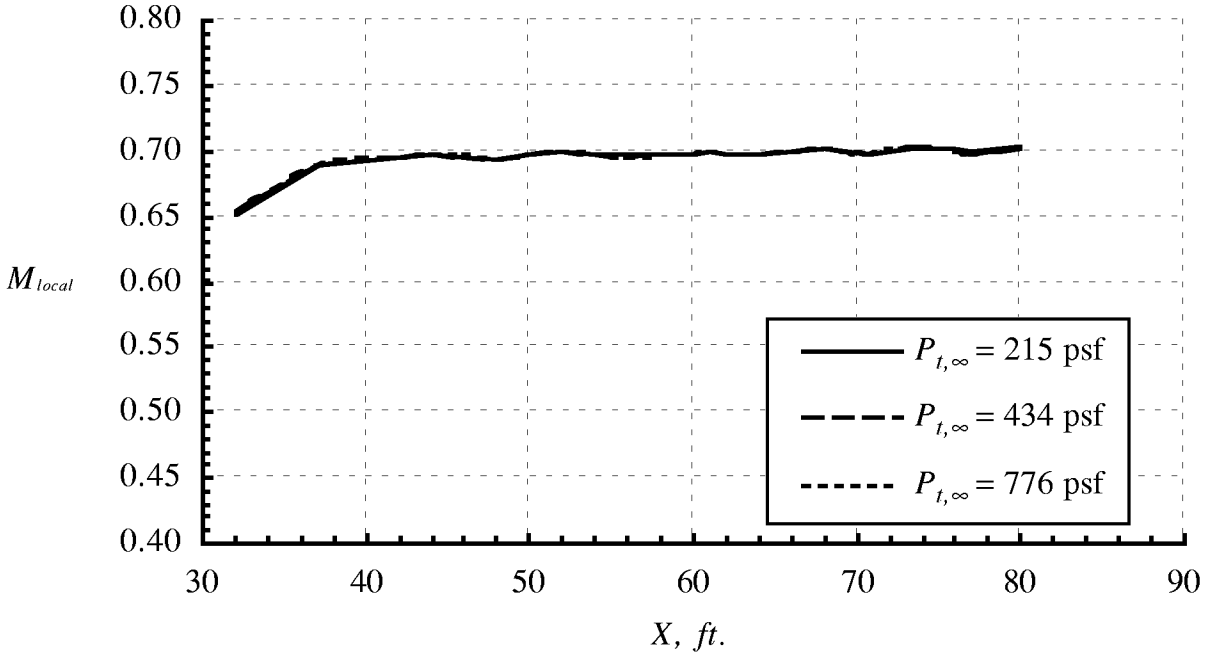

(c) Effect of $P_{t,\infty}$ at $M_\infty \approx 0.70$.
Figure 11. Continued.

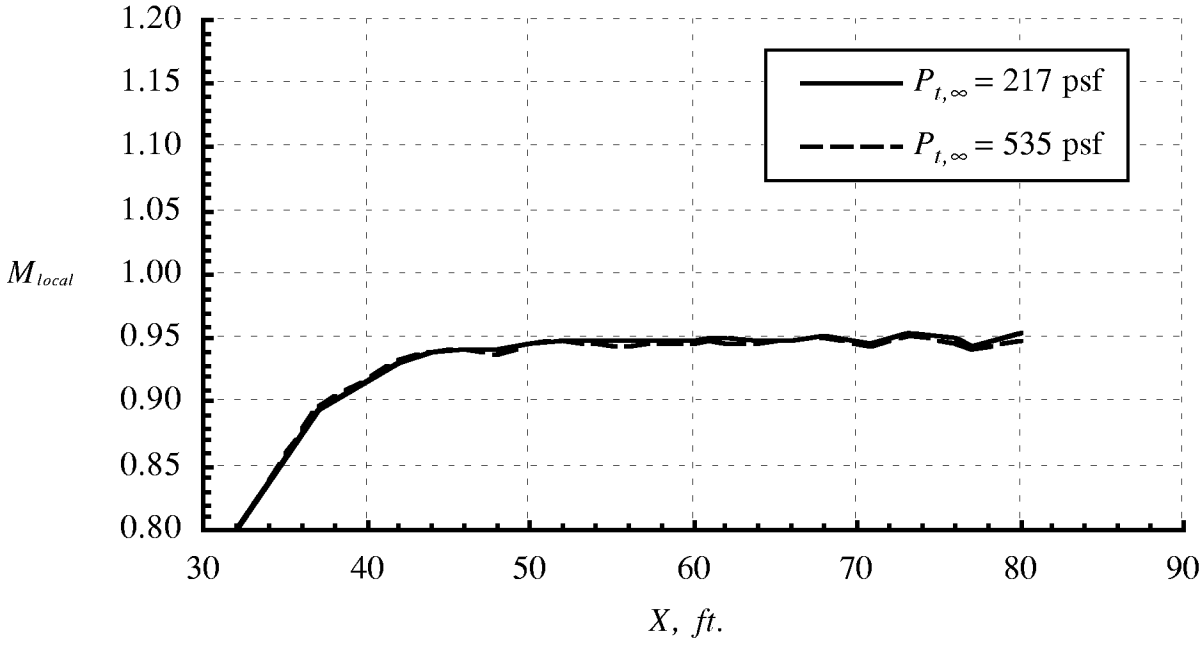

(d) Effect of $P_{t,\infty}$ at $M_\infty \approx 0.95$.
Figure 11. Continued.

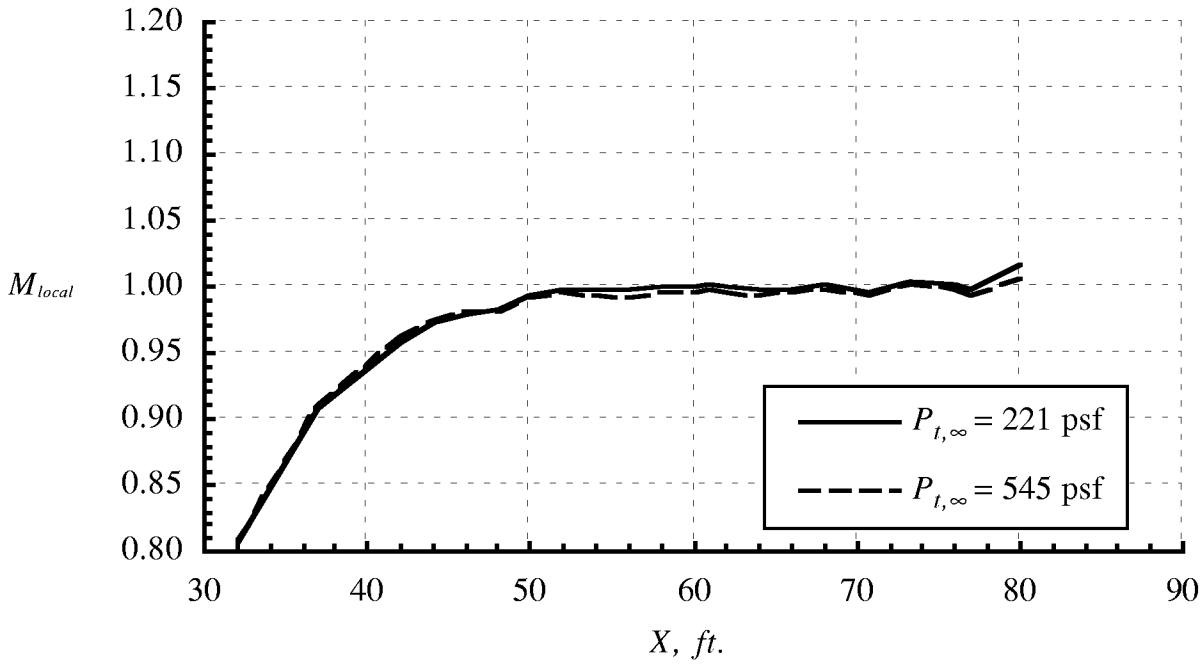

(e) Effect of $P_{t,\infty}$ at $M_\infty \approx 1.00$.
Figure 11. Concluded.

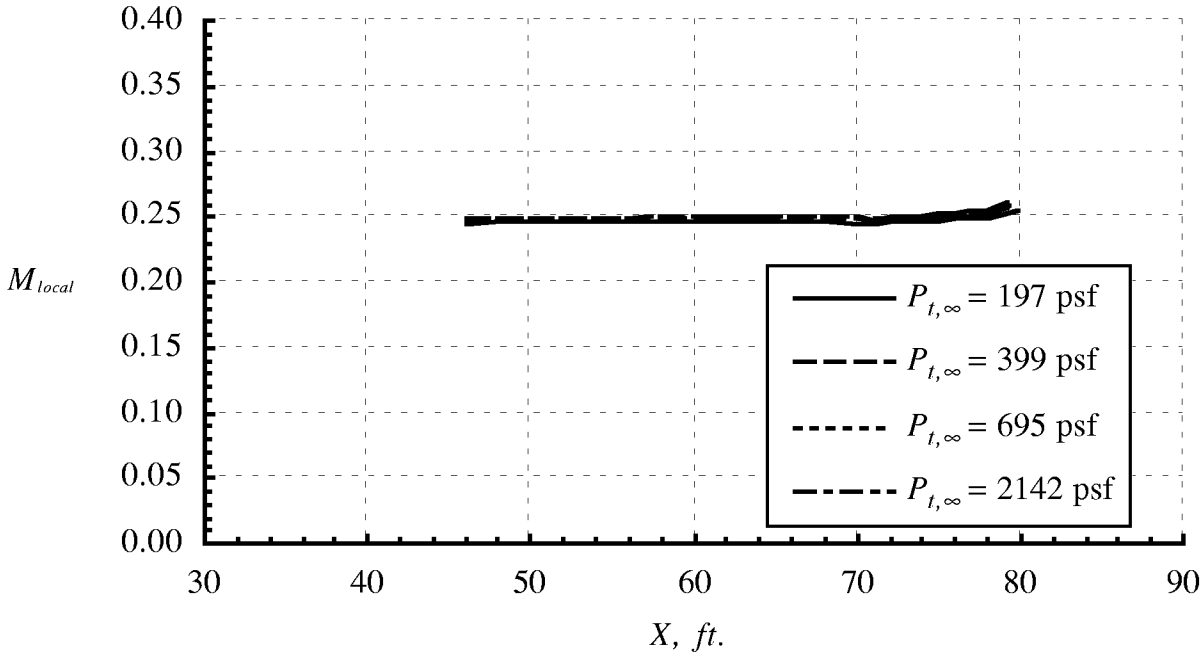

(a) Effect of $P_{t,\infty}$ at $M_\infty \approx 0.25$.

Figure 12. Variation in Mach number distribution on the ceiling of the test section in air due to $P_{t,\infty}$; re-entry flaps set to scheduled position.

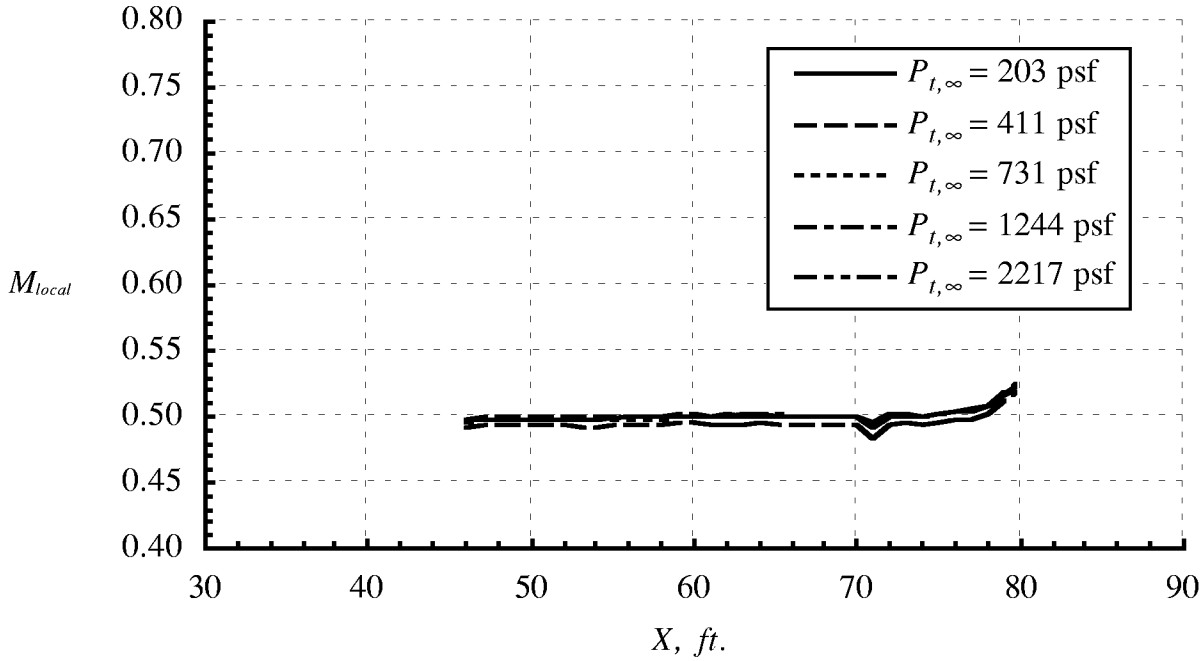

(b) Effect of $P_{t,\infty}$ at $M_\infty \approx 0.50$.

Figure 12. Continued.

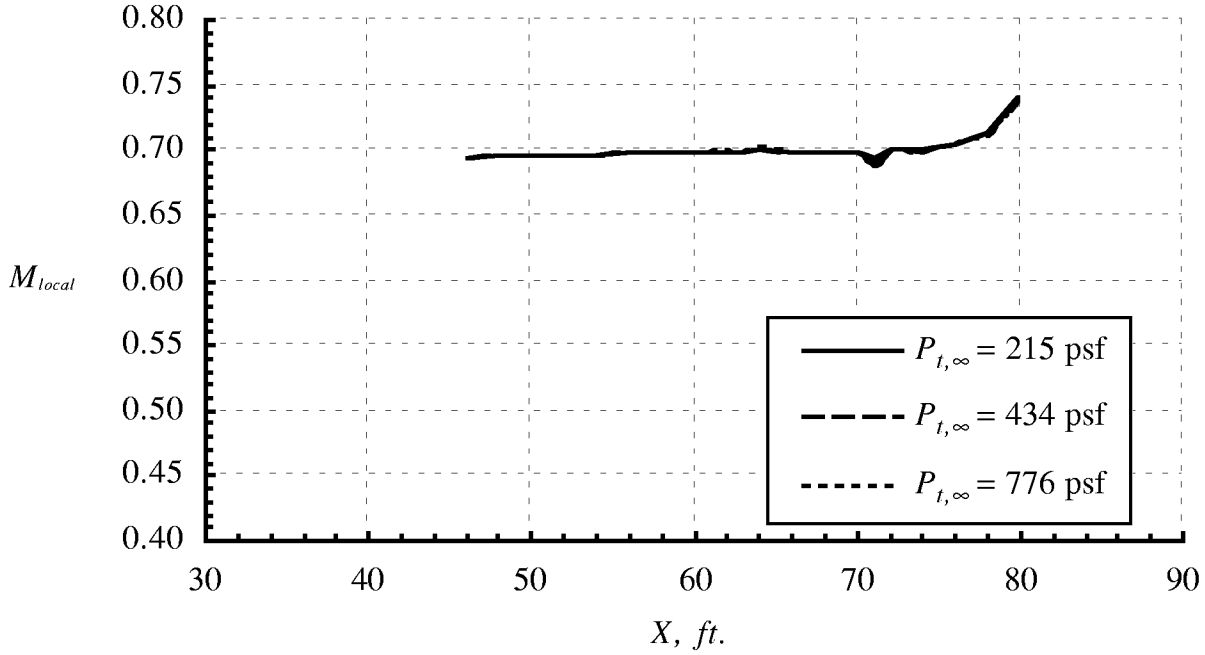

(c) Effect of $P_{t,\infty}$ at $M_\infty \approx 0.70$.
Figure 12. Continued.

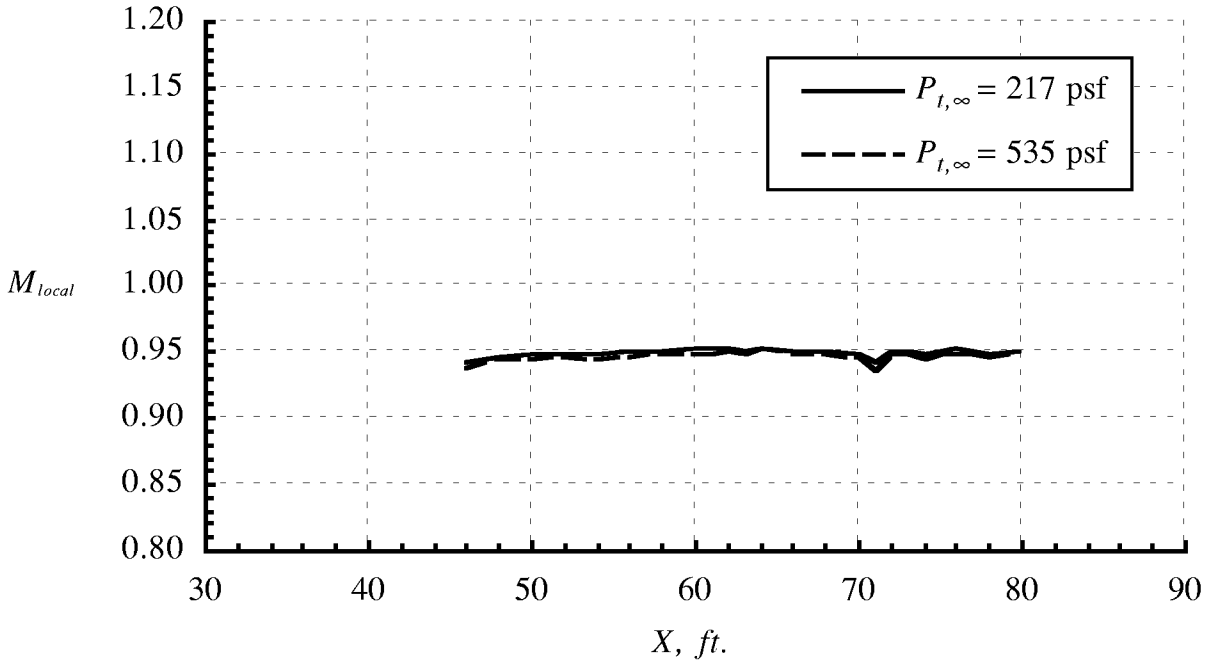

(d) Effect of $P_{t,\infty}$ at $M_\infty \approx 0.95$.
Figure 12. Continued.

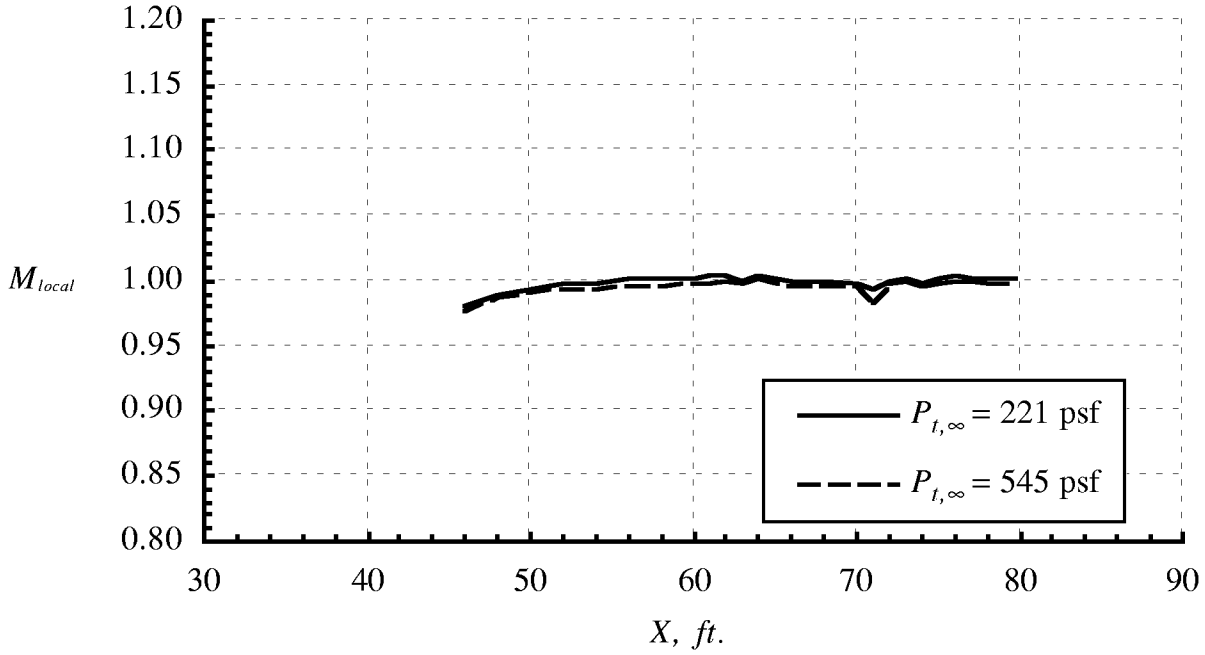

(e) Effect of $P_{t,\infty}$ at $M_\infty \approx 1.00$.

Figure 12. Concluded.

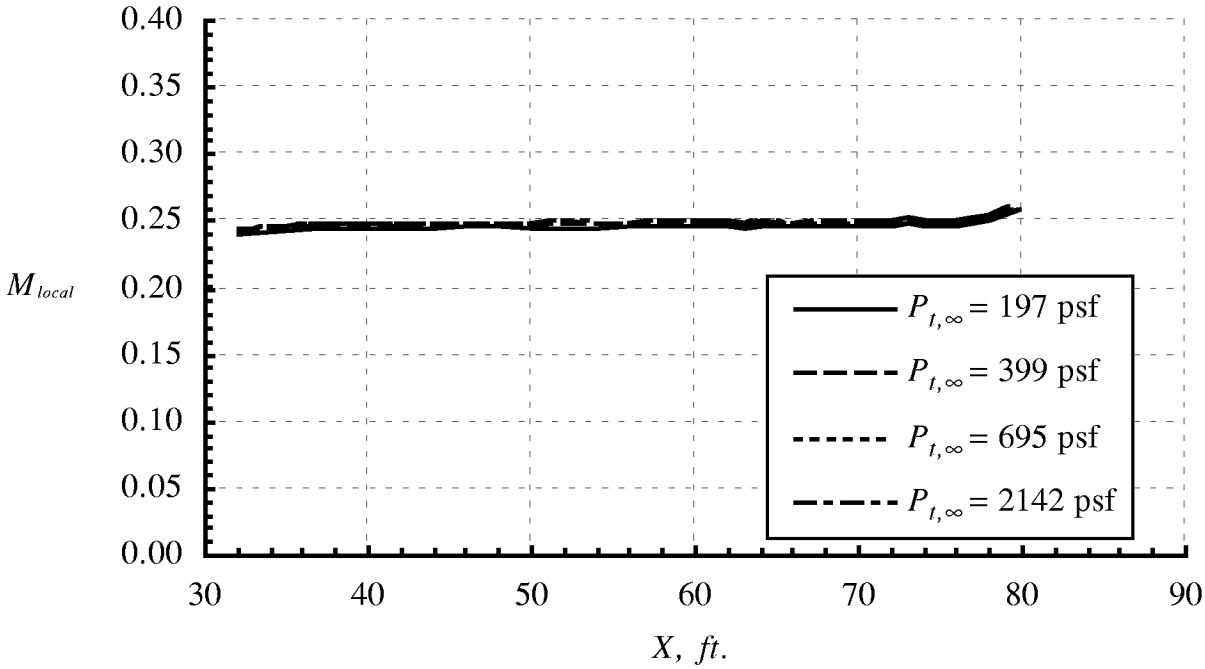

(a) Effect of $P_{t,\infty}$ at $M_\infty \approx 0.25$.

Figure 13. Variation in Mach number distribution on the floor of the test section in air due to $P_{t,\infty}$; re-entry flaps set to scheduled position.

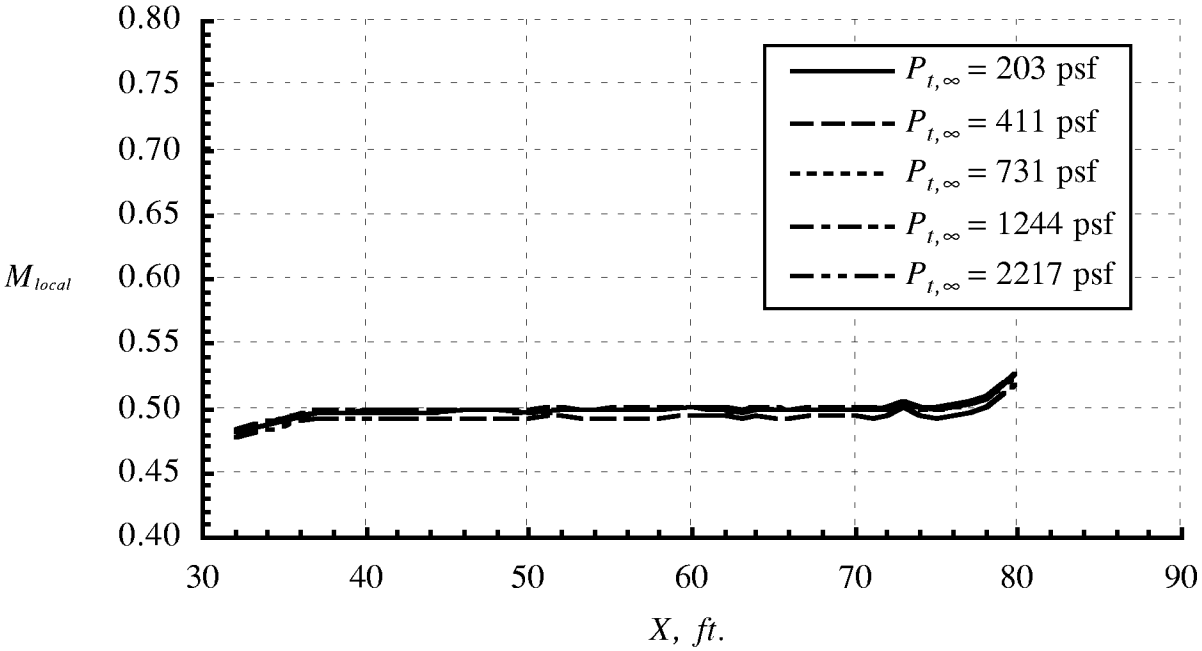

(b) Effect of $P_{t,\infty}$ at $M_\infty \approx 0.50$.
Figure 13. Continued.

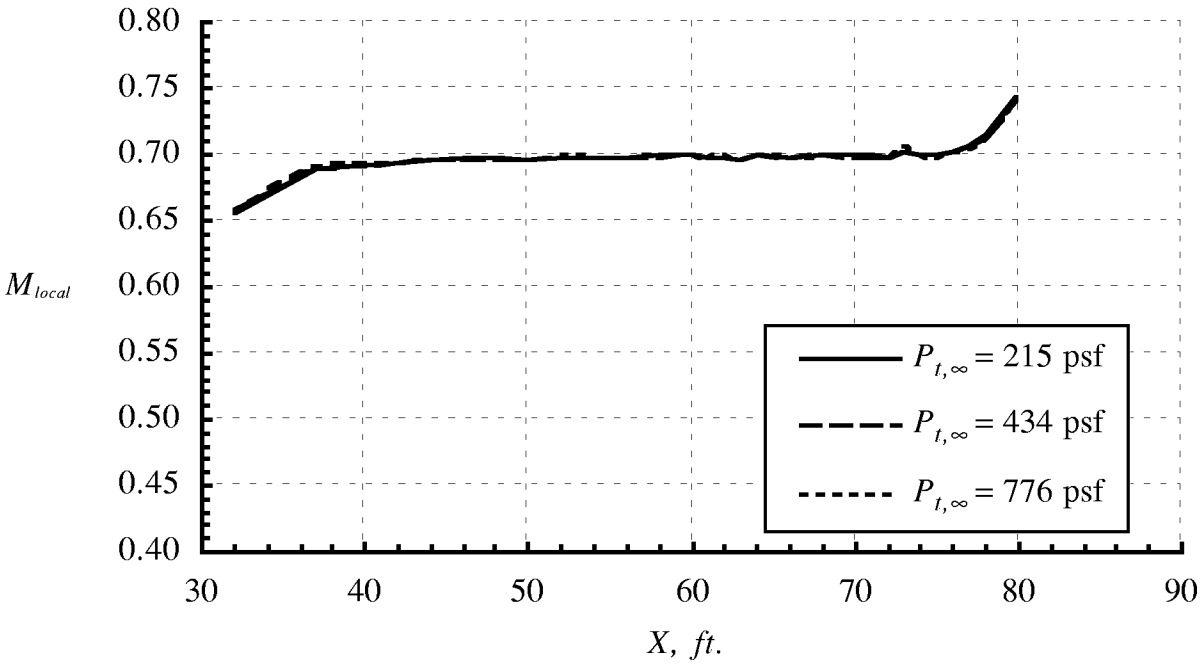

(c) Effect of $P_{t,\infty}$ at $M_\infty \approx 0.70$.
Figure 13. Continued.

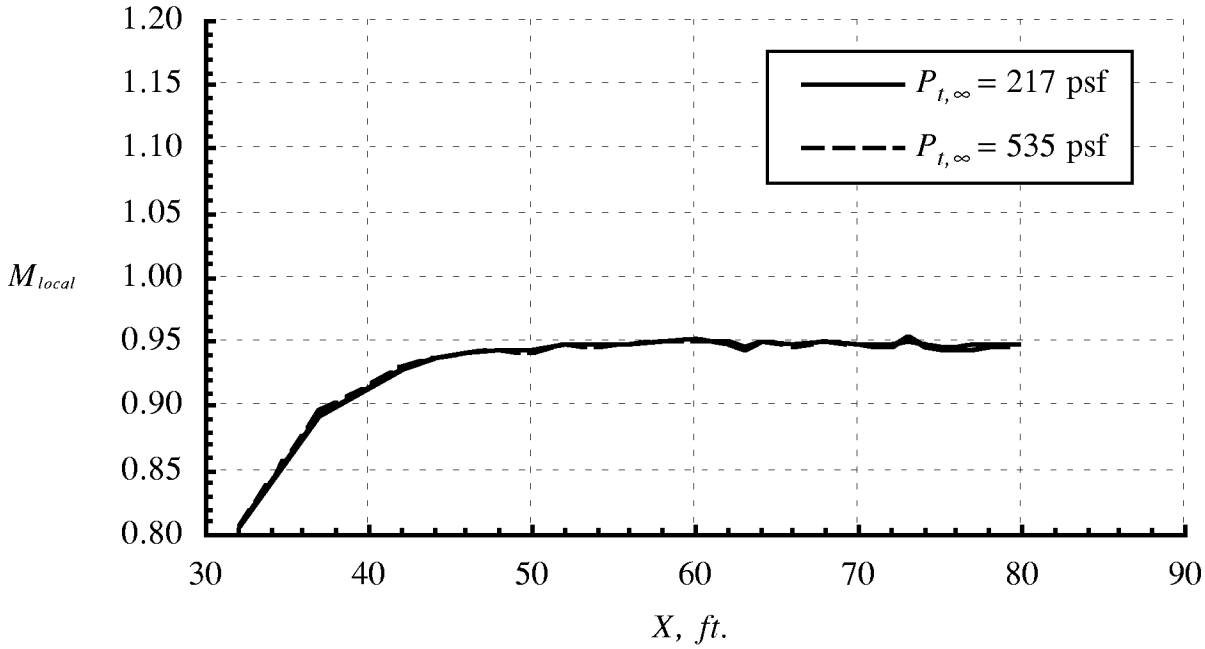

(d) Effect of $P_{t,\infty}$ at $M_\infty \approx 0.95$.
Figure 13. Continued.

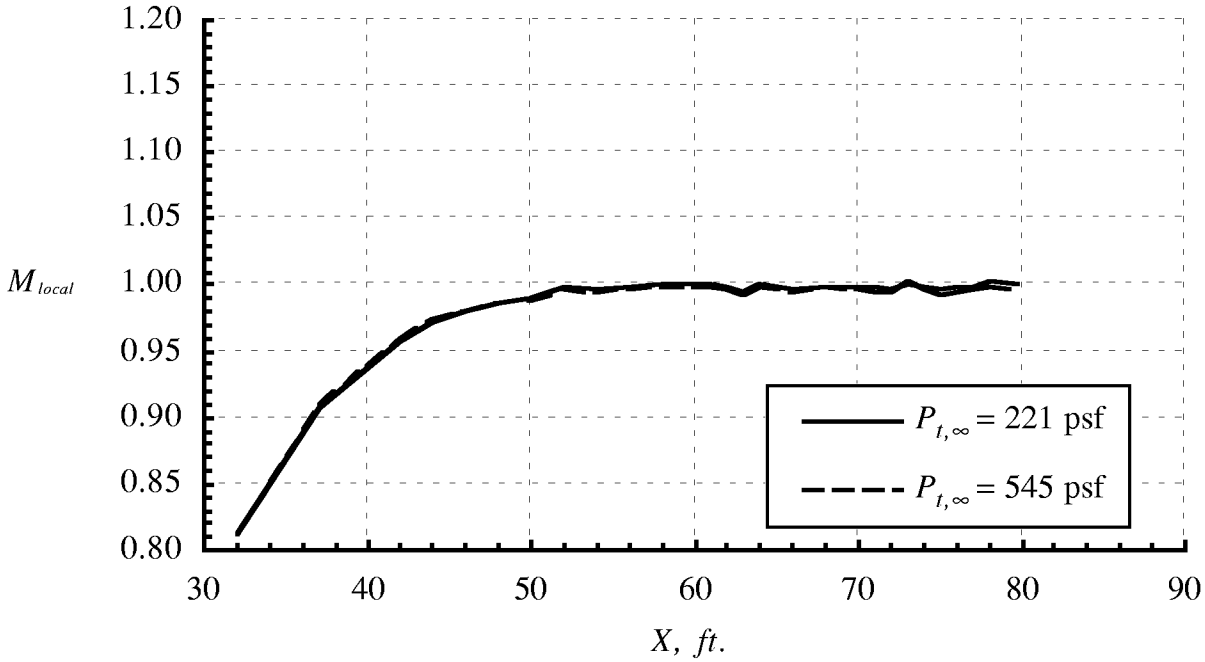

(e) Effect of $P_{t,\infty}$ at $M_\infty \approx 1.00$.
Figure 13. Concluded.

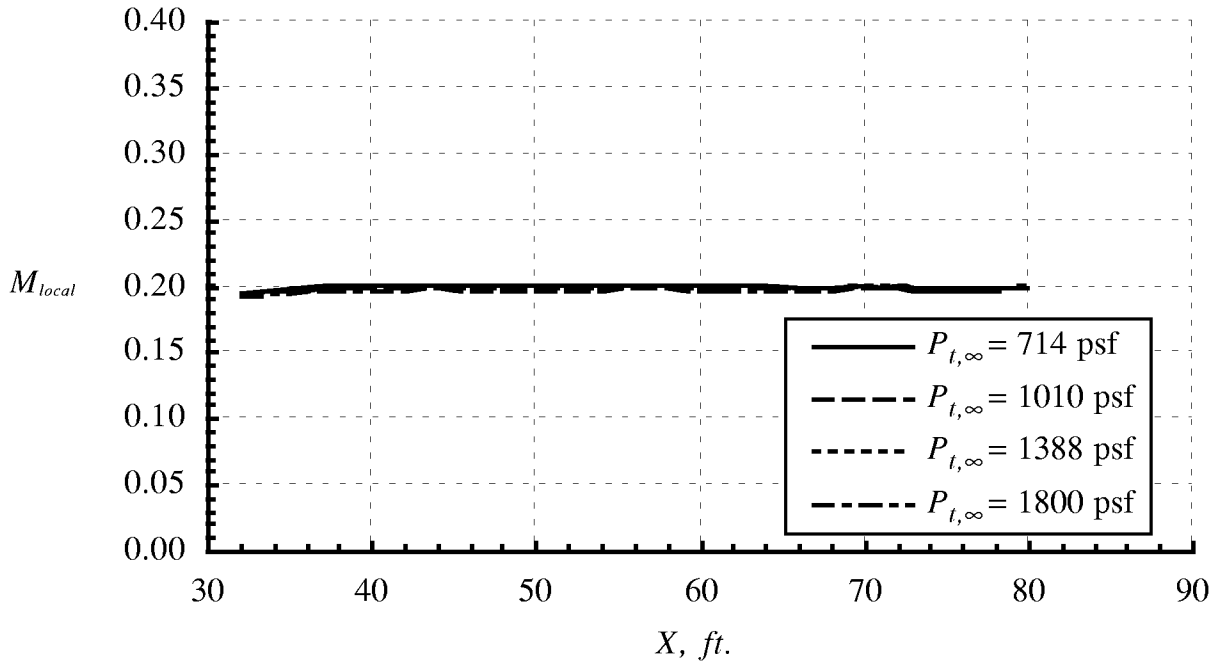

(a) Effect of $P_{t,\infty}$ at $M_\infty \approx 0.20$.

Figure 14. Variation in Mach number distribution on the test section east wall in R-134a due to $P_{t,\infty}$; re-entry flaps set to scheduled position.

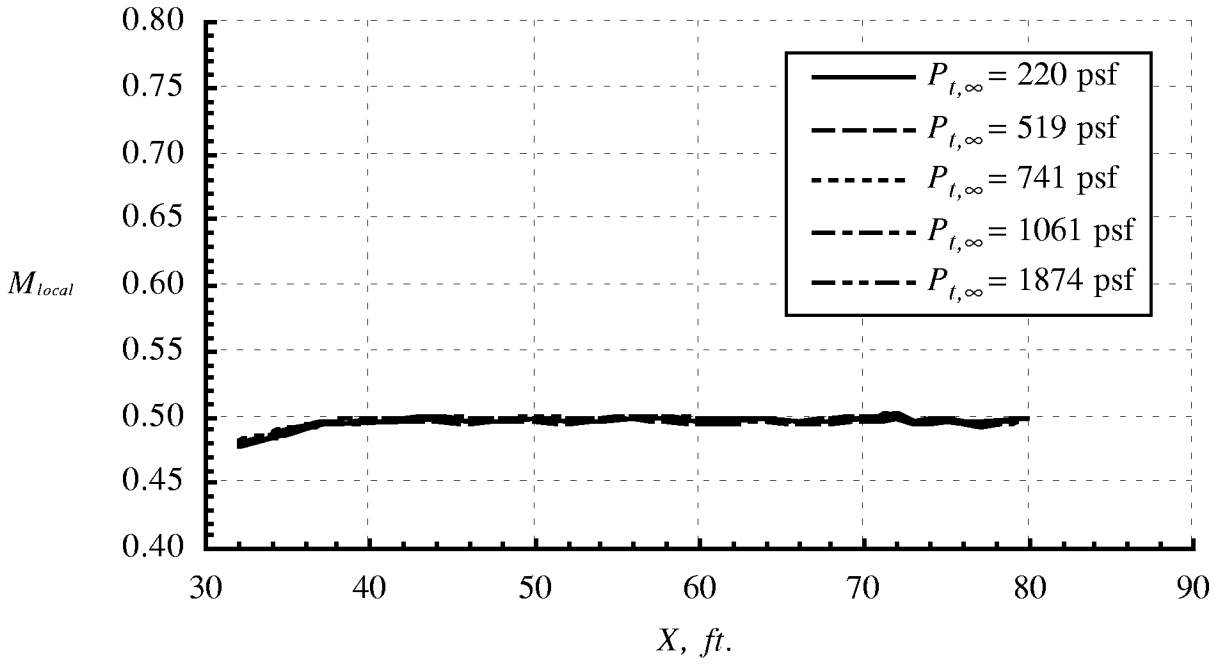

(b) Effect of $P_{t,\infty}$ at $M_\infty \approx 0.50$.

Figure 14. Continued.

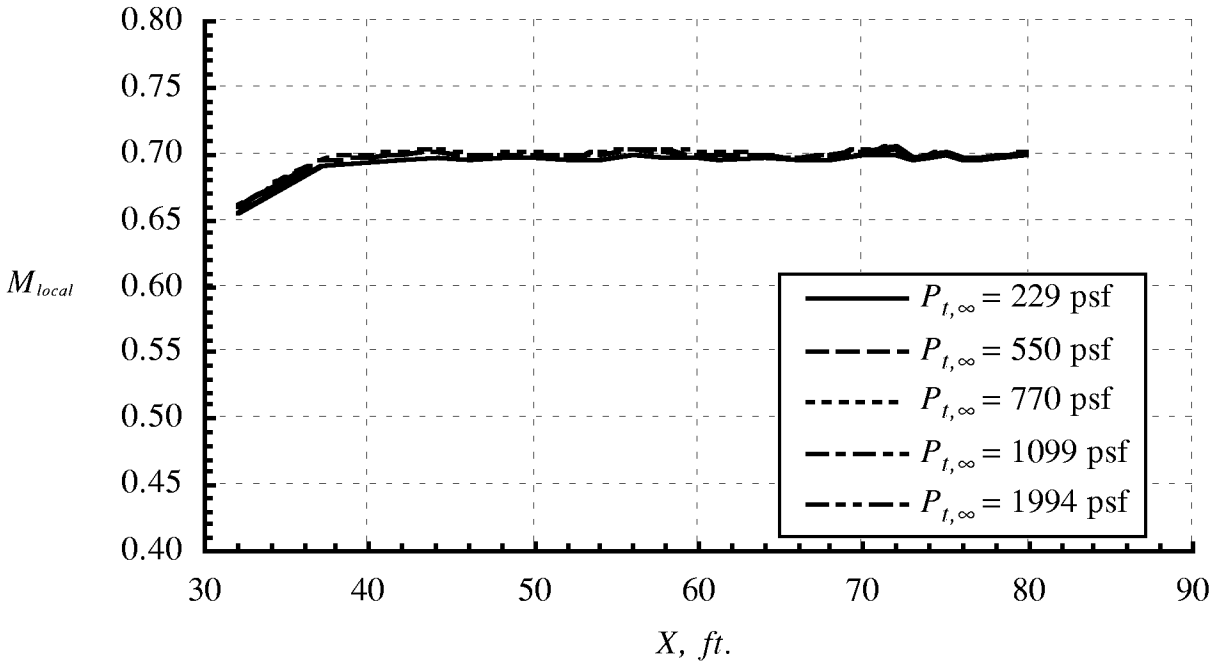

(c) Effect of $P_{t,\infty}$ at $M_\infty \approx 0.70$.
Figure 14. Continued.

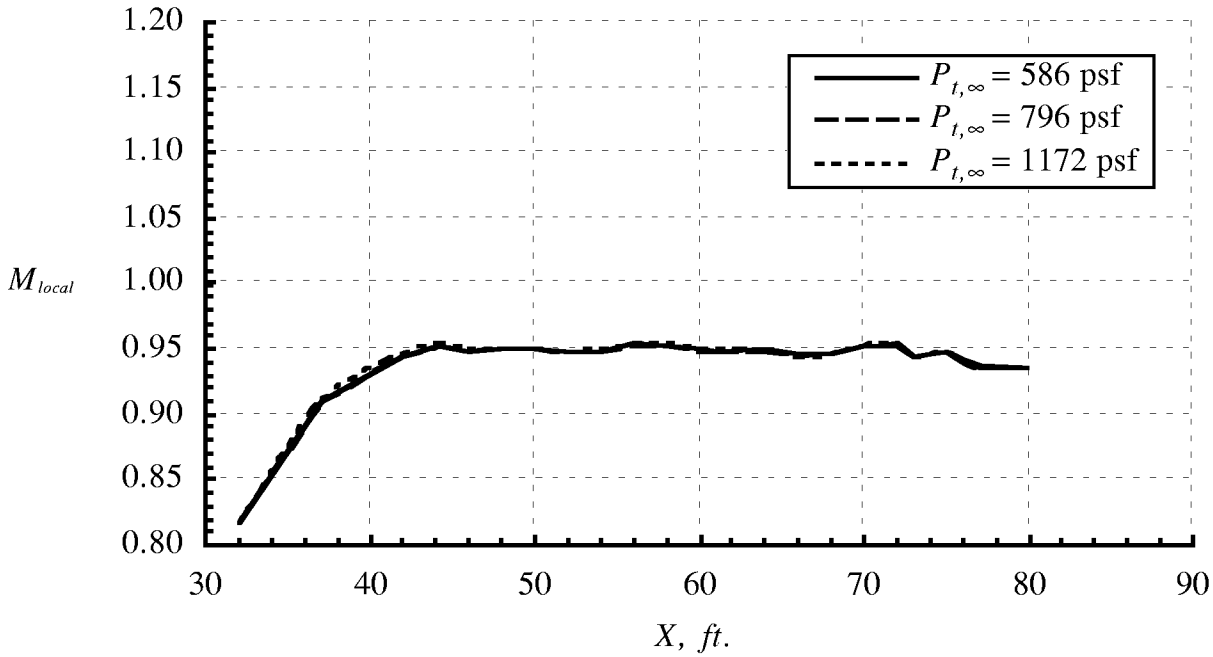

(d) Effect of $P_{t,\infty}$ at $M_\infty \approx 0.95$.
Figure 14. Continued.

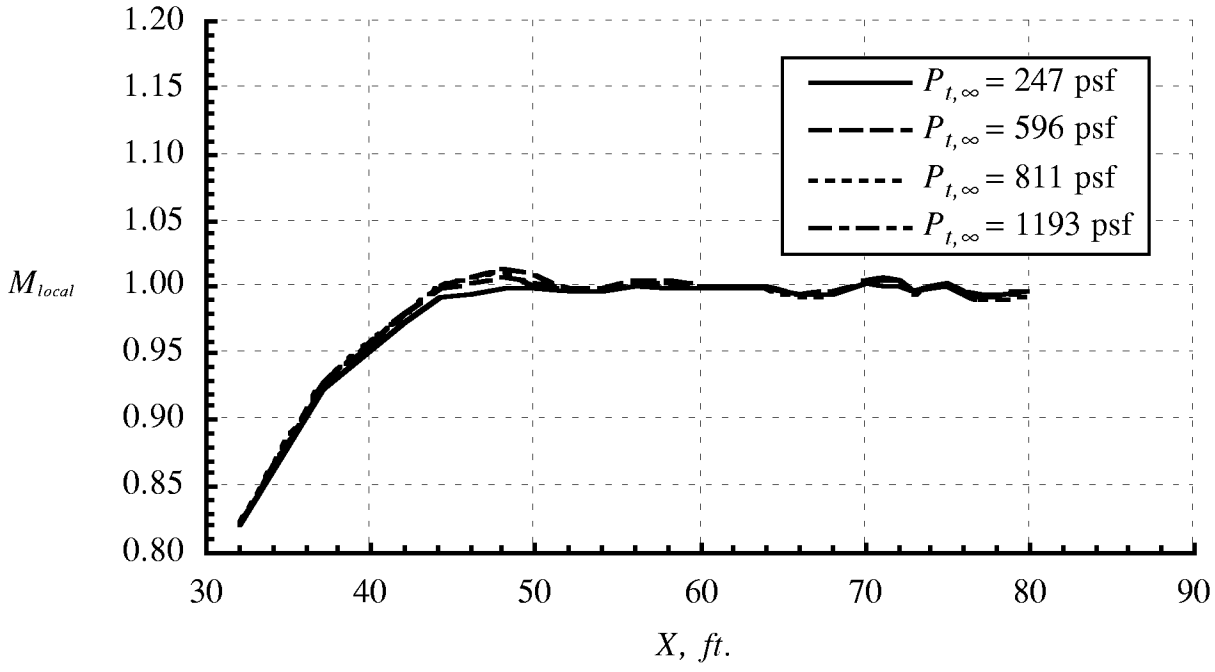

(e) Effect of $P_{t,\infty}$ at $M_\infty \approx 1.00$.
Figure 14. Continued.

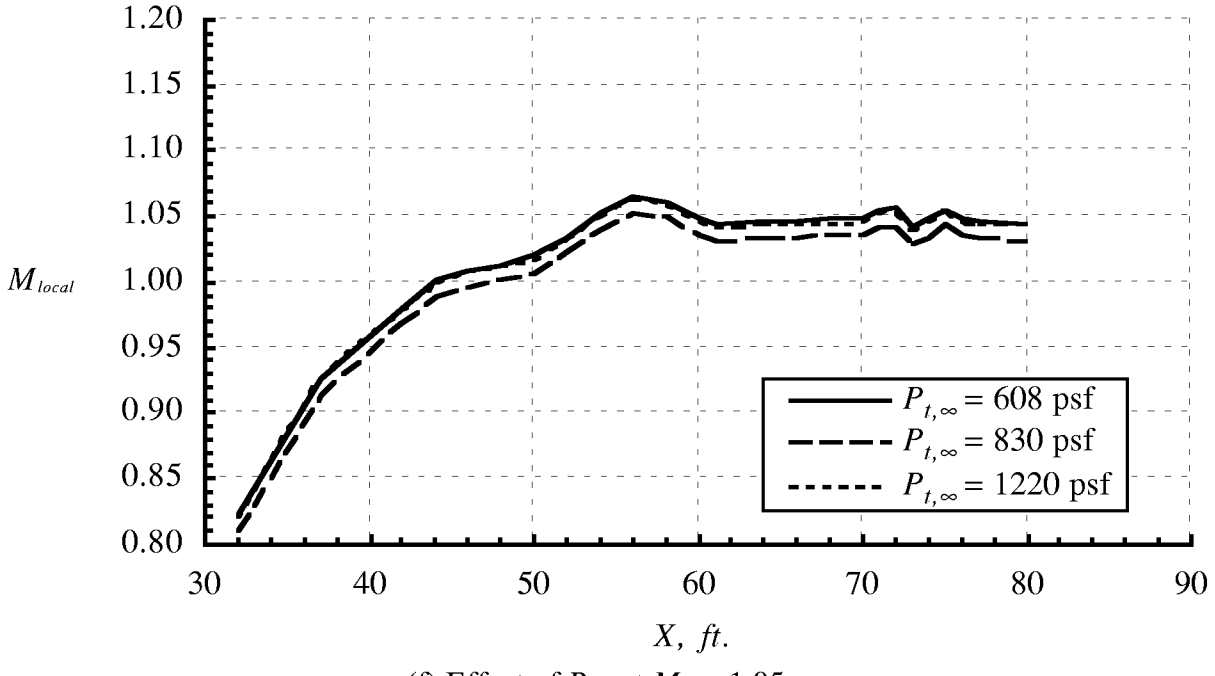

(f) Effect of $P_{t,\infty}$ at $M_\infty \approx 1.05$.
Figure 14. Continued.

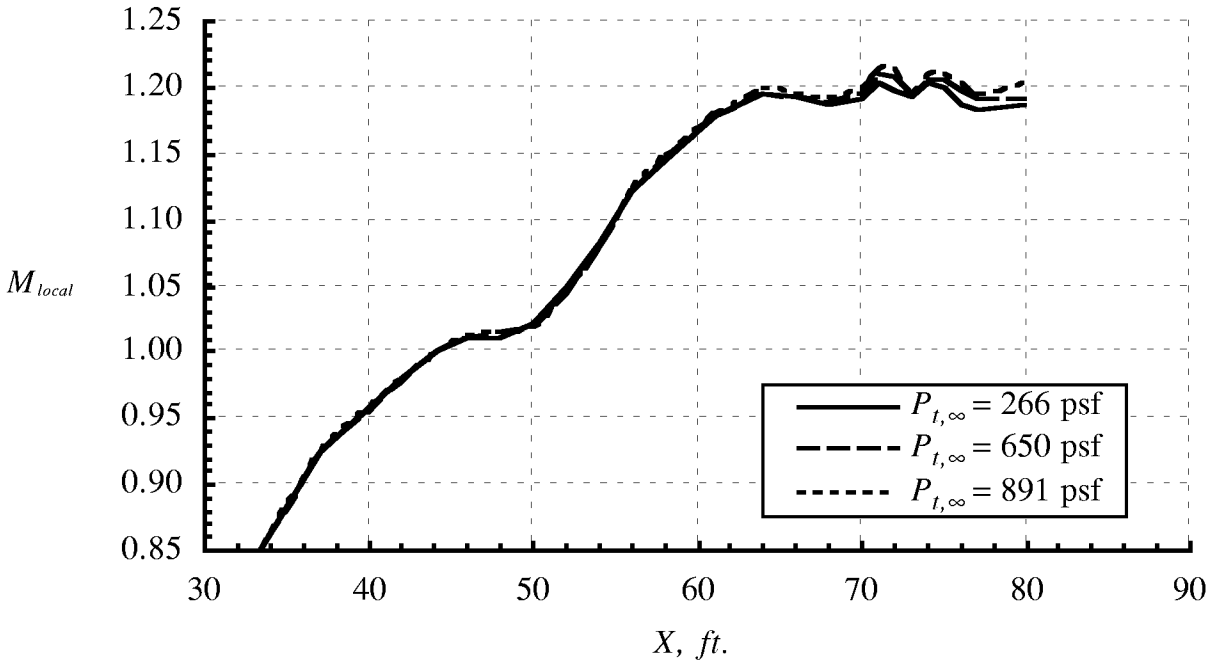

(g) Effect of $P_{t,\infty}$ at $M_\infty \approx 1.20$.

Figure 14. Concluded.

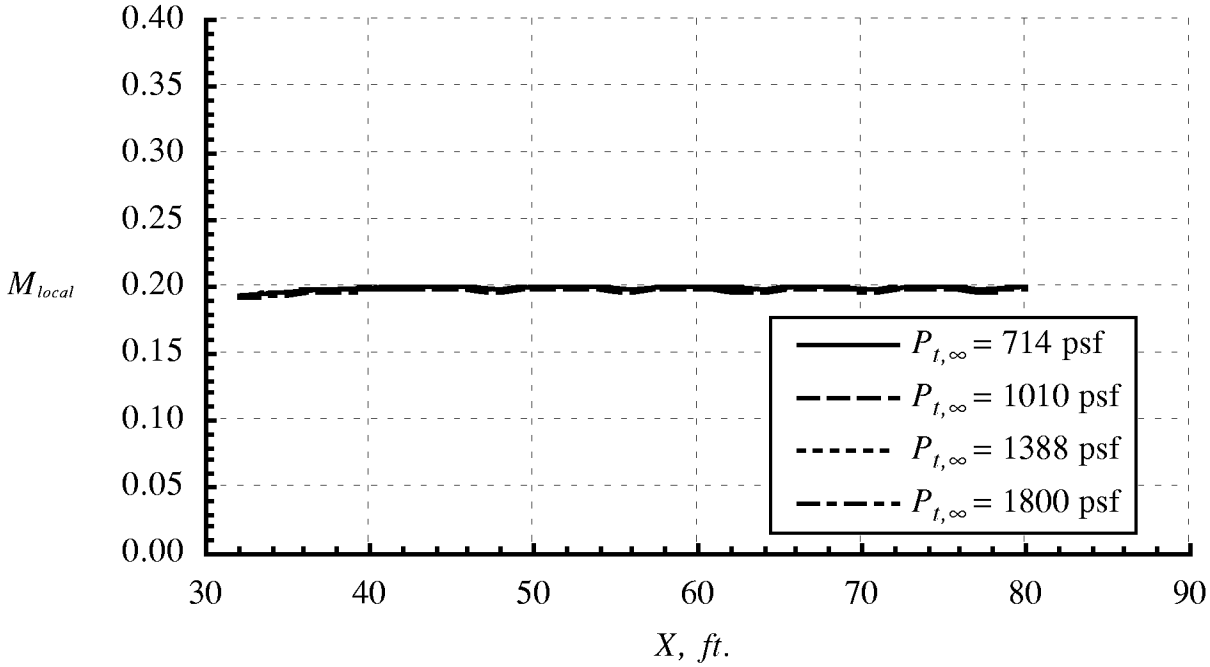

(a) Effect of $P_{t,\infty}$ at $M_\infty \approx 0.20$.

Figure 15. Variation in Mach number distribution on the test section west wall in R-134a due to $P_{t,\infty}$; re-entry flaps set to scheduled position.

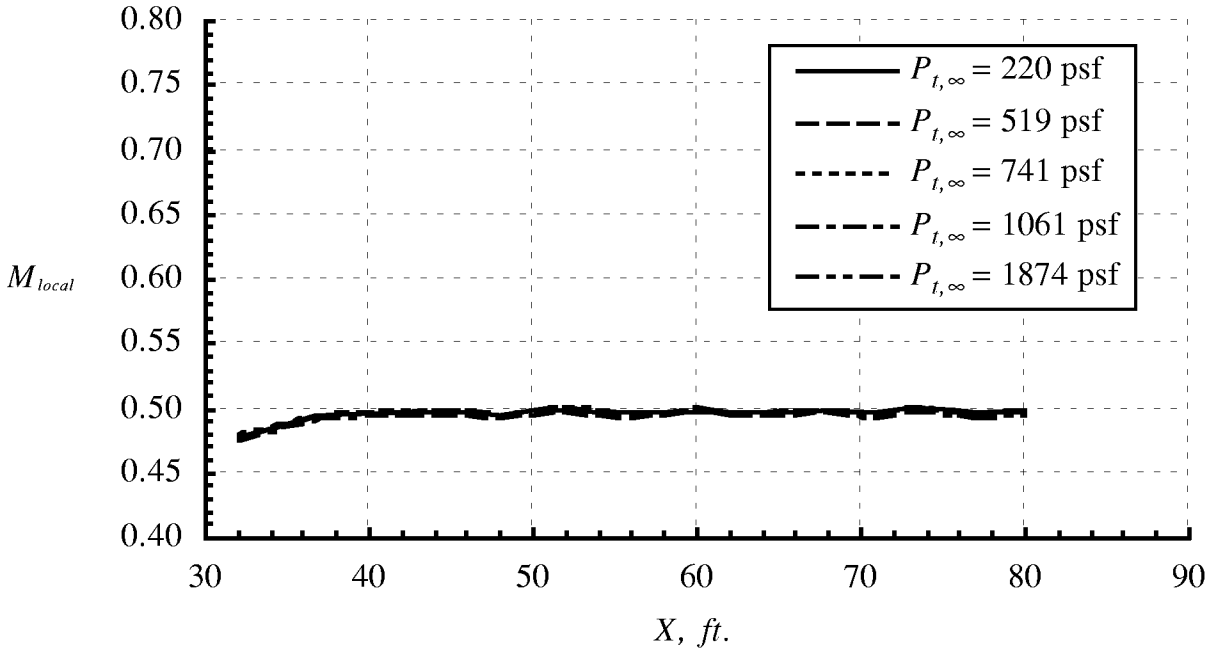

(b) Effect of $P_{t,\infty}$ at $M_\infty \approx 0.50$.
Figure 15. Continued.

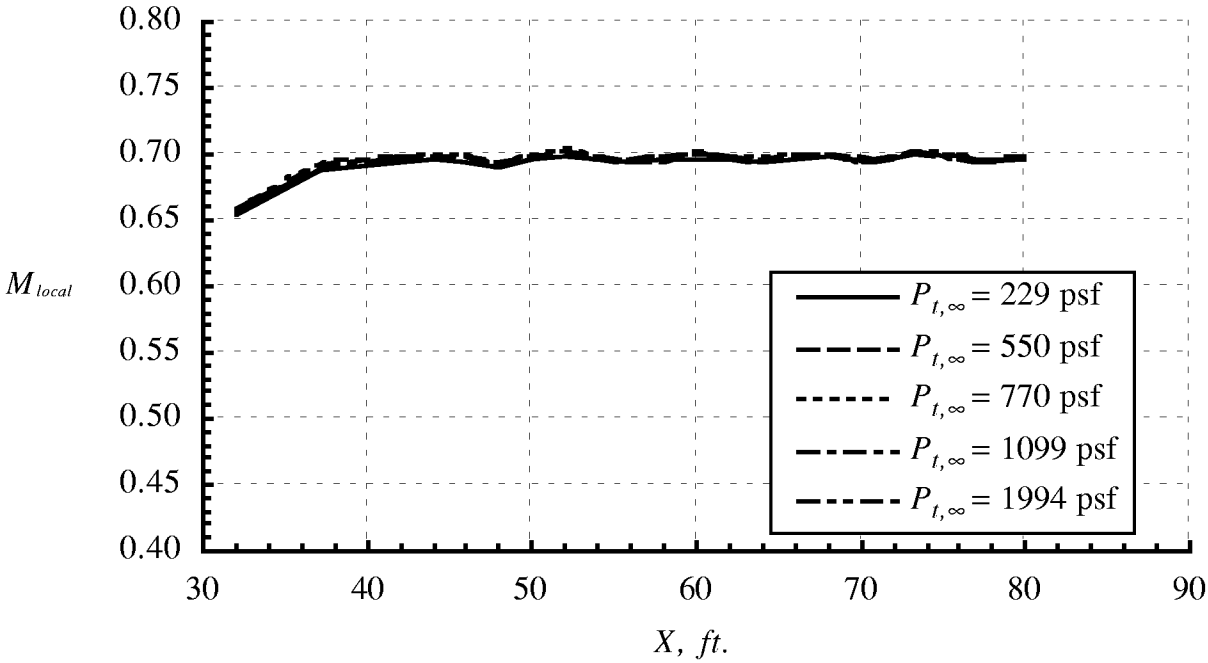

(c) Effect of $P_{t,\infty}$ at $M_\infty \approx 0.70$.
Figure 15. Continued.

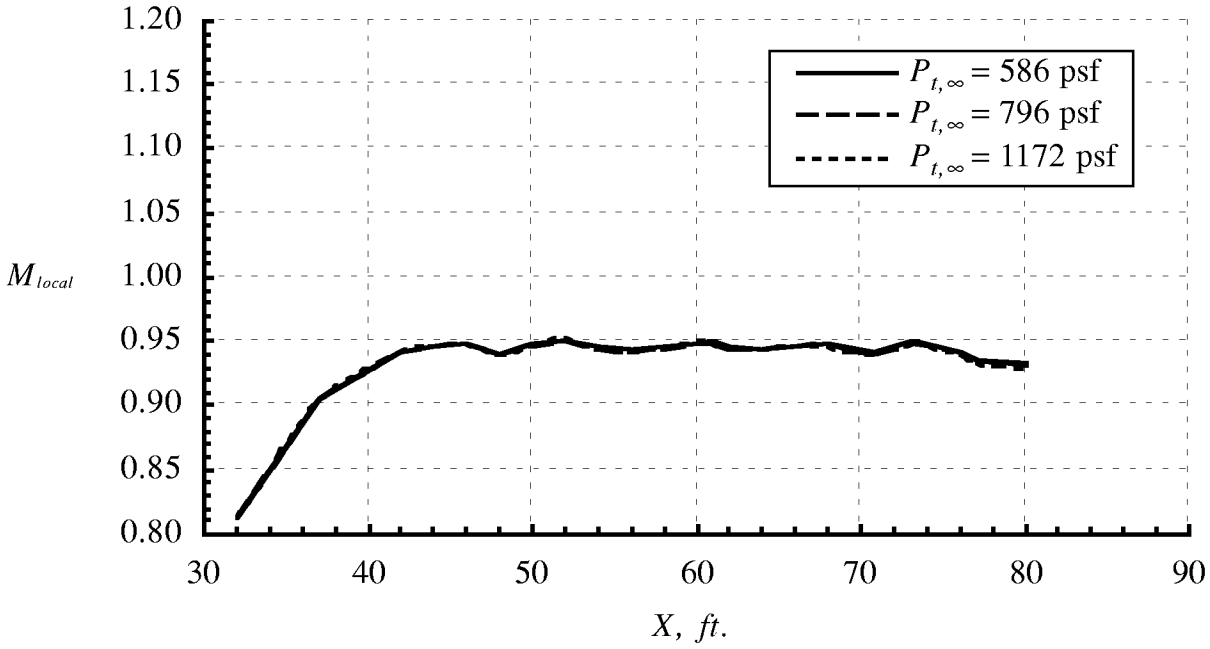

(d) Effect of $P_{t,\infty}$ at $M_\infty \approx 0.95$.
Figure 15. Continued.

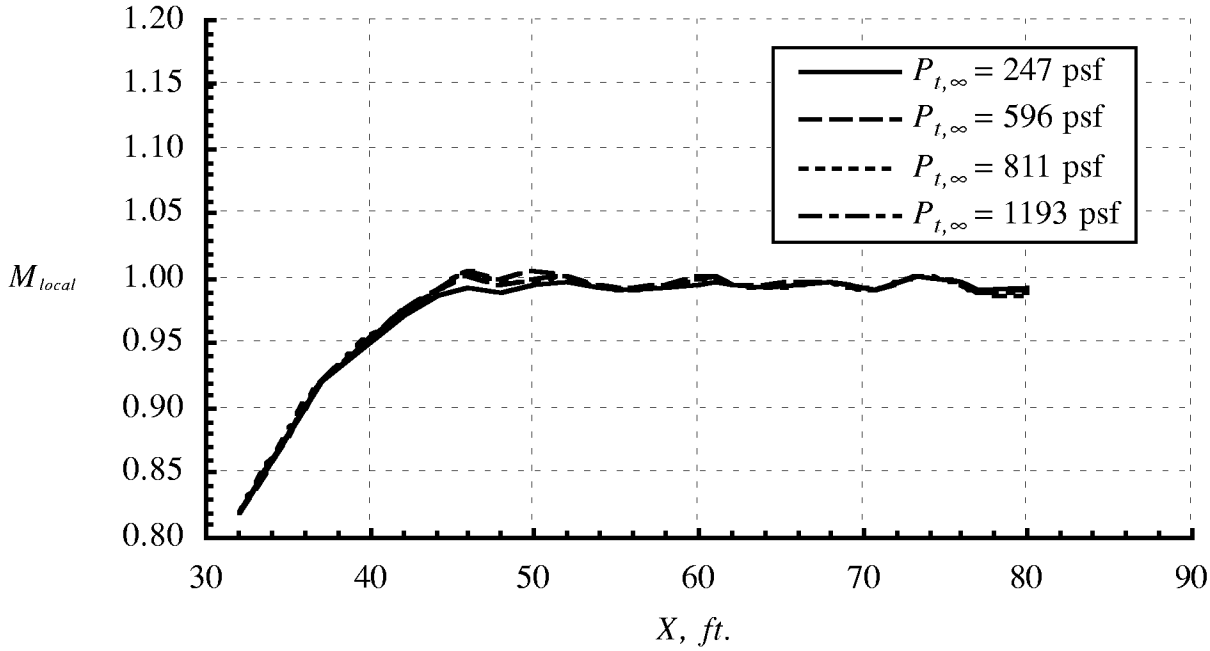

(e) Effect of $P_{t,\infty}$ at $M_\infty \approx 1.00$.
Figure 15. Continued.

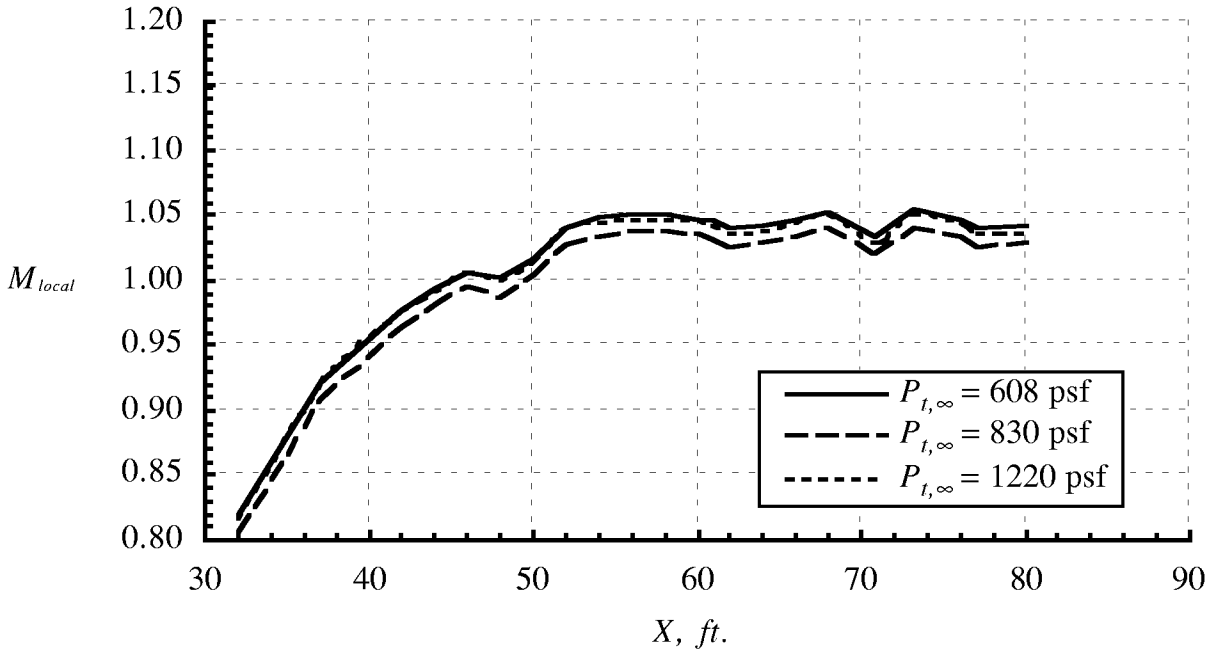

(f) Effect of $P_{t,\infty}$ at $M_\infty \approx 1.05$.
Figure 15. Continued.

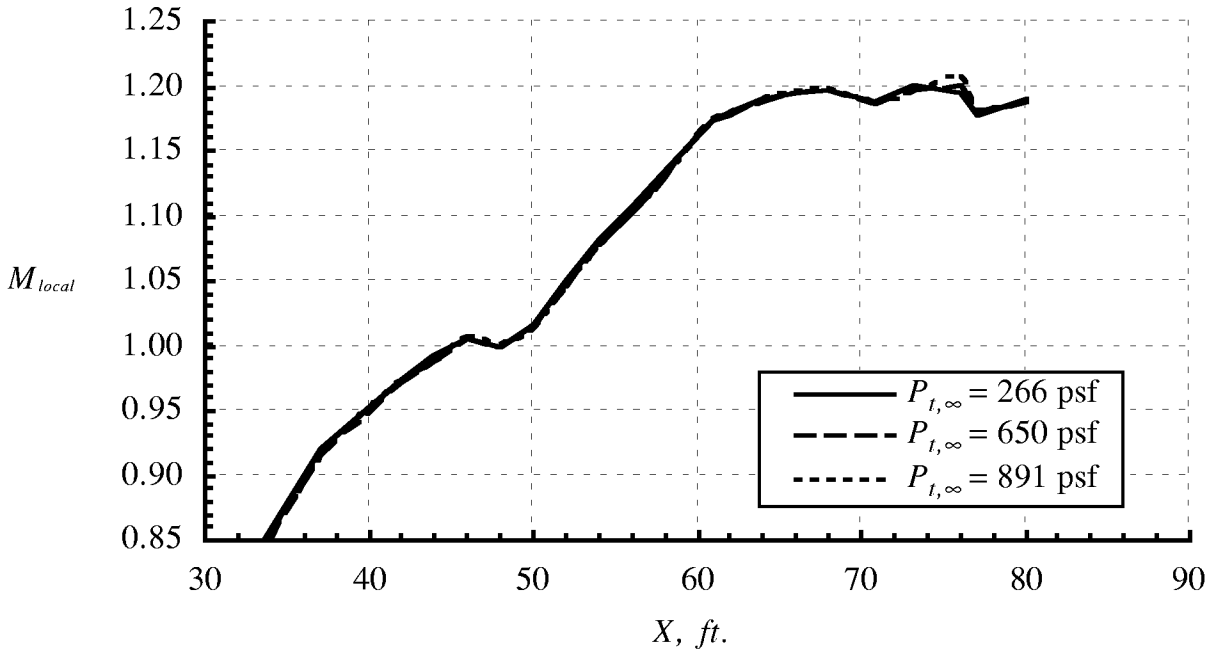

(g) Effect of $P_{t,\infty}$ at $M_\infty \approx 1.20$.
Figure 15. Concluded.

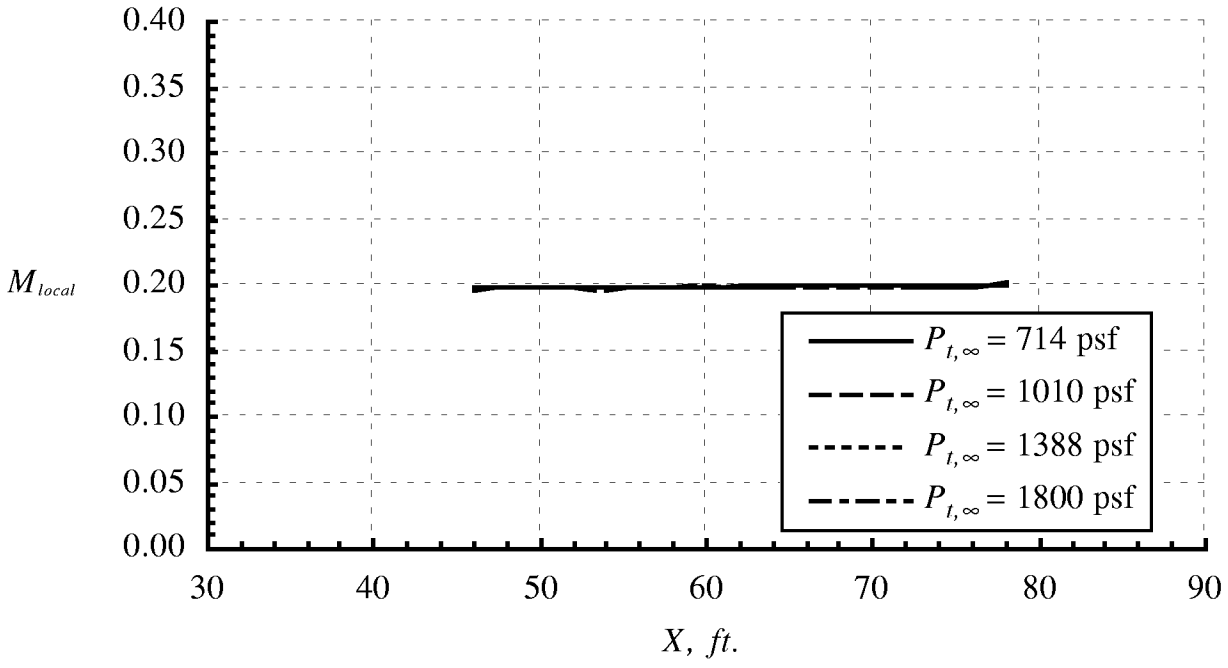

(a) Effect of $P_{t,\infty}$ at $M_\infty \approx 0.20$.

Figure 16. Variation in Mach number distribution on the test section ceiling in R-134a due to $P_{t,\infty}$; re-entry flaps set to scheduled position.

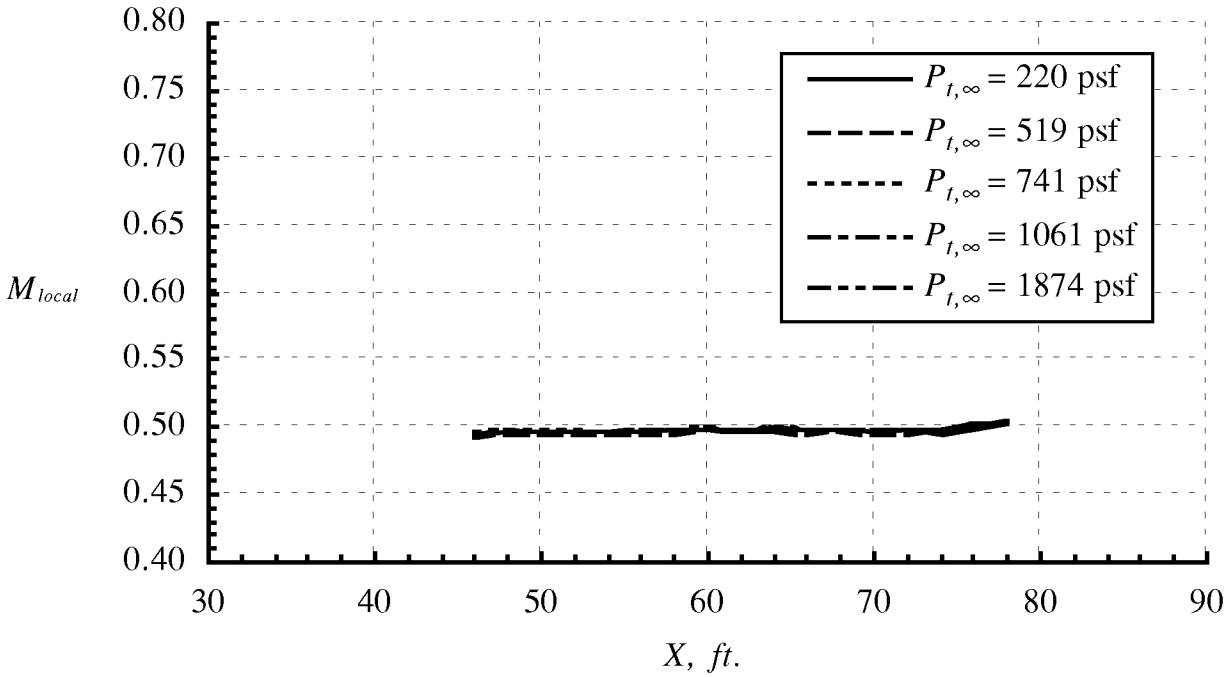

(b) Effect of $P_{t,\infty}$ at $M_\infty \approx 0.50$.

Figure 16. Continued.

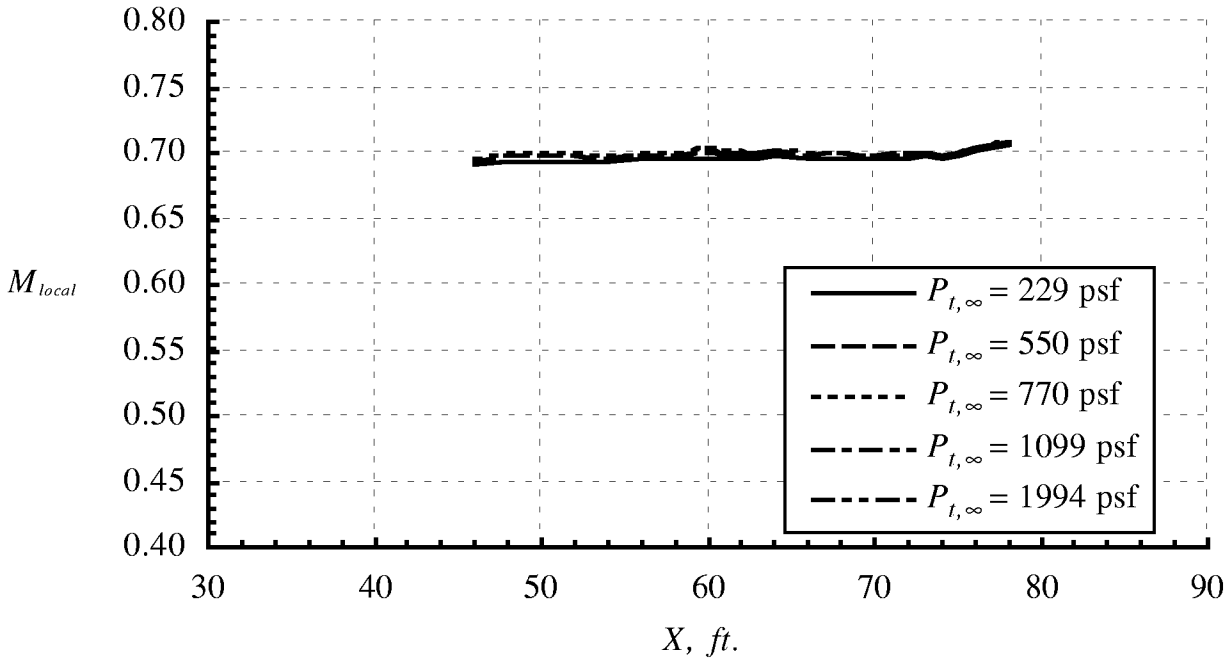

(c) Effect of $P_{t,\infty}$ at $M_\infty \approx 0.70$.
Figure 16. Continued.

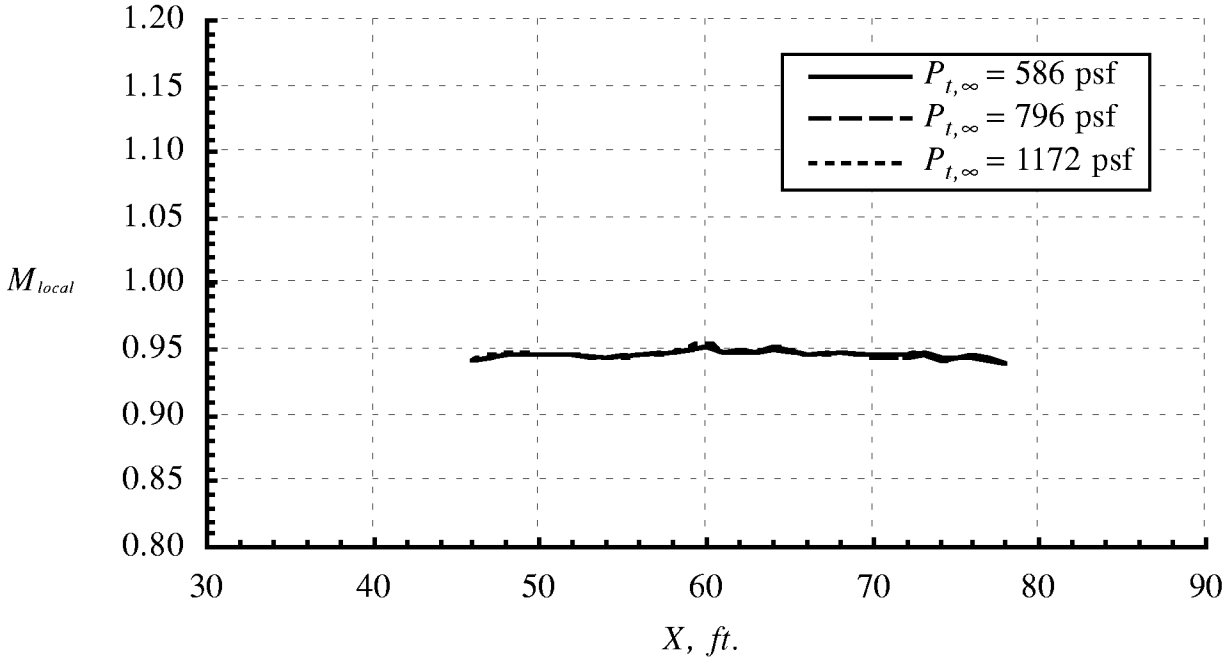

(d) Effect of $P_{t,\infty}$ at $M_\infty \approx 0.95$.
Figure 16. Continued.

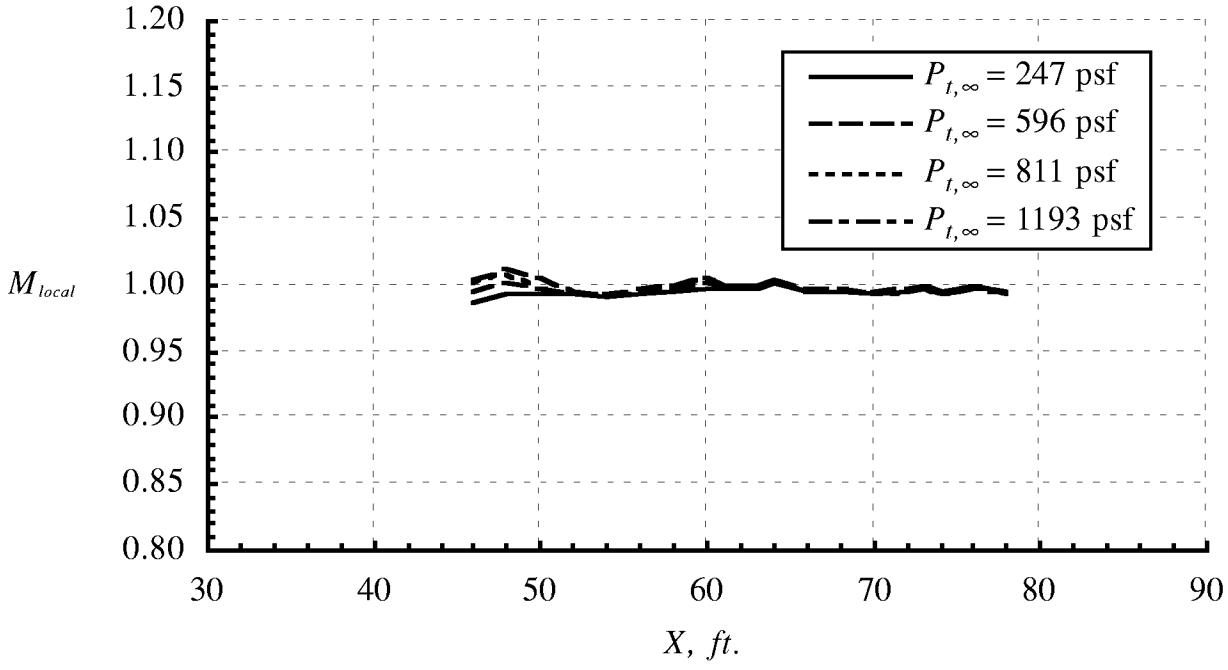

(e) Effect of $P_{t,\infty}$ at $M_\infty \approx 1.00$.
Figure 16. Continued.

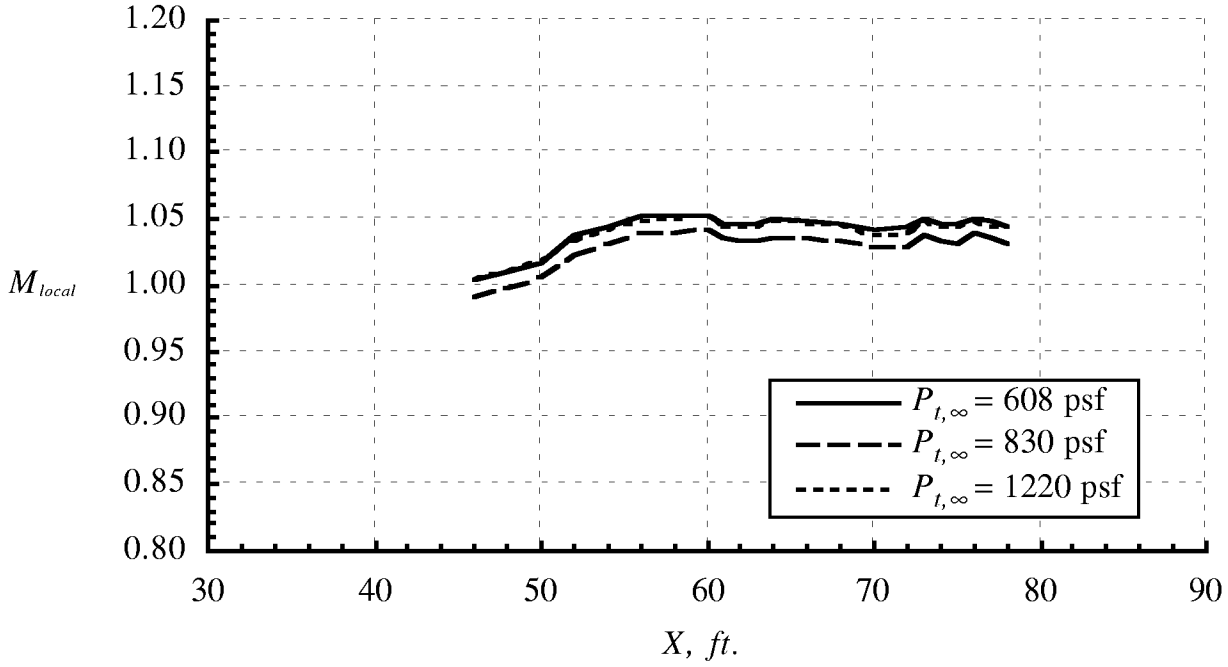

(f) Effect of $P_{t,\infty}$ at $M_\infty \approx 1.05$.
Figure 16. Continued.

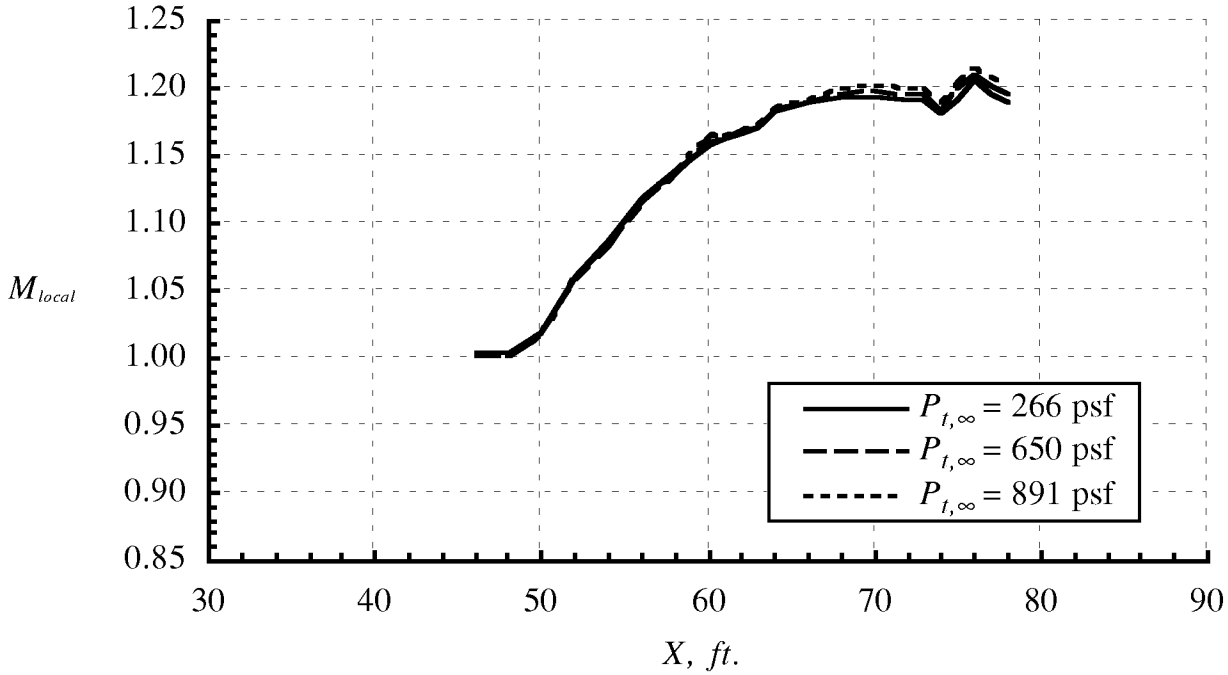

(g) Effect of $P_{t,\infty}$ at $M_\infty \approx 1.20$.

Figure 16. Concluded.

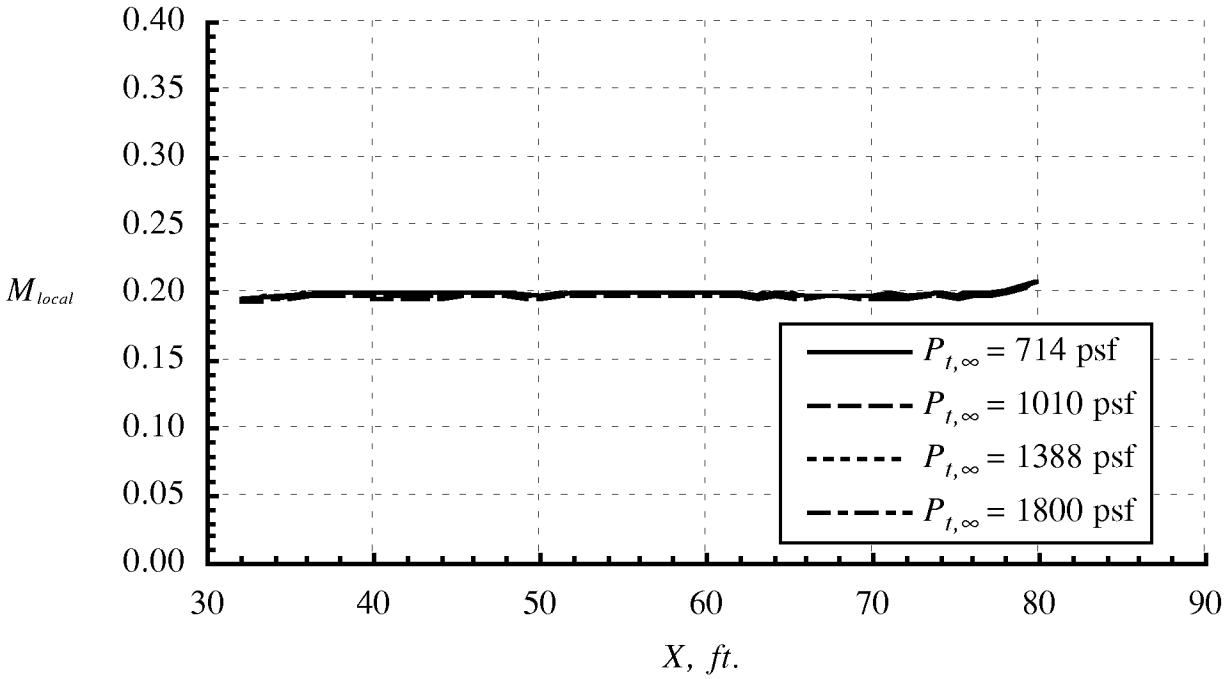

(a) Effect of $P_{t,\infty}$ at $M_\infty \approx 0.20$.

Figure 17. Variation in Mach number distribution on the test section floor in R-134a due to $P_{t,\infty}$; re-entry flaps set to scheduled position.

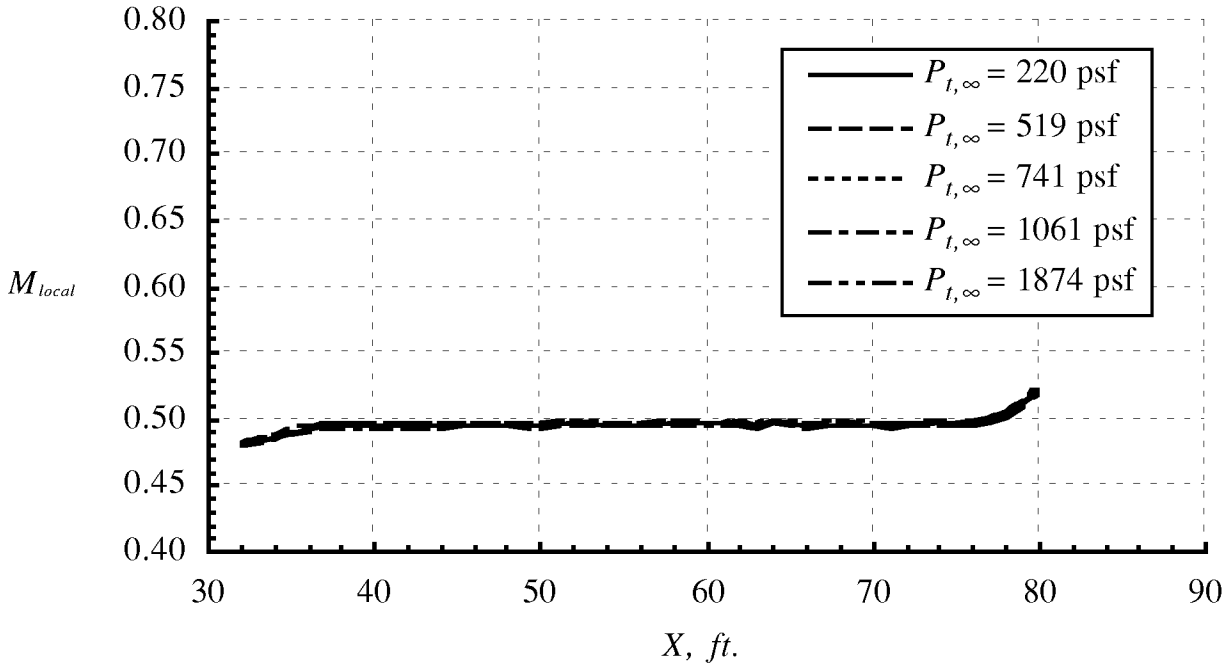

(b) Effect of $P_{t,\infty}$ at $M_\infty \approx 0.50$.
Figure 17. Continued.

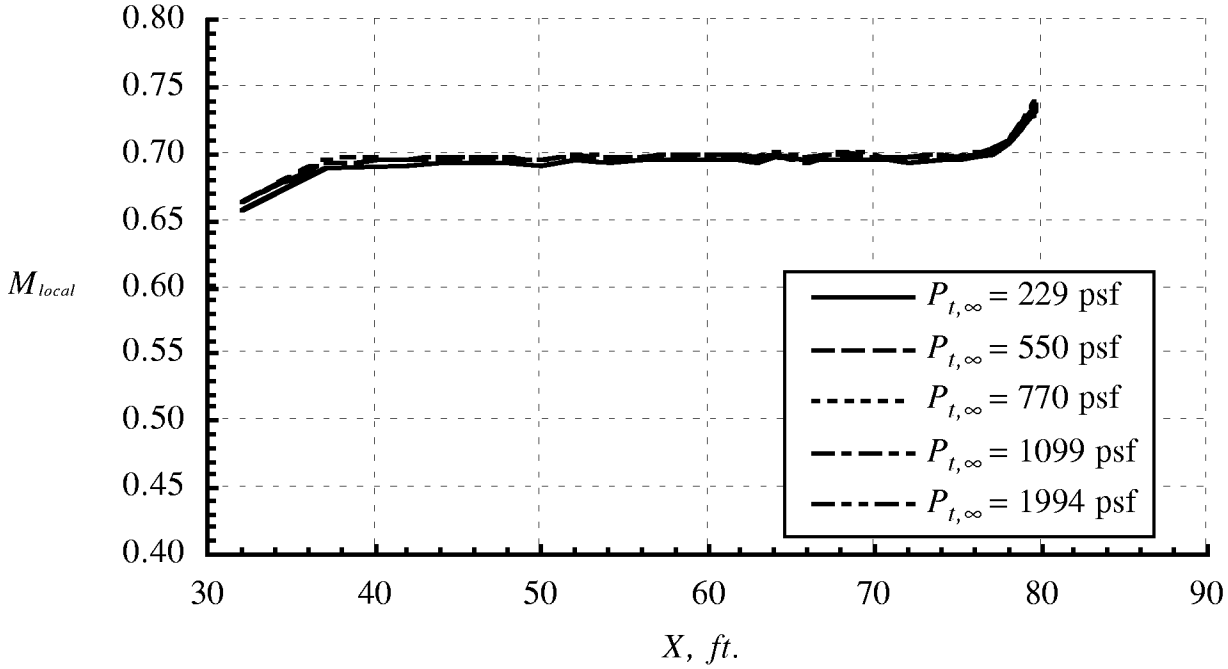

(c) Effect of $P_{t,\infty}$ at $M_\infty \approx 0.70$.
Figure 17. Continued.

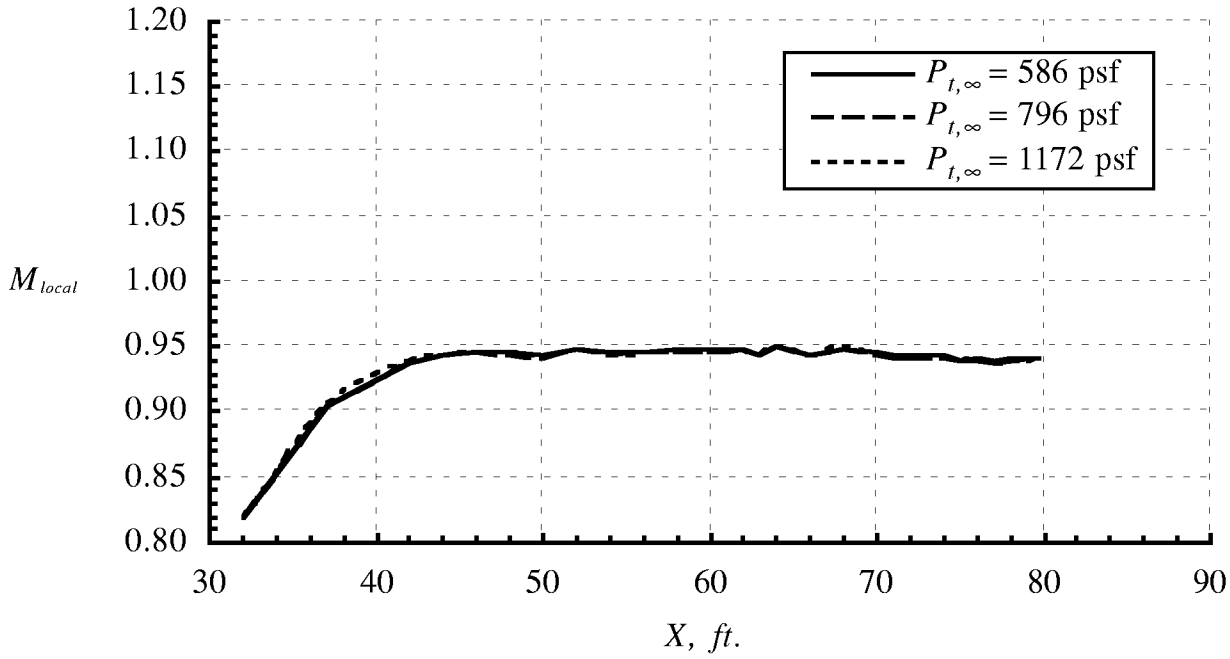

(d) Effect of $P_{t,\infty}$ at $M_\infty \approx 0.95$.
Figure 17. Continued.

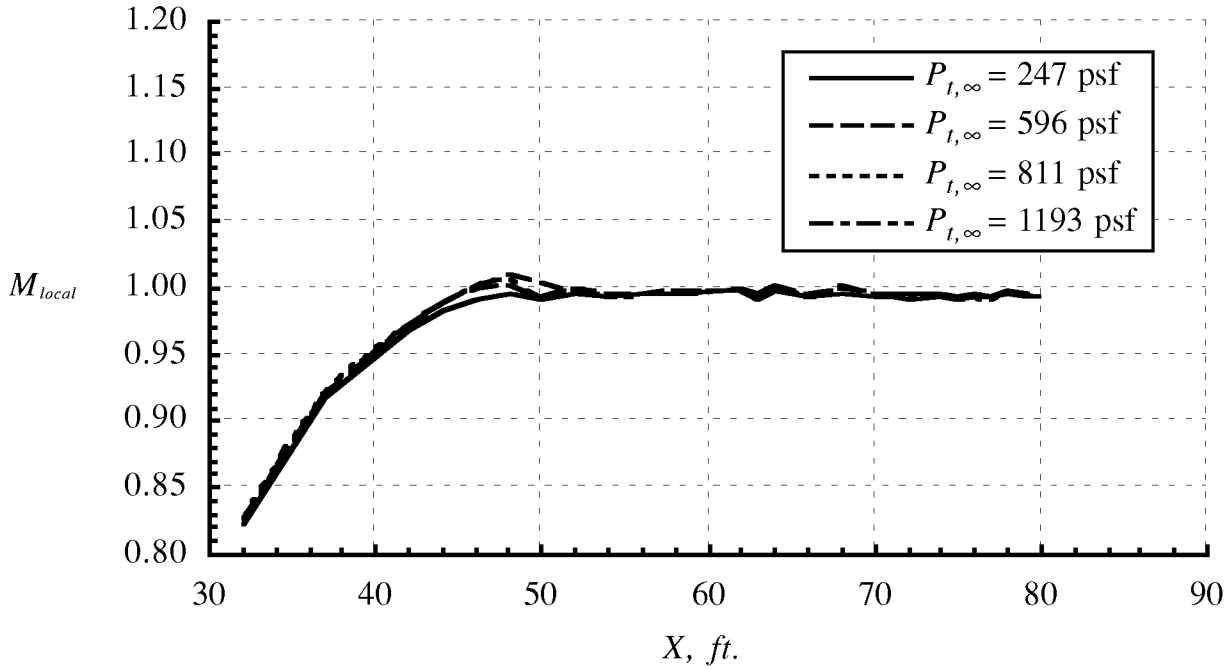

(e) Effect of $P_{t,\infty}$ at $M_\infty \approx 1.00$.
Figure 17. Continued.

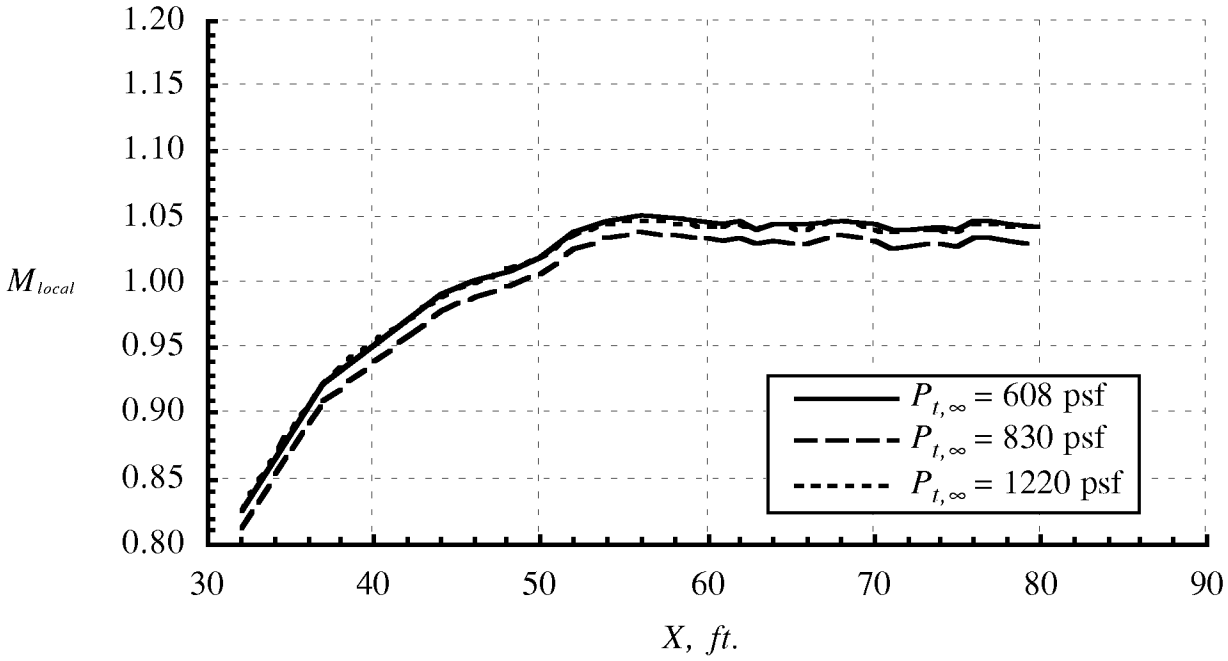

(f) Effect of $P_{t,\infty}$ at $M_\infty \approx 1.05$.
Figure 17. Continued.

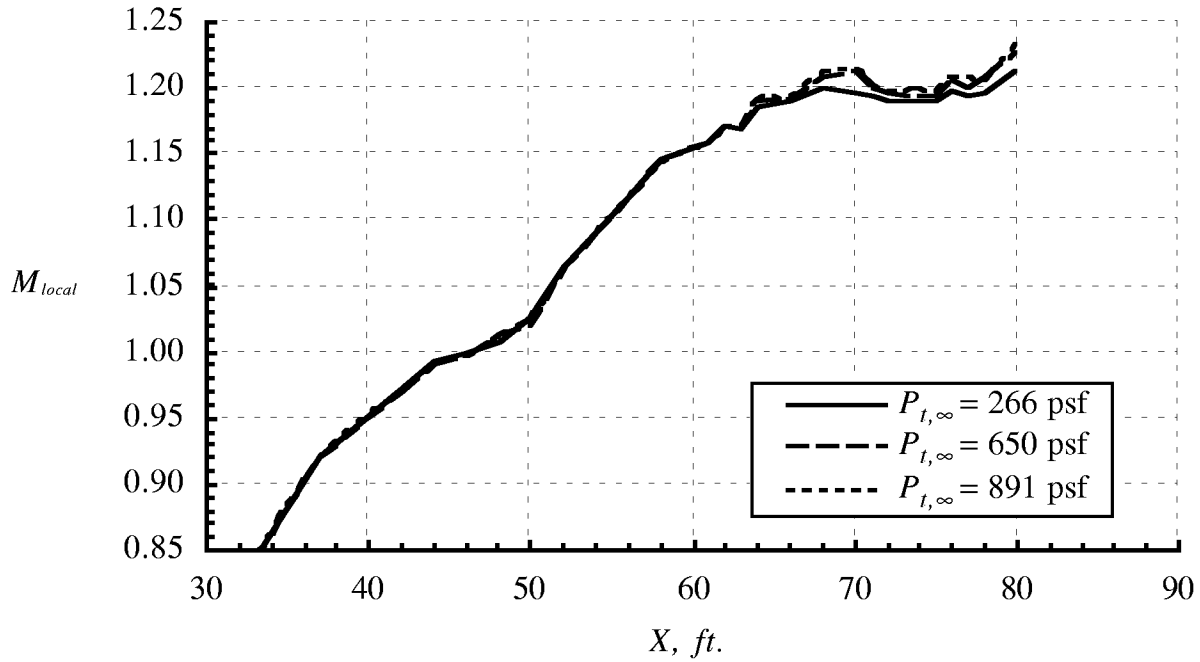

(g) Effect of $P_{t,\infty}$ at $M_\infty \approx 1.20$.
Figure 17. Concluded.

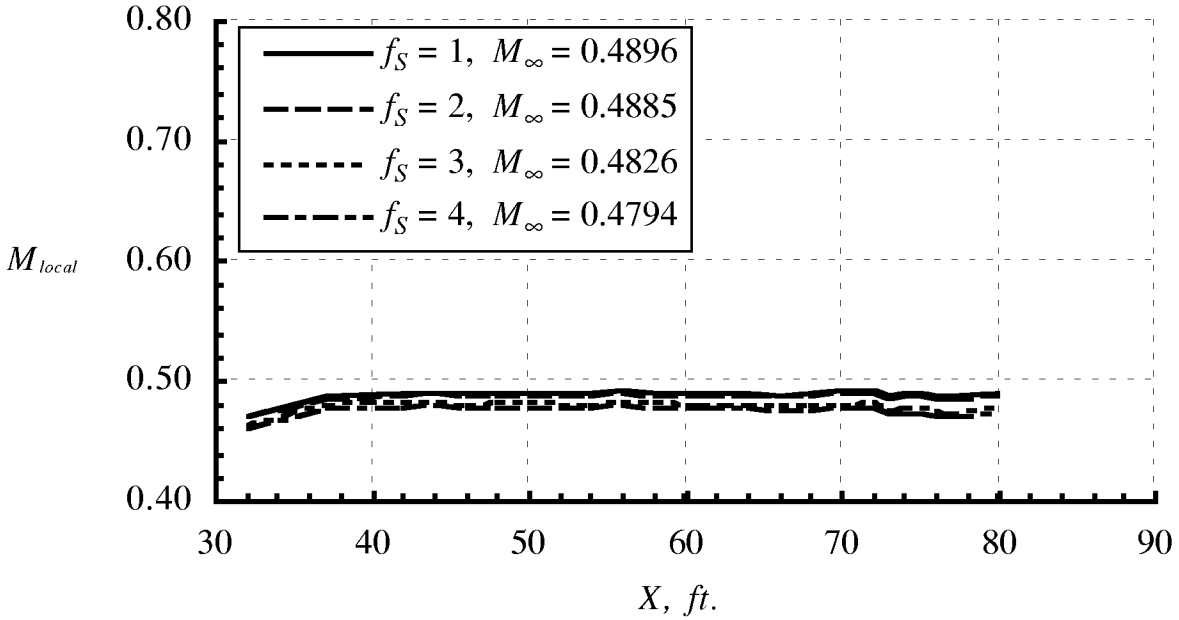

(a) Effect of re-entry flap position on east wall Mach number distribution.
Figure 18. Mach number distribution on the test section walls in air;
$P_{t,\infty} \approx 1235$ psf, $M_\infty \approx 0.49$.

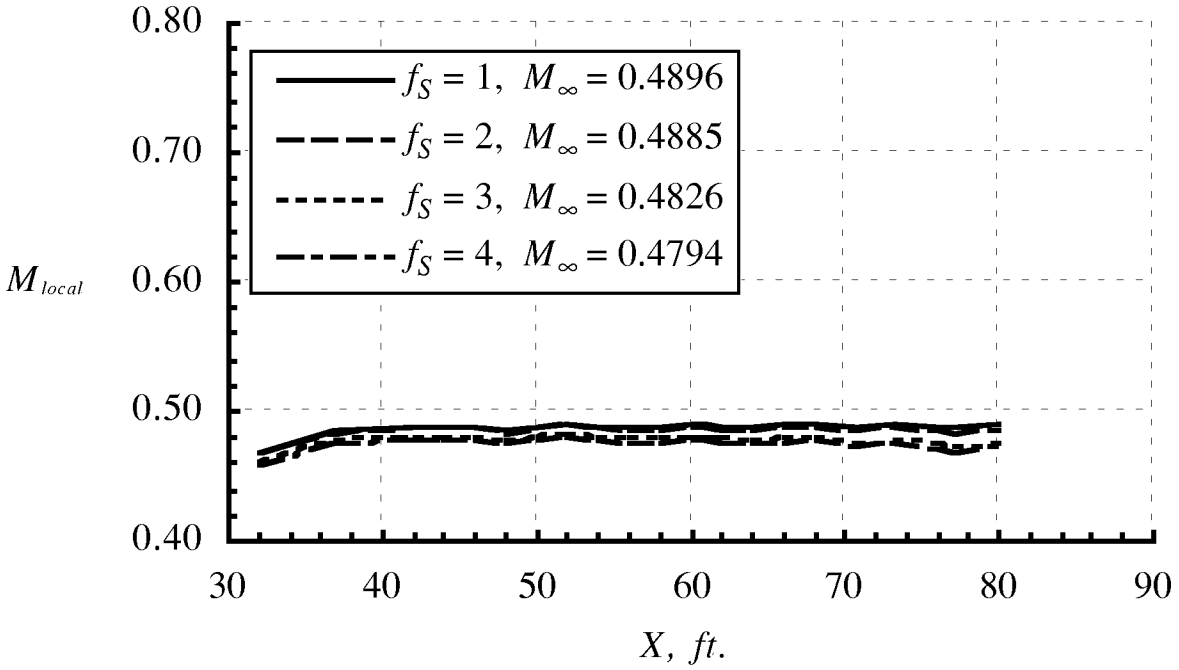

(b) Effect of re-entry flap position on west wall Mach number distribution.
Figure 18. Continued.

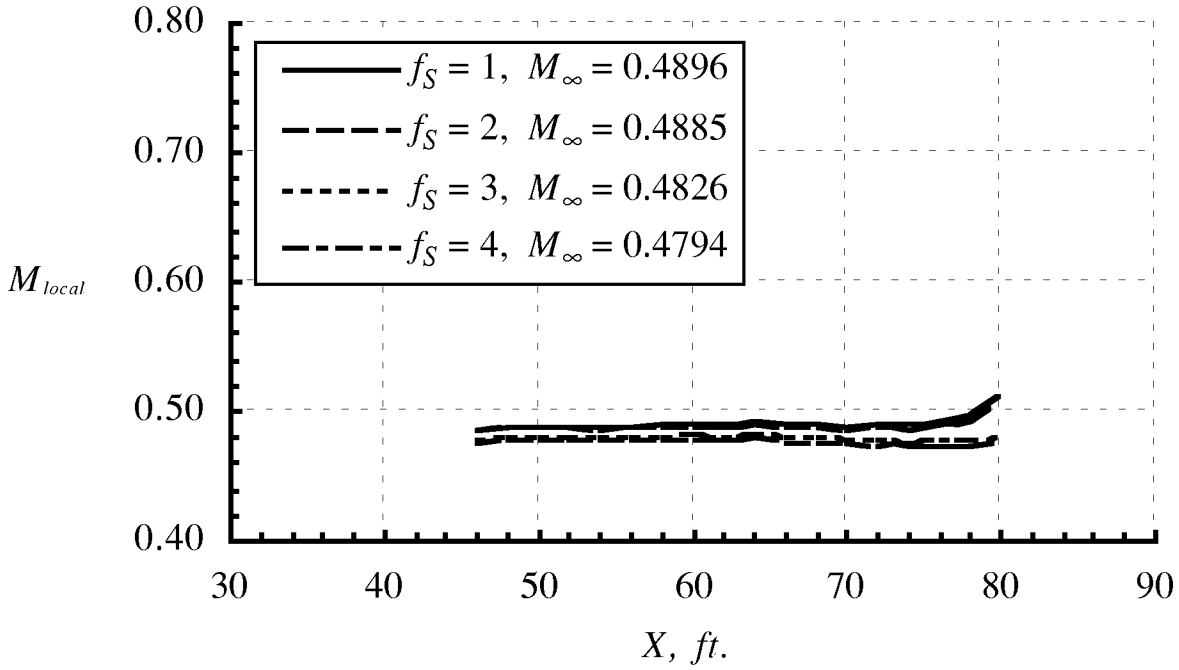

(c) Effect of re-entry flap position on ceiling Mach number distribution.
Figure 18. Continued.

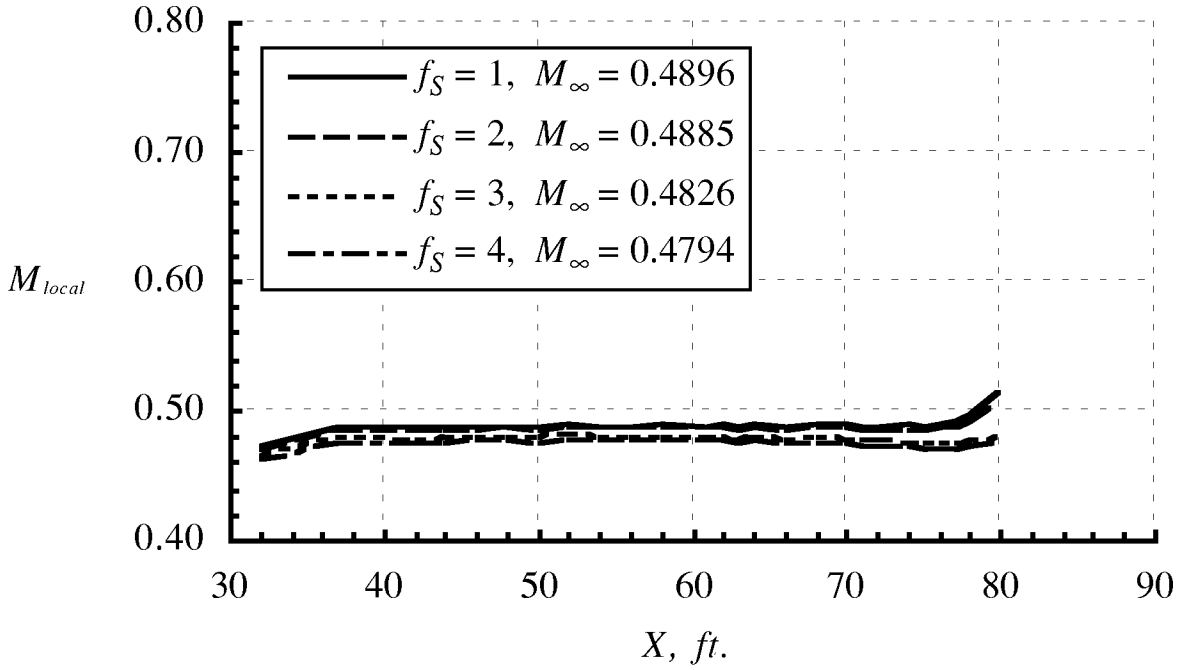

(d) Effect of re-entry flap position on floor Mach number distribution.
Figure 18. Concluded.

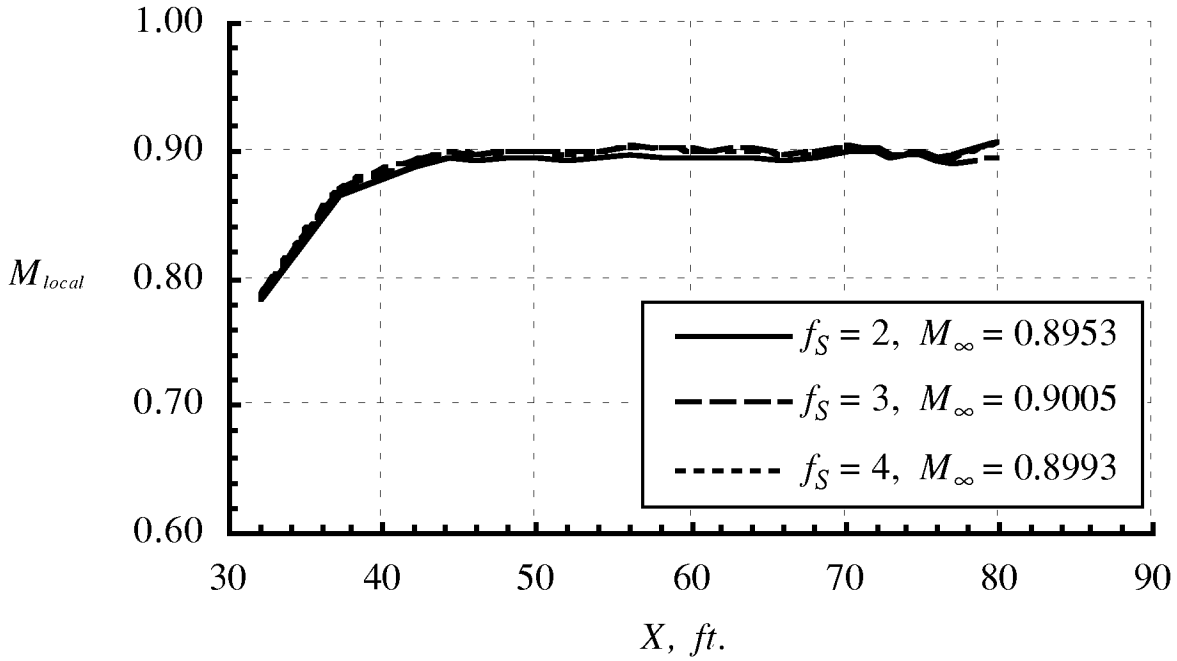

(a) Effect of re-entry flap position on east wall Mach number distribution.

Figure 19. Mach number distribution on the test section walls in air; $P_{t,\infty} \approx 500$ psf, $M_\infty \approx 0.90$.

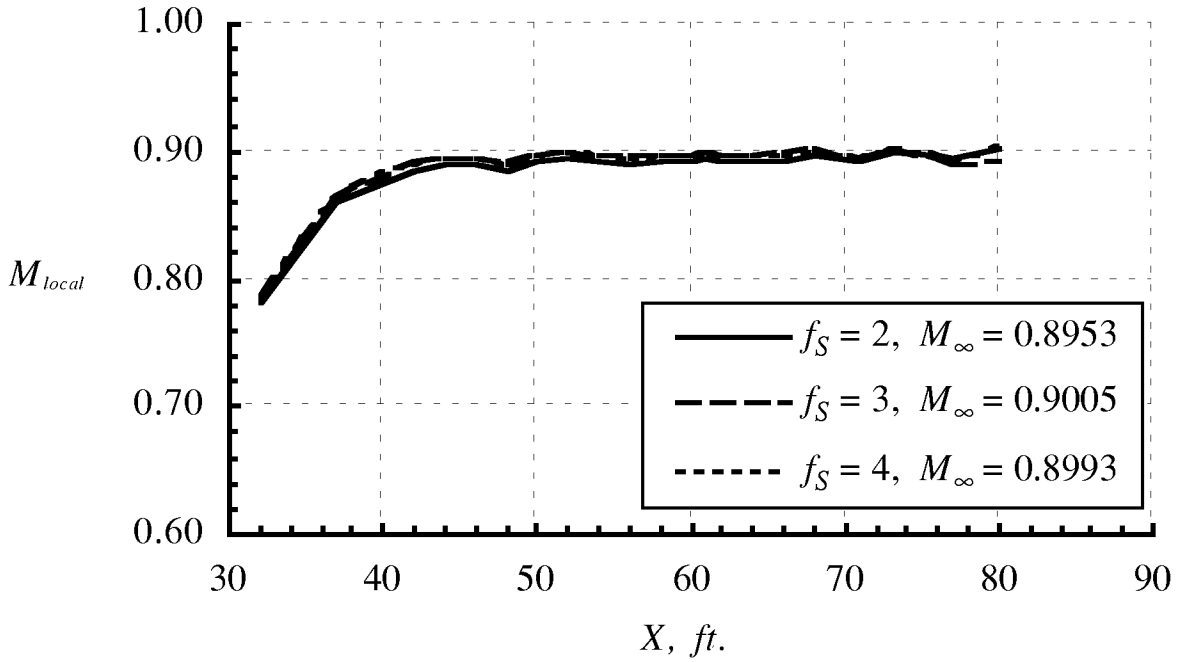

(b) Effect of re-entry flap position on west wall Mach number distribution.

Figure 19. Continued.

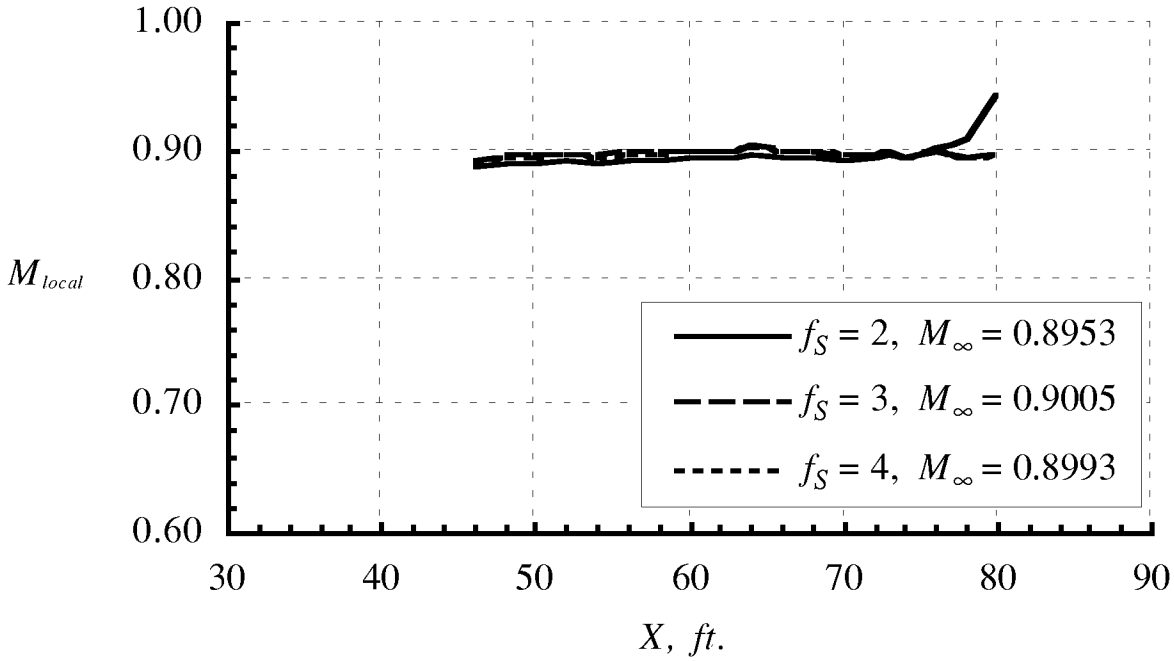

(c) Effect of re-entry flap position on ceiling Mach number distribution.
Figure 19. Continued.

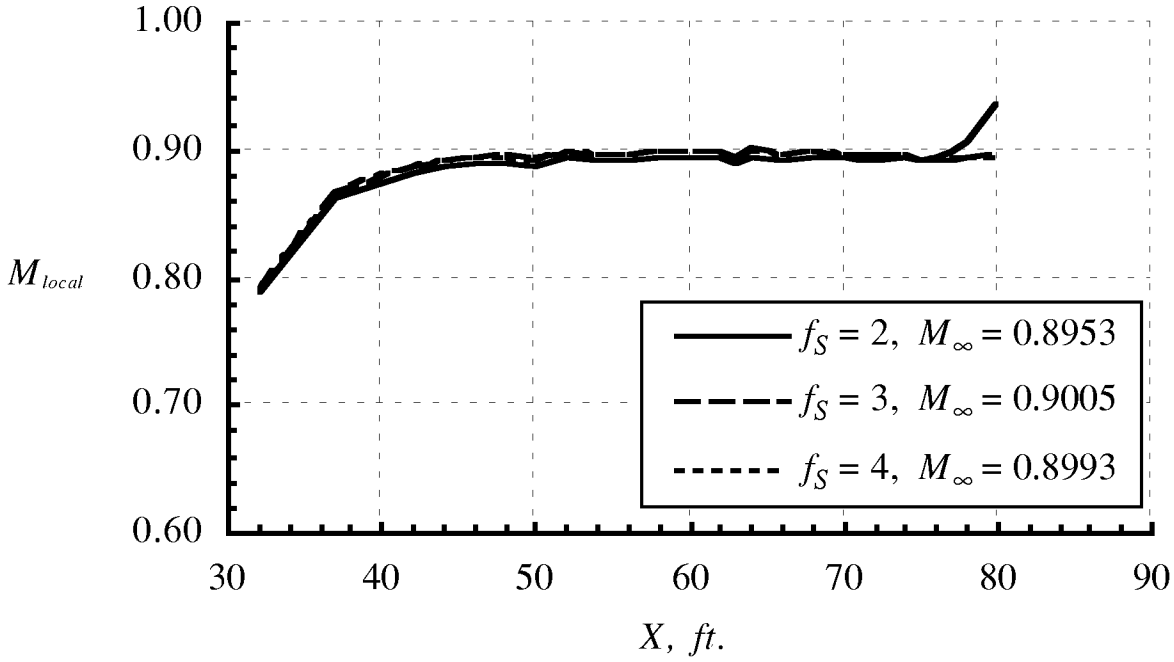

(d) Effect of re-entry flap position on floor Mach number distribution.
Figure 19. Concluded.

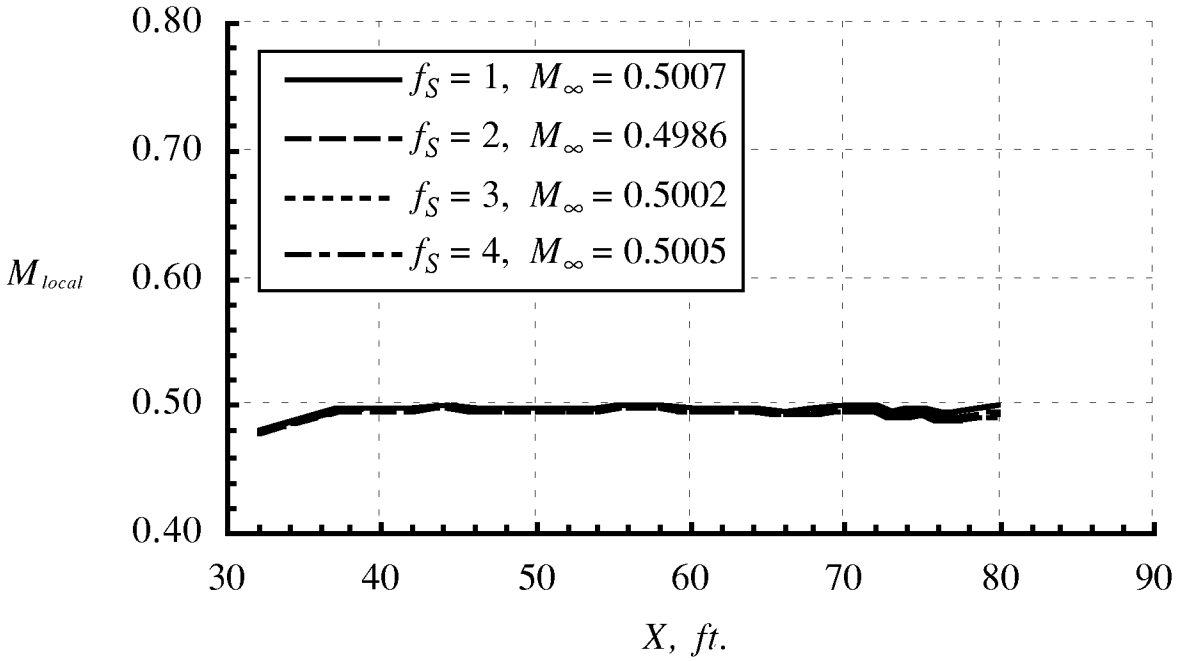

(a) Effect of re-entry flap position on east wall Mach number distribution.

Figure 20. Mach number distribution on the test section walls in R-134a; $P_{t,\infty} \approx 1875$ psf, $M_\infty \approx 0.50$.

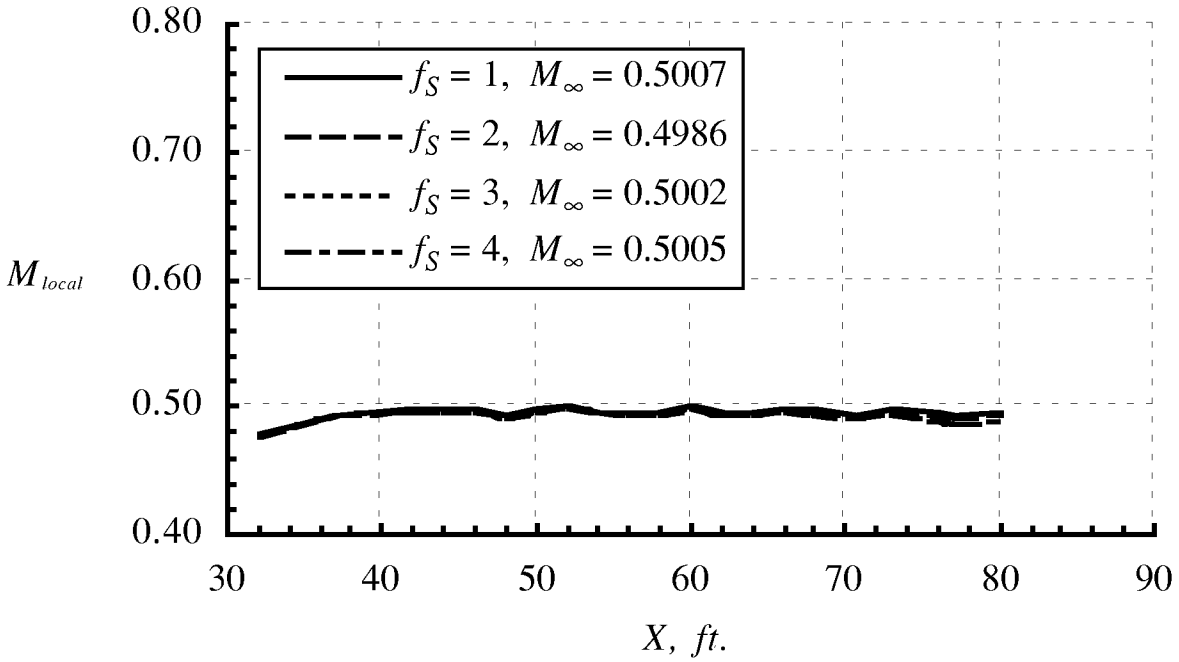

(b) Effect of re-entry flap position on west wall Mach number distribution.

Figure 20. Continued.

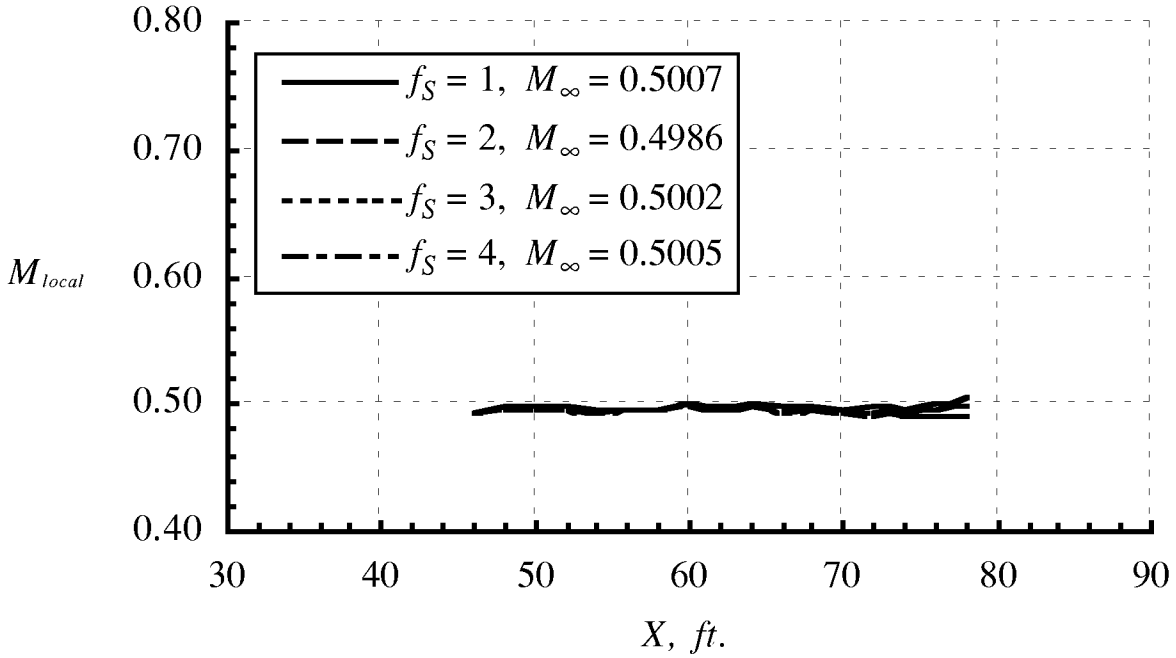

(c) Effect of re-entry flap position on ceiling Mach number distribution.
Figure 20. Continued.

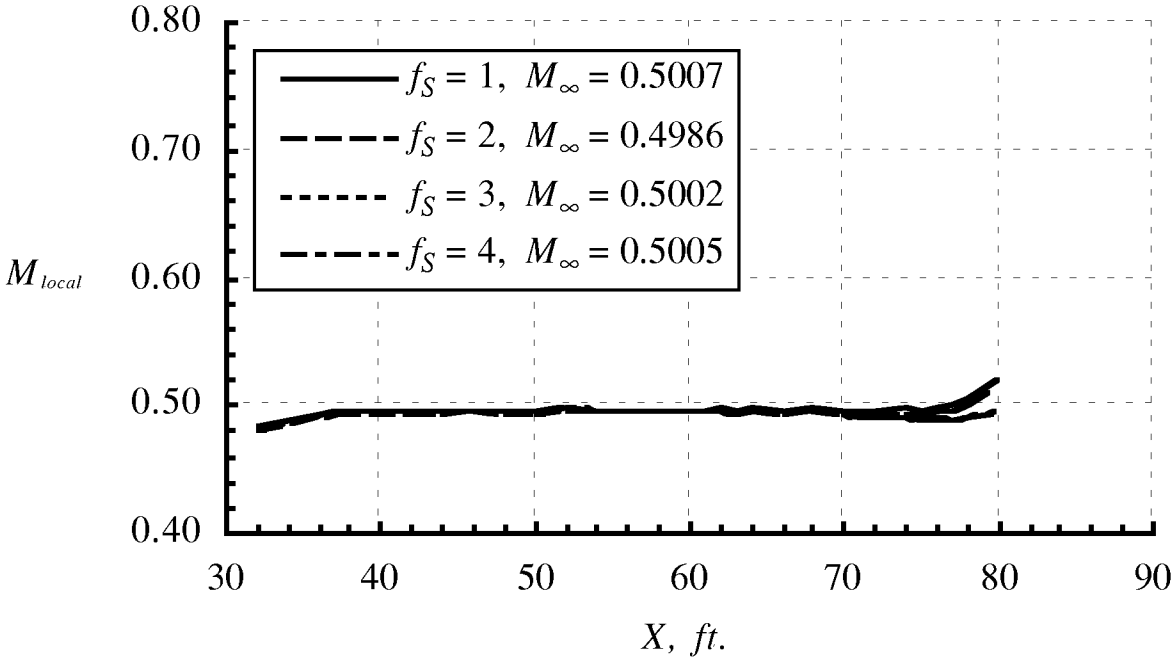

(d) Effect of re-entry flap position on floor Mach number distribution.
Figure 20. Concluded.

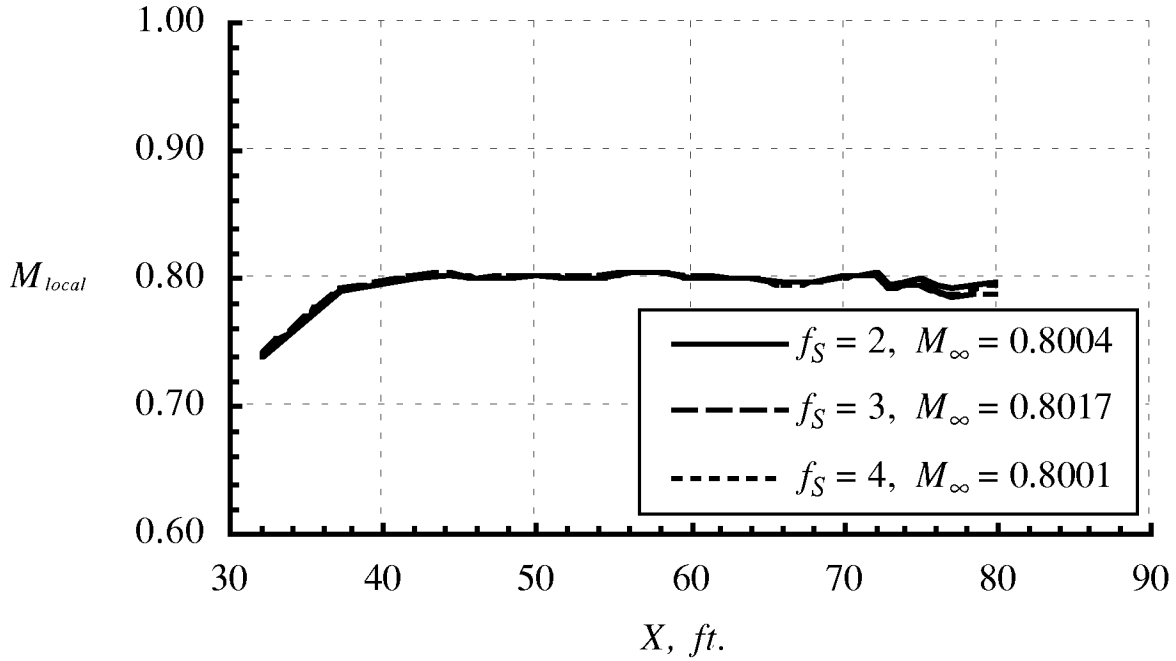

(a) Effect of re-entry flap position on east wall Mach number distribution.

Figure 21. Mach number distribution on the test section walls in R-134a; $P_{t,\infty} \approx 787$ psf, $M_\infty \approx 0.80$.

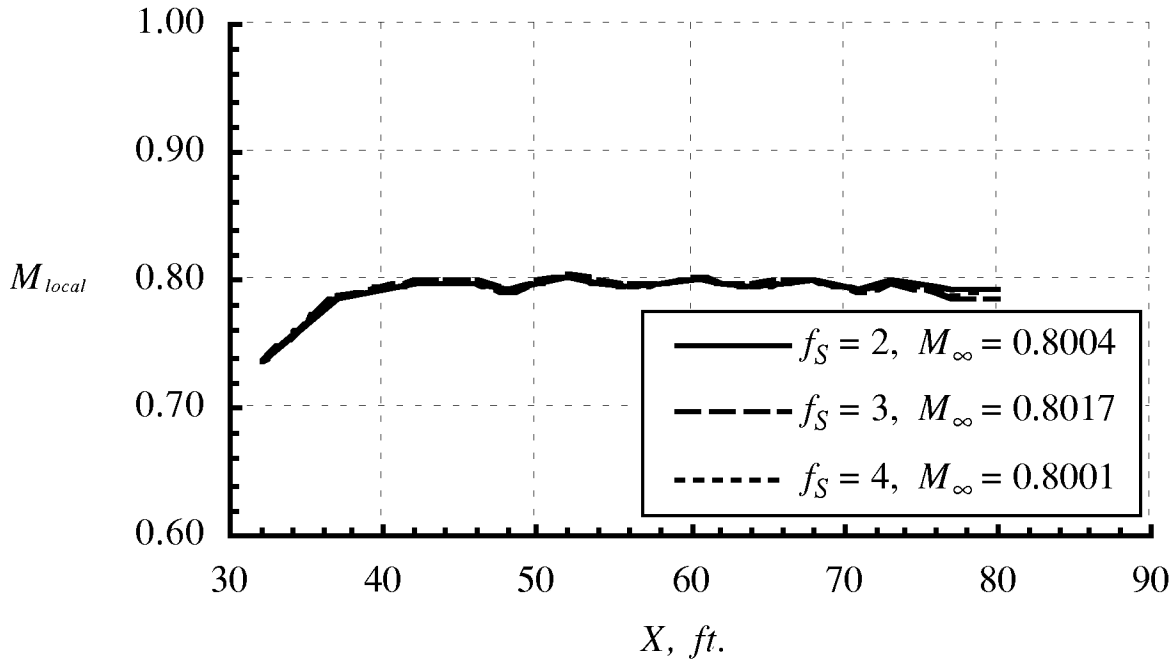

(b) Effect of re-entry flap position on west wall Mach number distribution.

Figure 21. Continued.

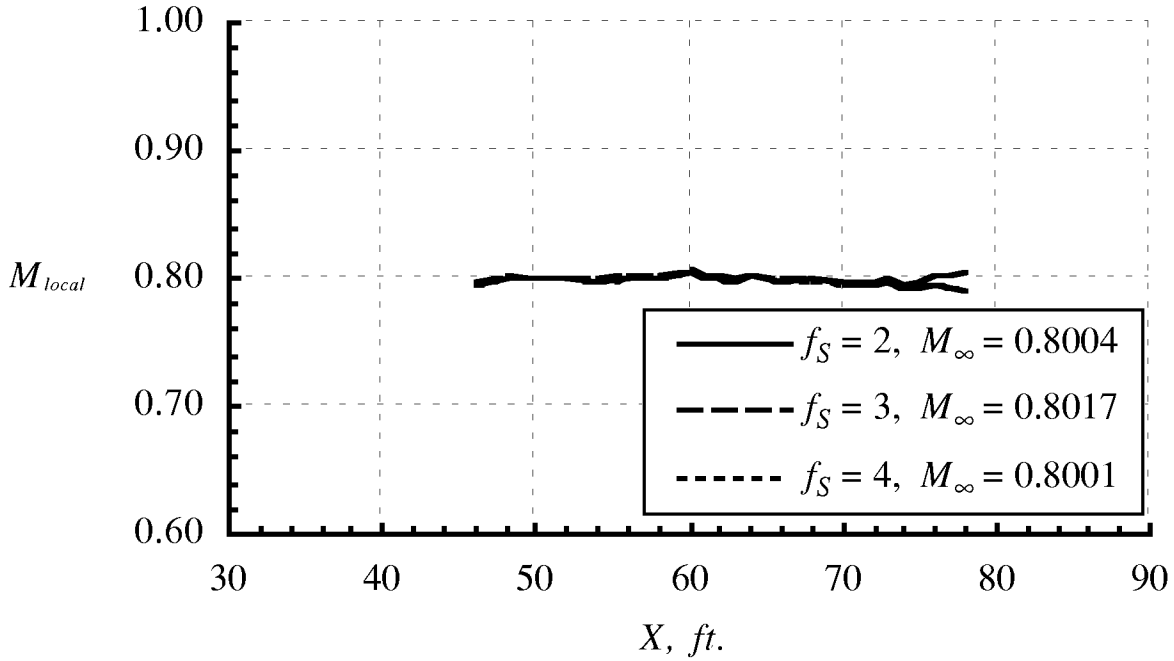

(c) Effect of re-entry flap position on ceiling Mach number distribution.
Figure 21. Continued.

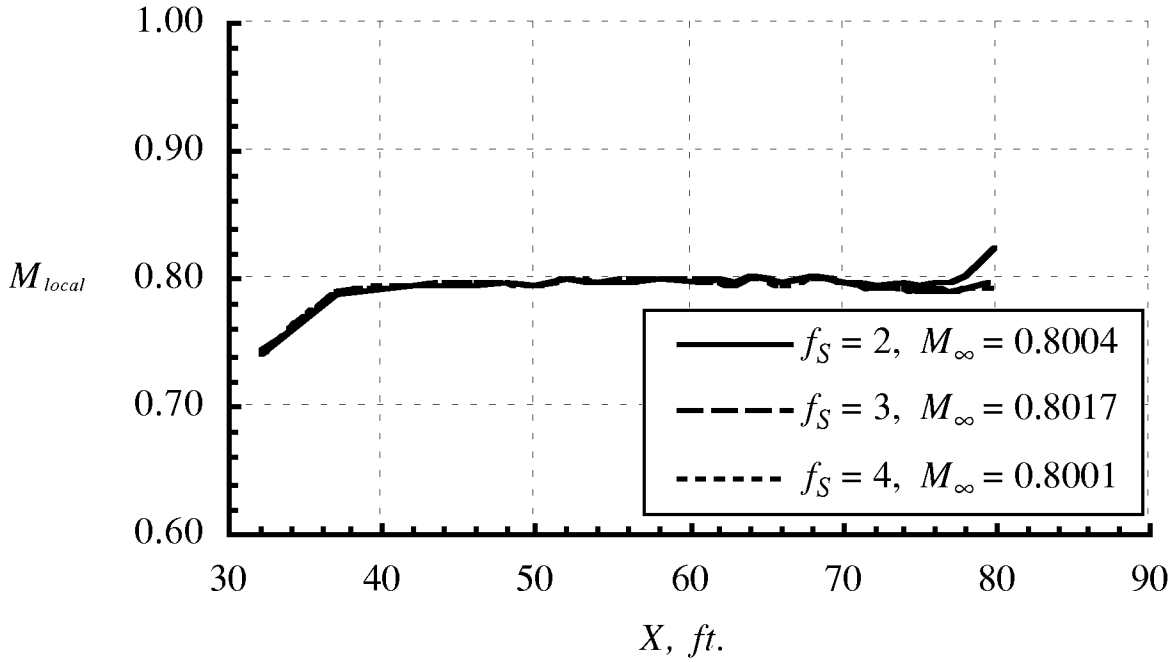

(d) Effect of re-entry flap position on floor Mach number distribution.
Figure 21. Concluded.

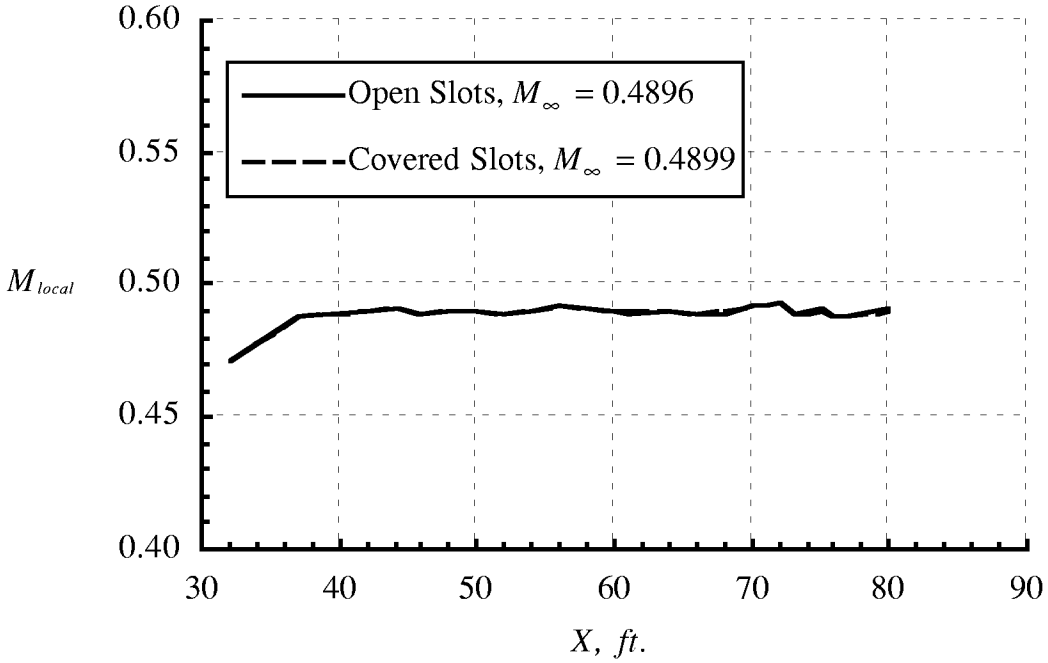

(a) Effect of sealing the east wall sidewall slots on east wall Mach number distribution.

Figure 22. Mach number distribution on the test section walls in air;
$P_{t,\infty} \approx 1250$ psf, $M_\infty \approx 0.49$.

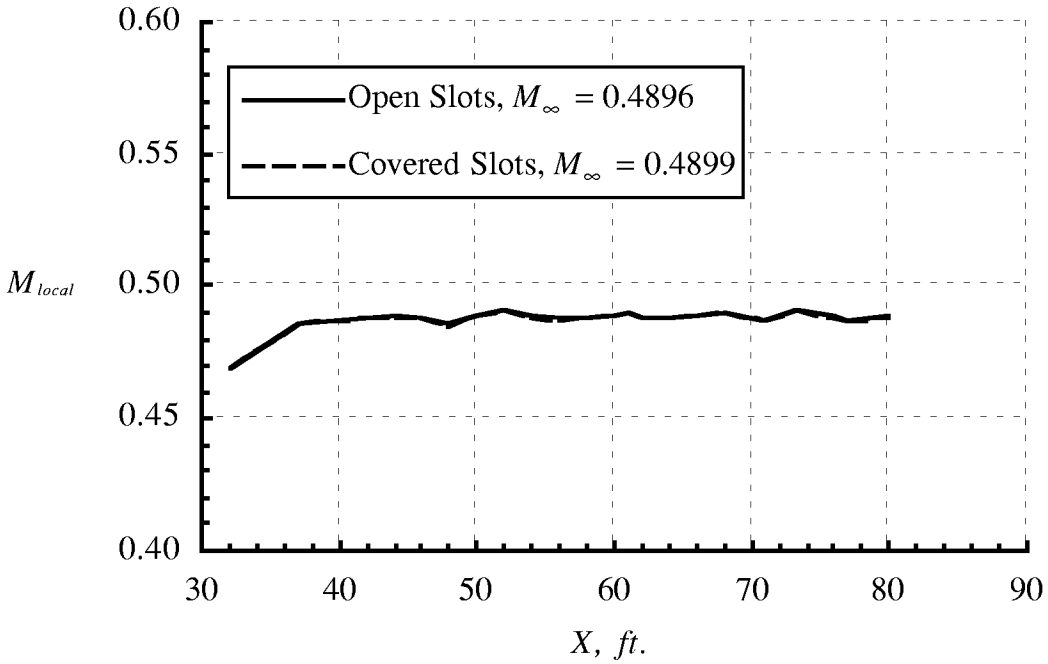

(b) Effect of sealing the east wall sidewall slots on west wall Mach number distribution.

Figure 22. Continued.

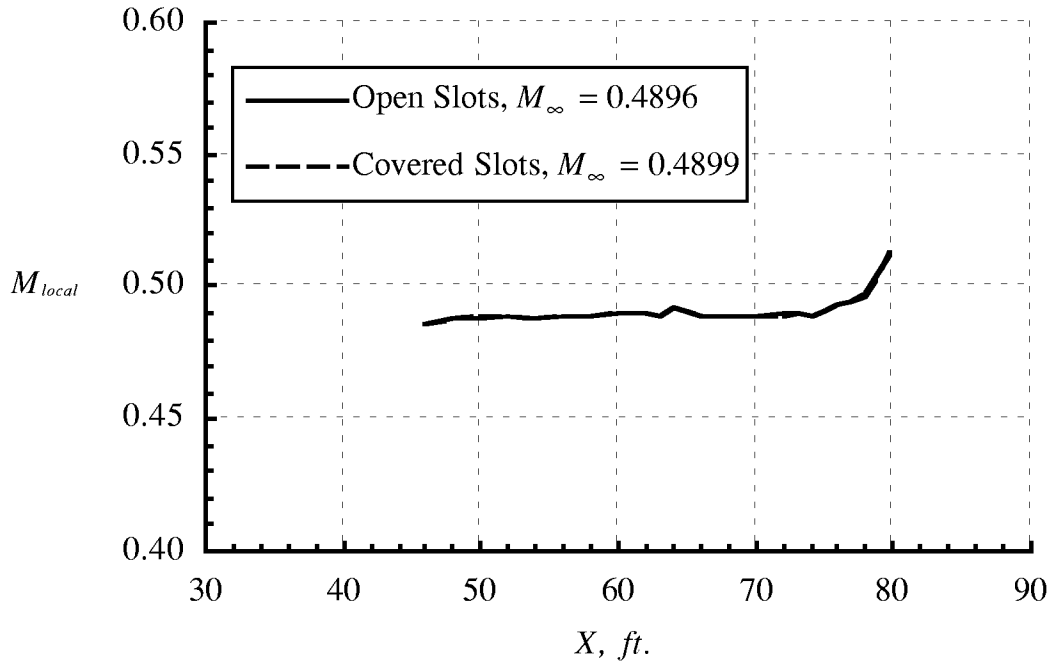

(c) Effect of sealing the east wall sidewall slots on ceiling Mach number distribution.
Figure 22. Continued.

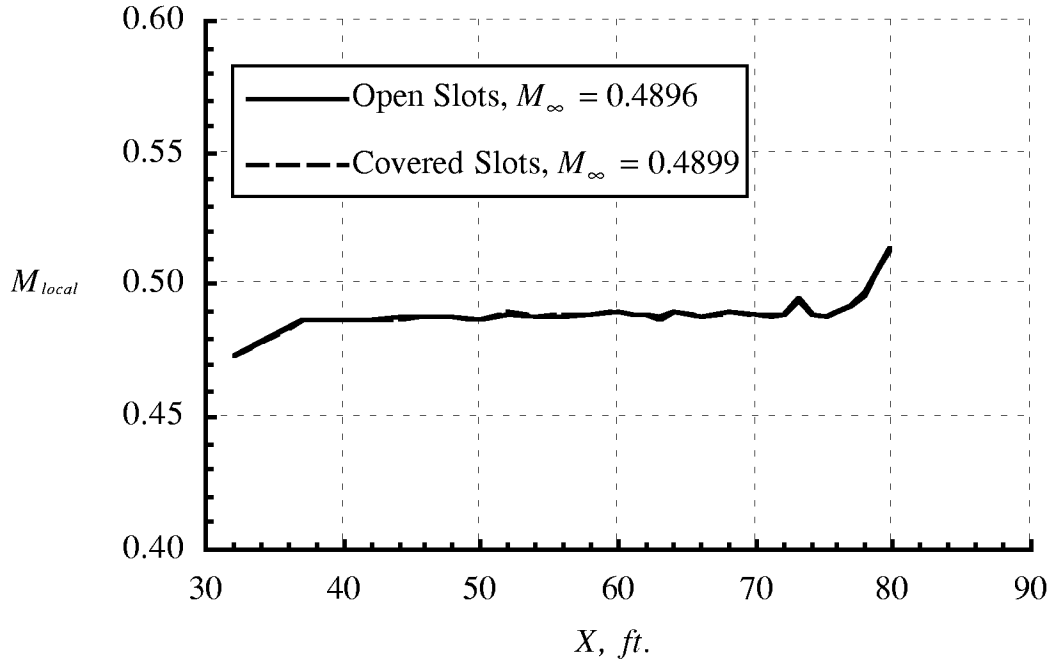

(d) Effect of sealing the east wall sidewall slots on floor Mach number distribution.
Figure 22. Concluded.

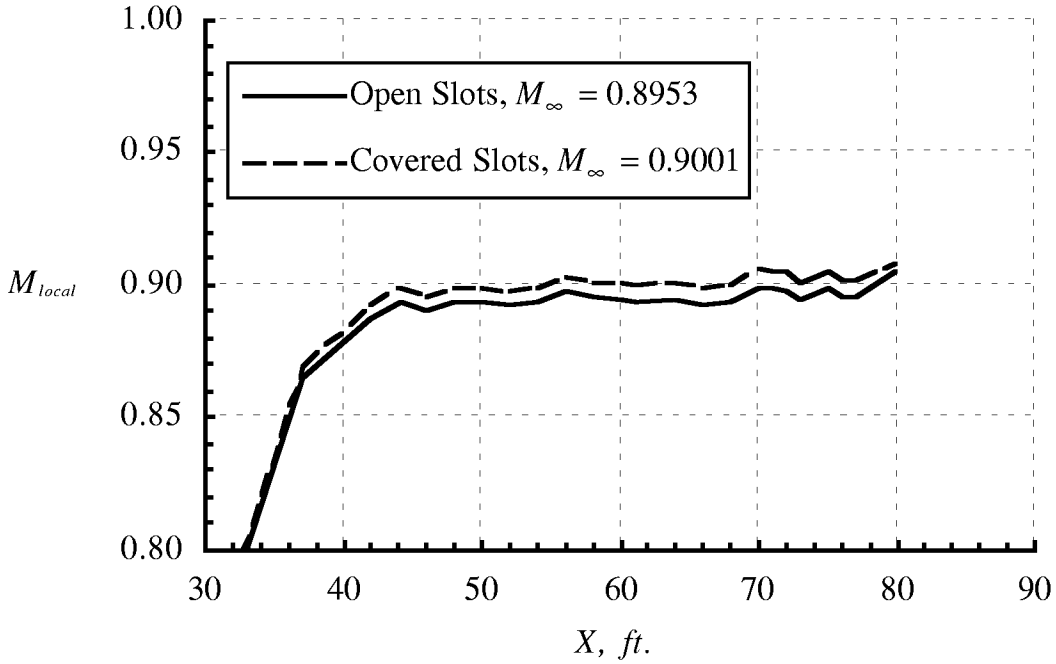

(a) Effect of sealing the east wall sidewall slots on east wall Mach number distribution.

Figure 23. Mach number distribution on the test section walls in air; $P_{t,\infty} \approx 475$ psf, $M_\infty \approx 0.90$.

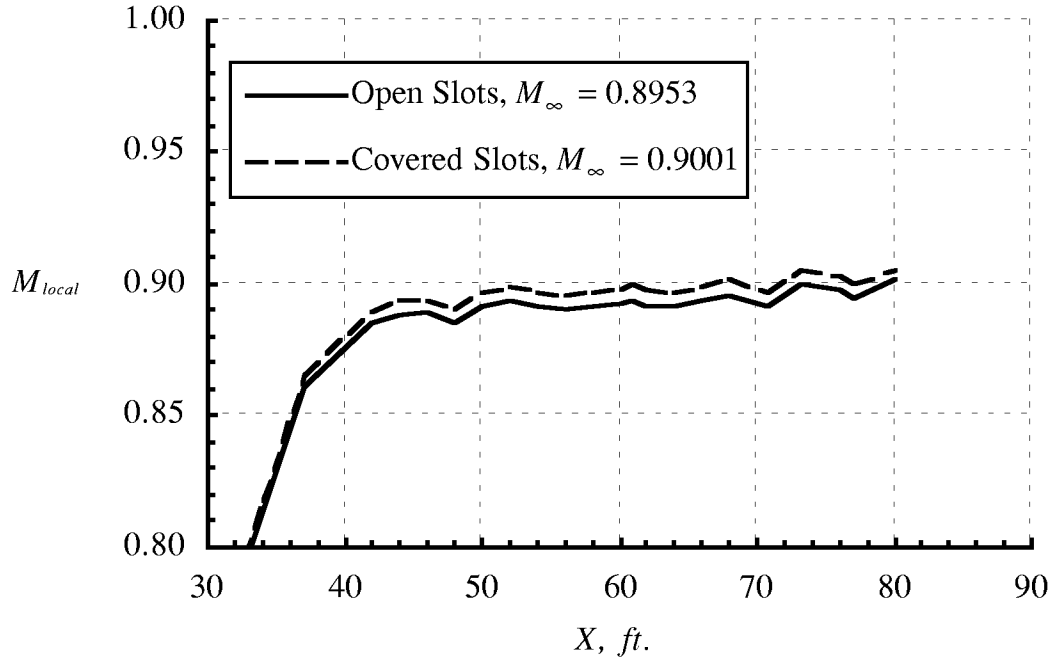

(b) Effect of sealing the east wall sidewall slots on west wall Mach number distribution.

Figure 23. Continued.

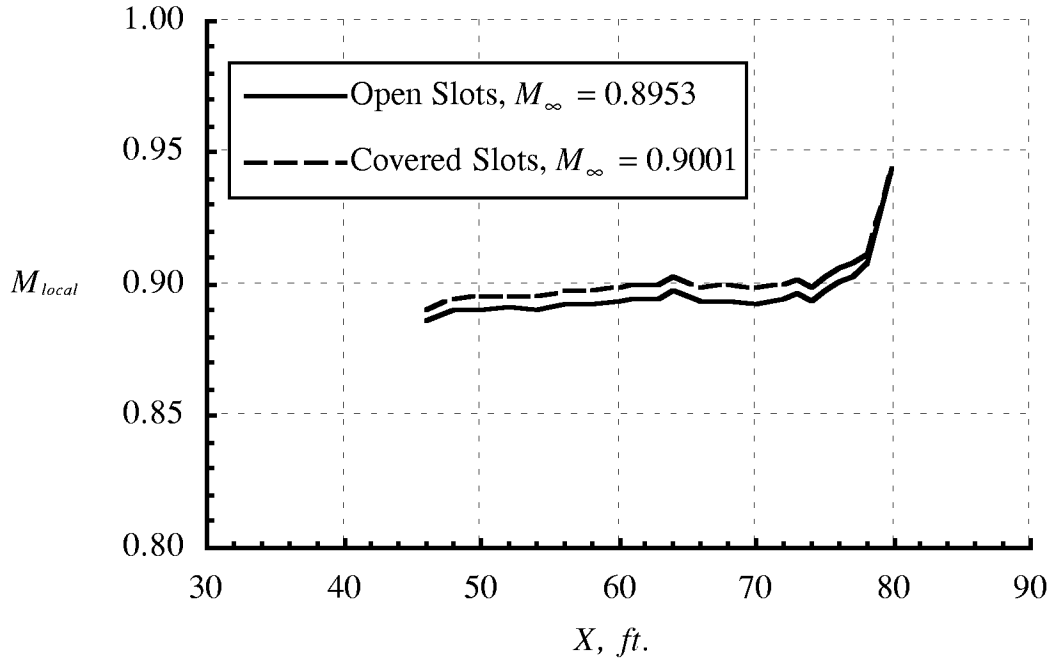

(c) Effect of sealing the east wall sidewall slots on ceiling Mach number distribution.
Figure 23. Continued.

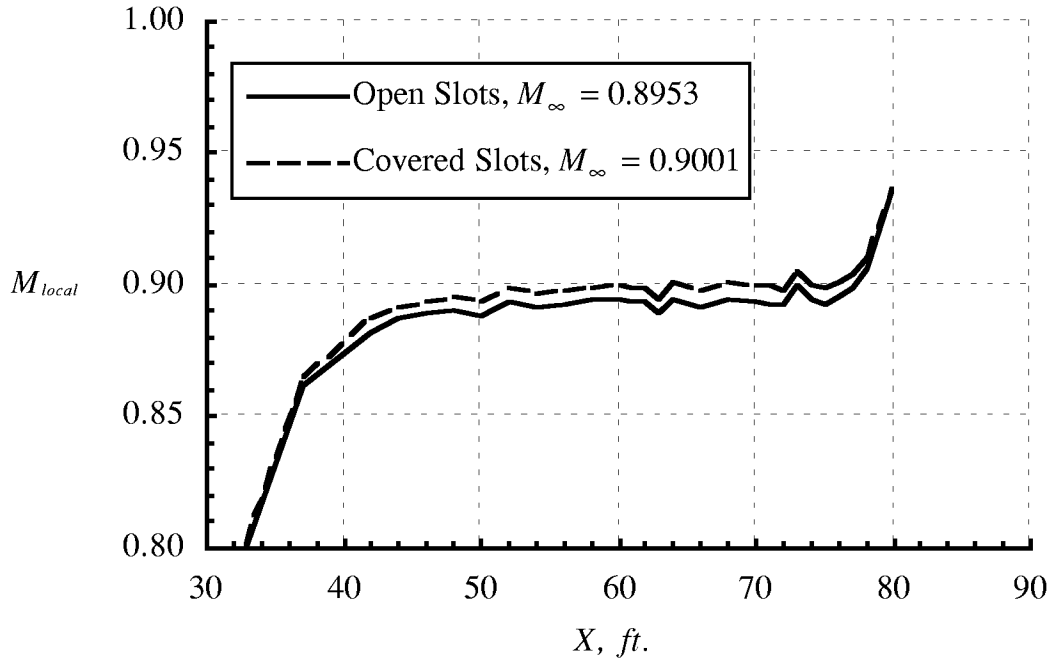

(d) Effect of sealing the east wall sidewall slots on floor Mach number distribution.
Figure 23. Concluded.

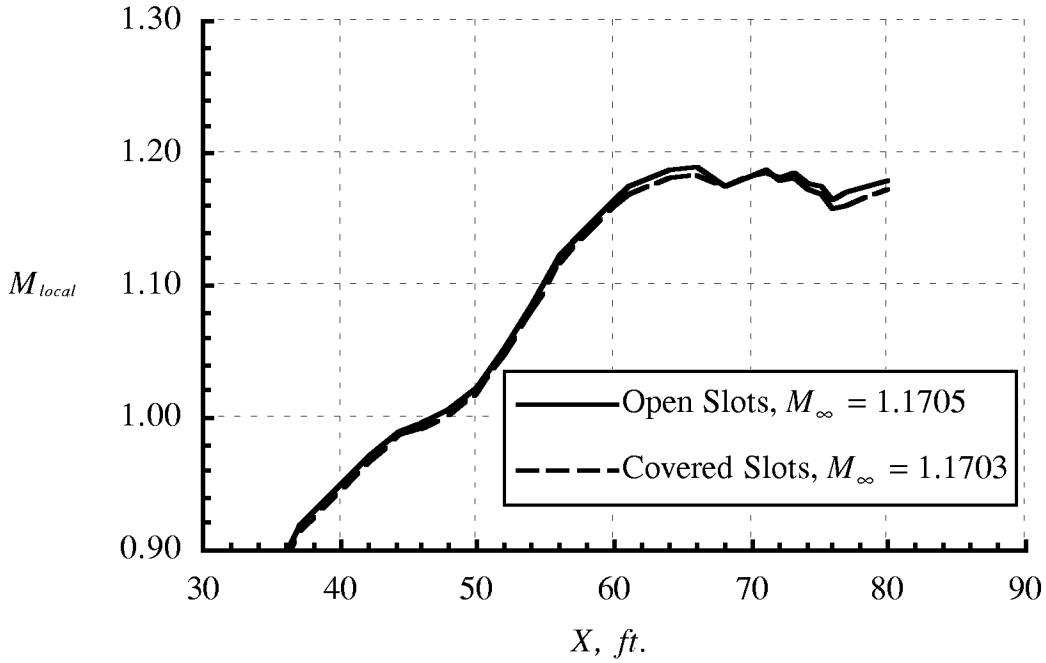

(a) Effect of sealing the east wall sidewall slots on east wall Mach number distribution.

Figure 24. Mach number distribution on the test section walls in air; $P_{t,\infty} \approx 250$ psf, $M_\infty \approx 1.17$.

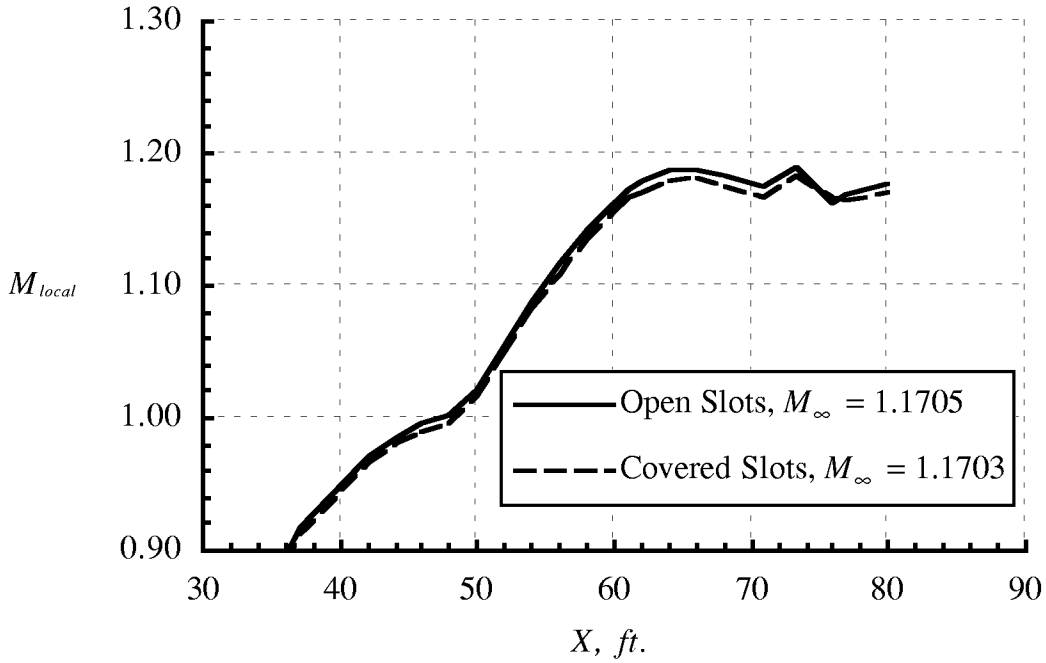

(b) Effect of sealing the east wall sidewall slots on west wall Mach number distribution.

Figure 24. Continued.

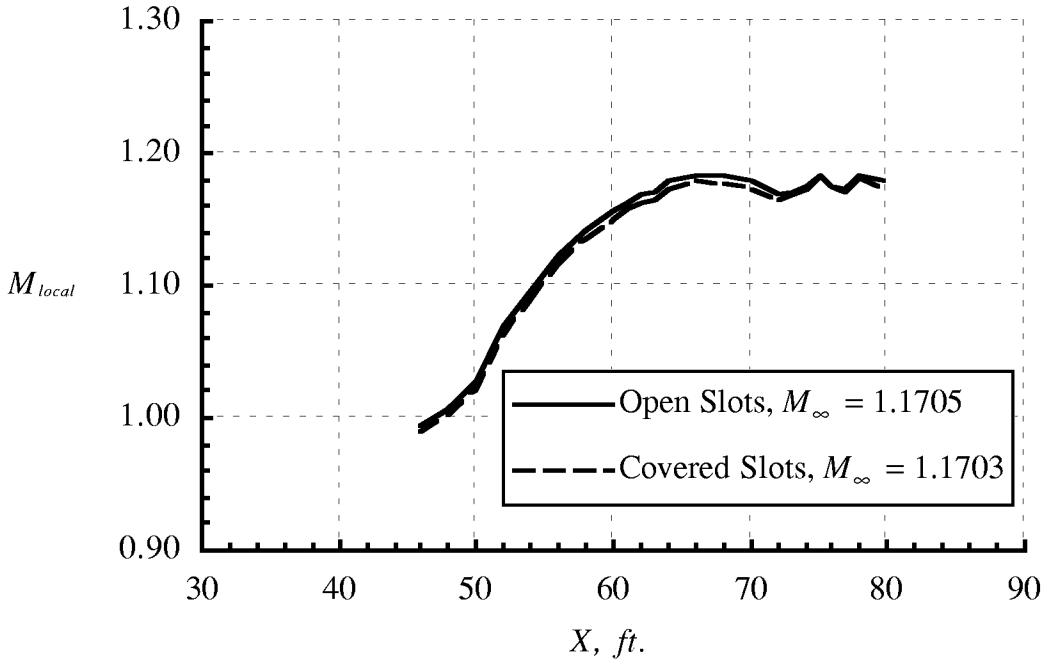

(c) Effect of sealing the east wall sidewall slots on ceiling Mach number distribution.
Figure 24. Continued.

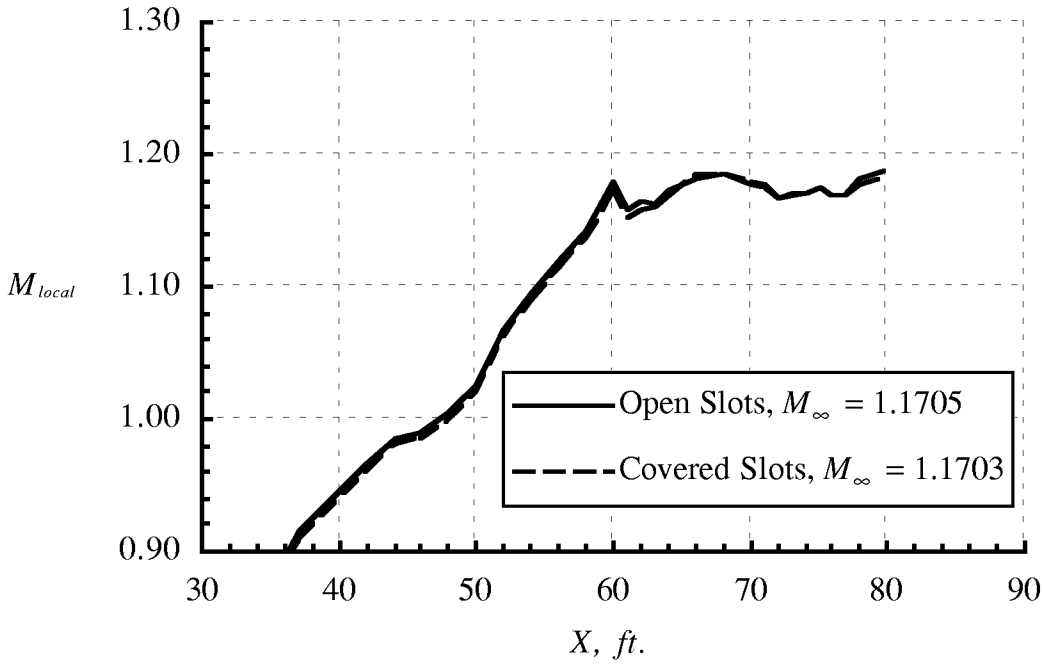

(d) Effect of sealing the east wall sidewall slots on floor Mach number distribution.
Figure 24. Concluded.

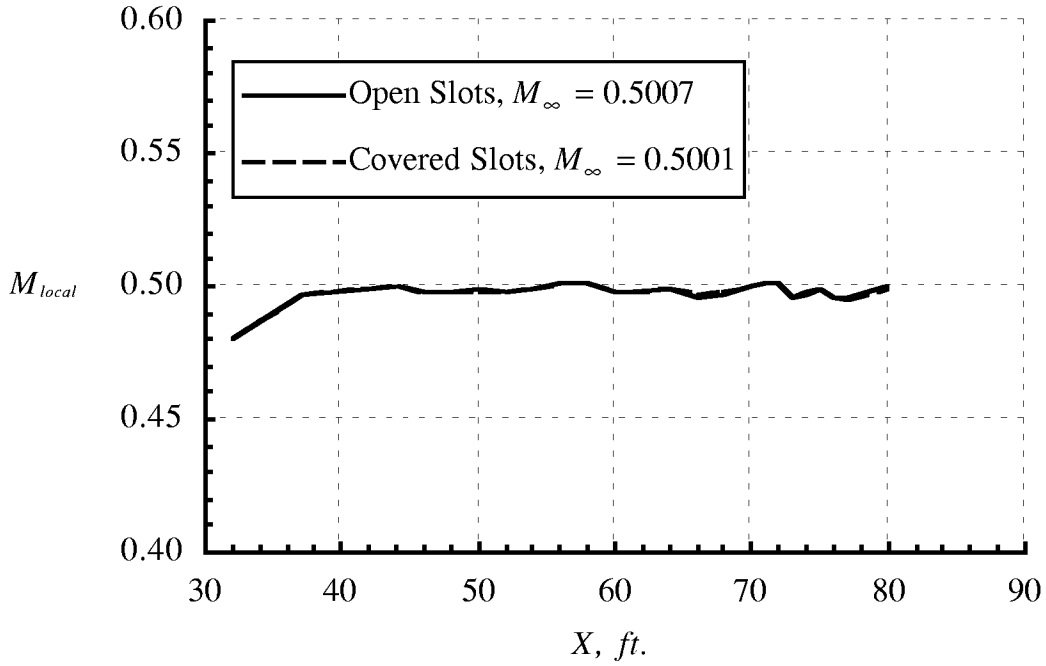

(a) Effect of sealing the east wall sidewall slots on east wall Mach number distribution.

Figure 25. Mach number distribution on the test section walls in R-134a; $P_{t,\infty} \approx 1875$ psf, $M_\infty \approx 0.50$.

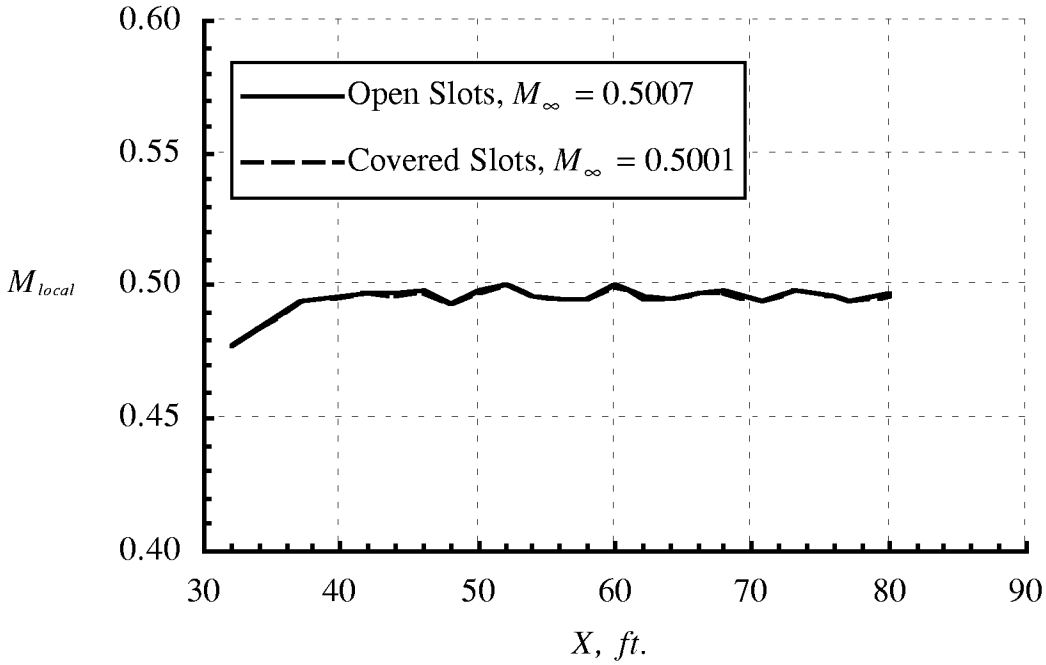

(b) Effect of sealing the east wall sidewall slots on west wall Mach number distribution.

Figure 25. Continued.

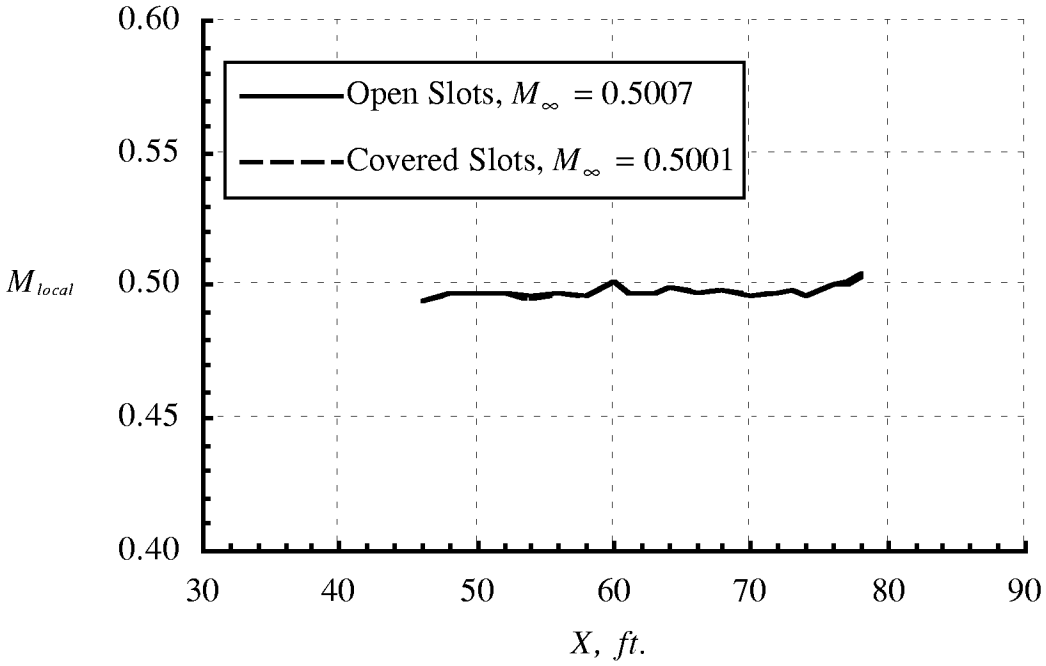

(c) Effect of sealing the east wall sidewall slots on ceiling Mach number distribution.
Figure 25. Continued.

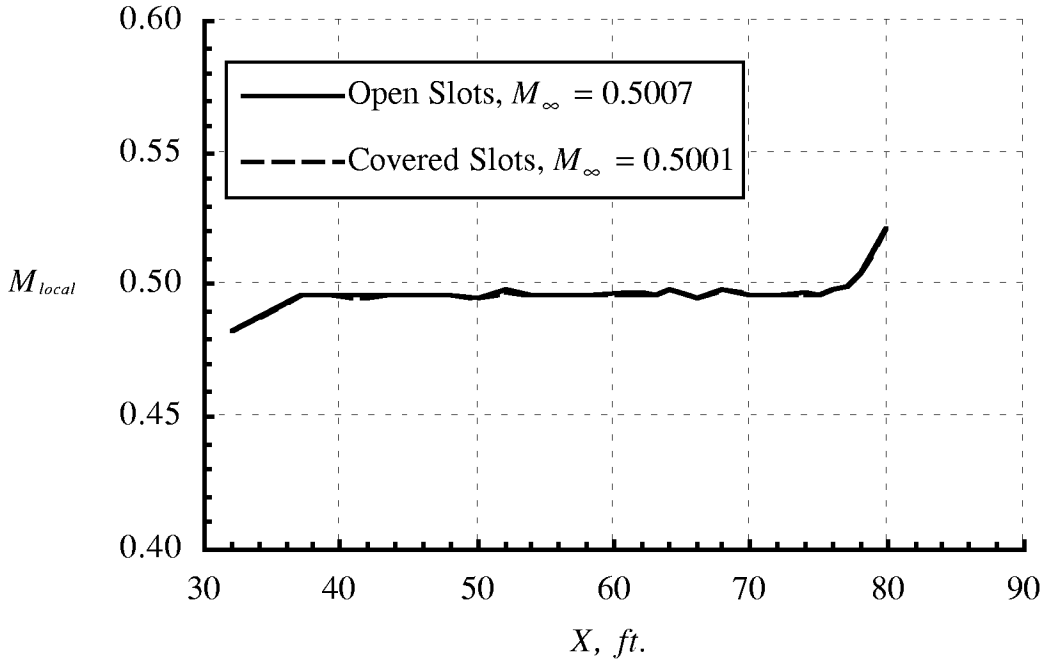

(d) Effect of sealing the east wall sidewall slots on floor Mach number distribution.
Figure 25. Concluded.

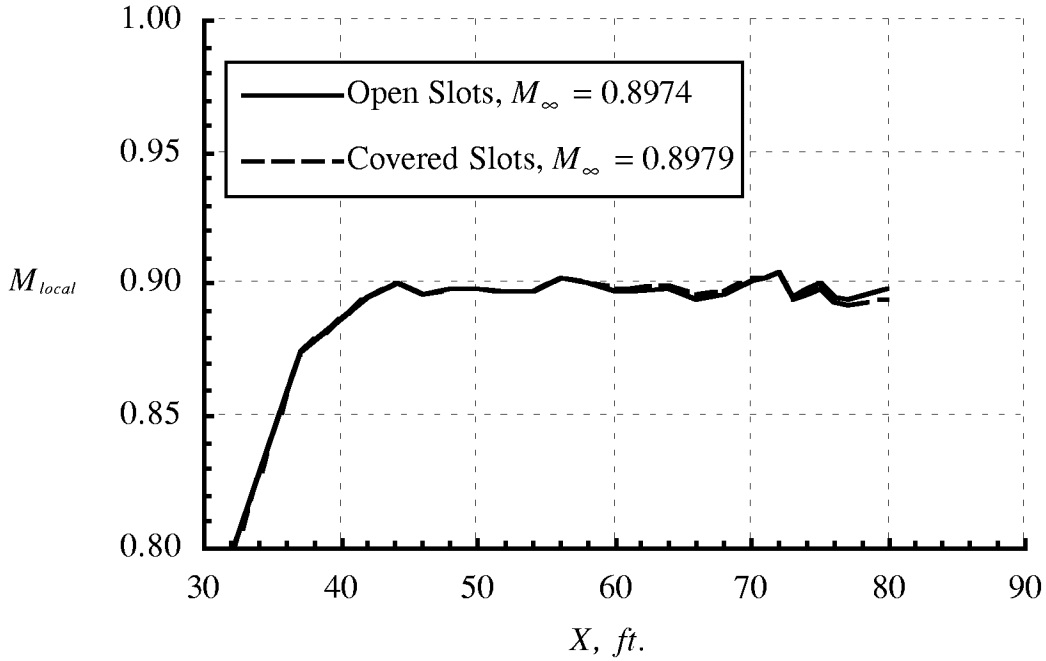

(a) Effect of sealing the east wall sidewall slots on east wall Mach number distribution.

Figure 26. Mach number distribution on the test section walls in R-134a; $P_{t,\infty} \approx 575$ psf, $M_\infty \approx 0.90$.

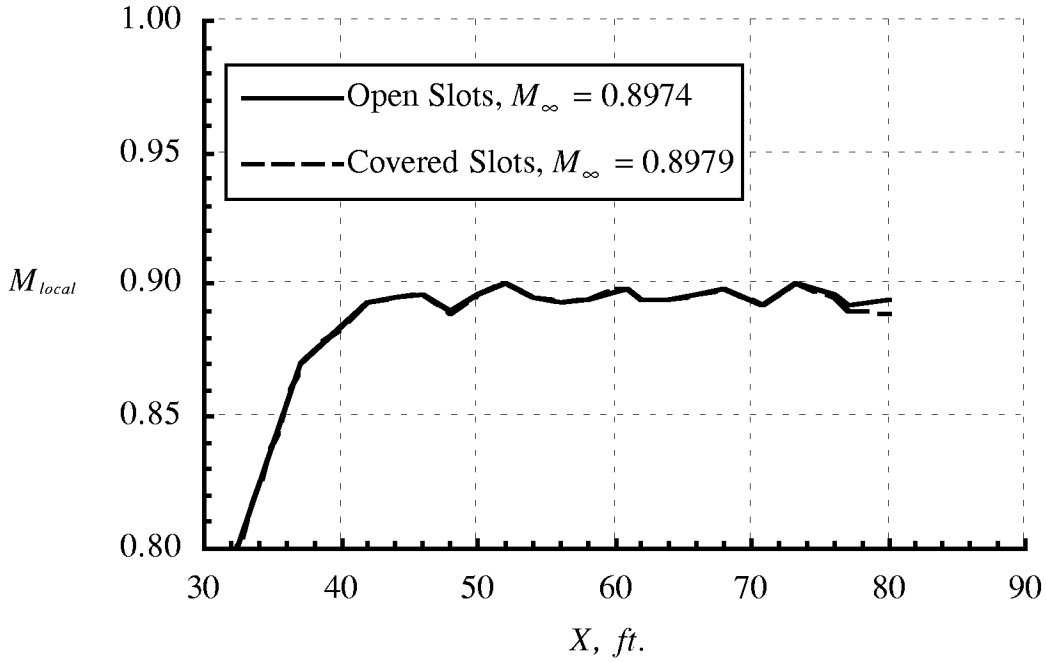

(b) Effect of sealing the east wall sidewall slots on west wall Mach number distribution.

Figure 26. Continued.

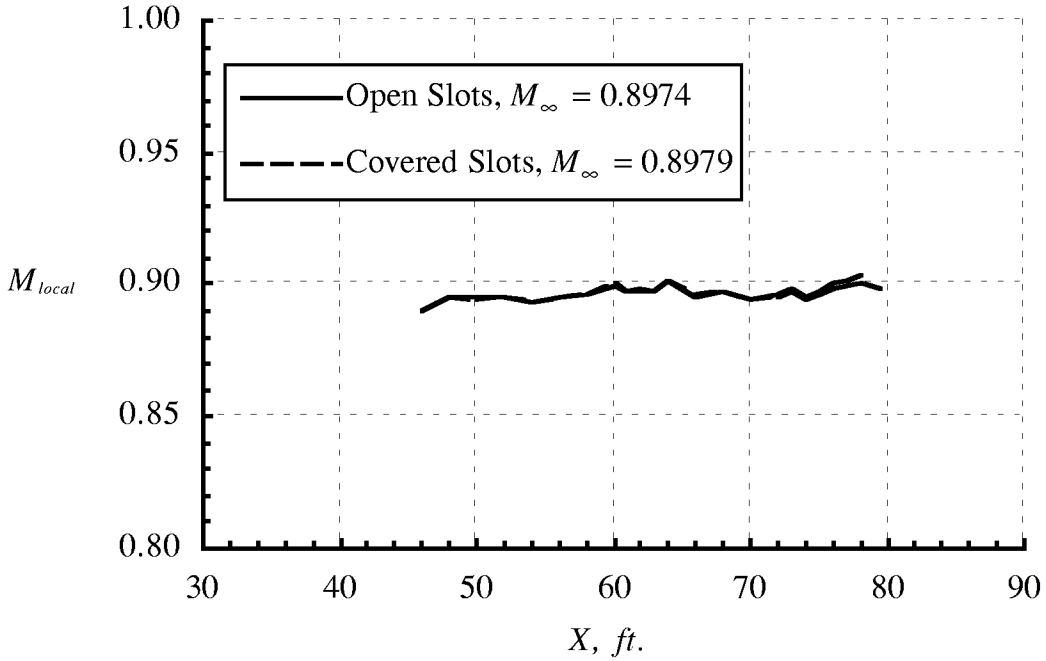

(c) Effect of sealing the east wall sidewall slots on ceiling Mach number distribution.
Figure 26. Continued.

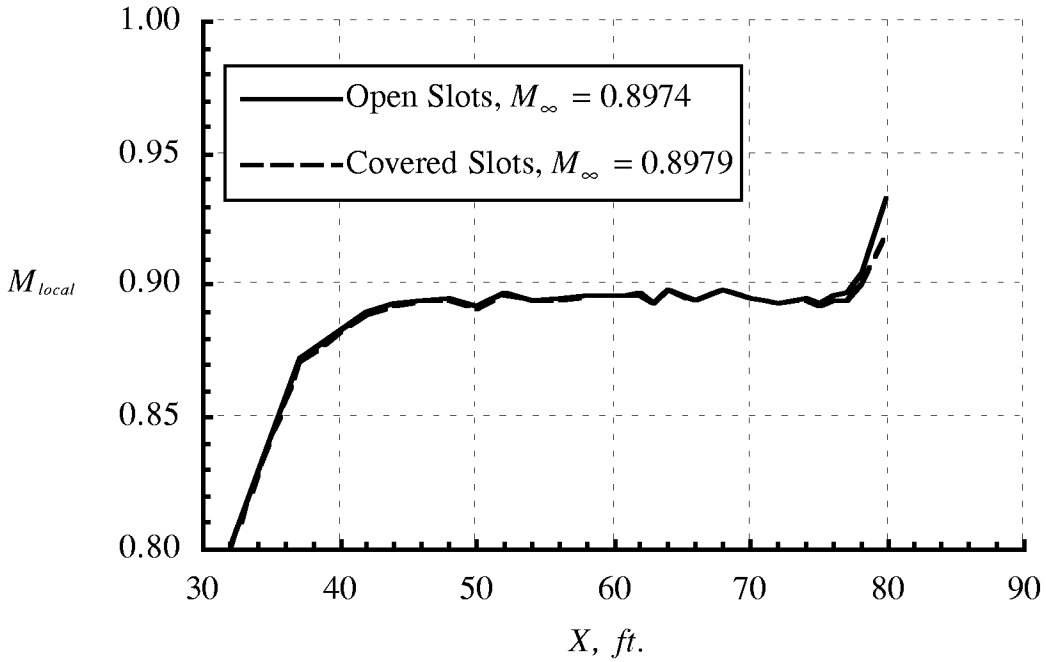

(d) Effect of sealing the east wall sidewall slots on floor Mach number distribution.
Figure 26. Concluded.

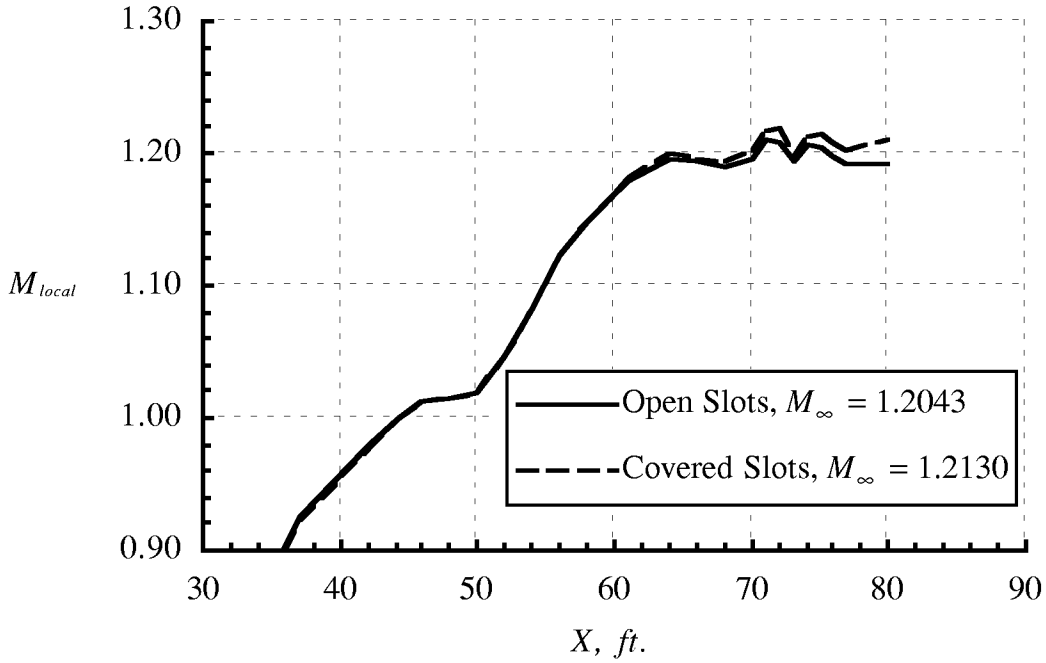

(a) Effect of sealing the east wall sidewall slots on east wall Mach number distribution.

Figure 27. Mach number distribution on the test section walls in R-134a; $P_{t,\infty} \approx 650$ psf, $M_\infty \approx 1.2$.

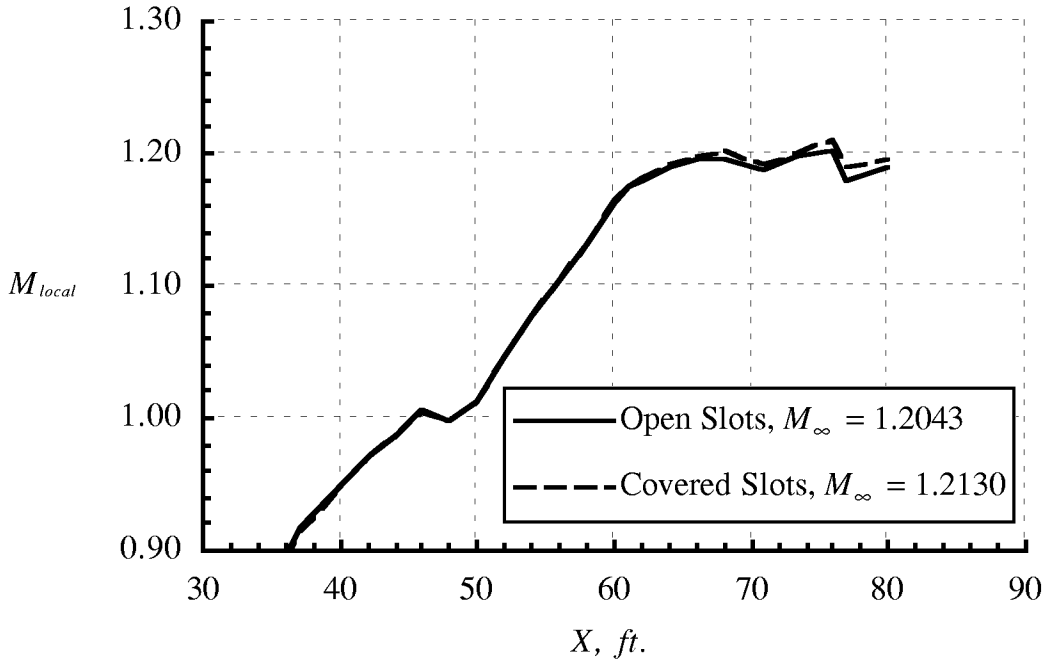

(b) Effect of sealing the east wall sidewall slots on west wall Mach number distribution.

Figure 27. Continued.

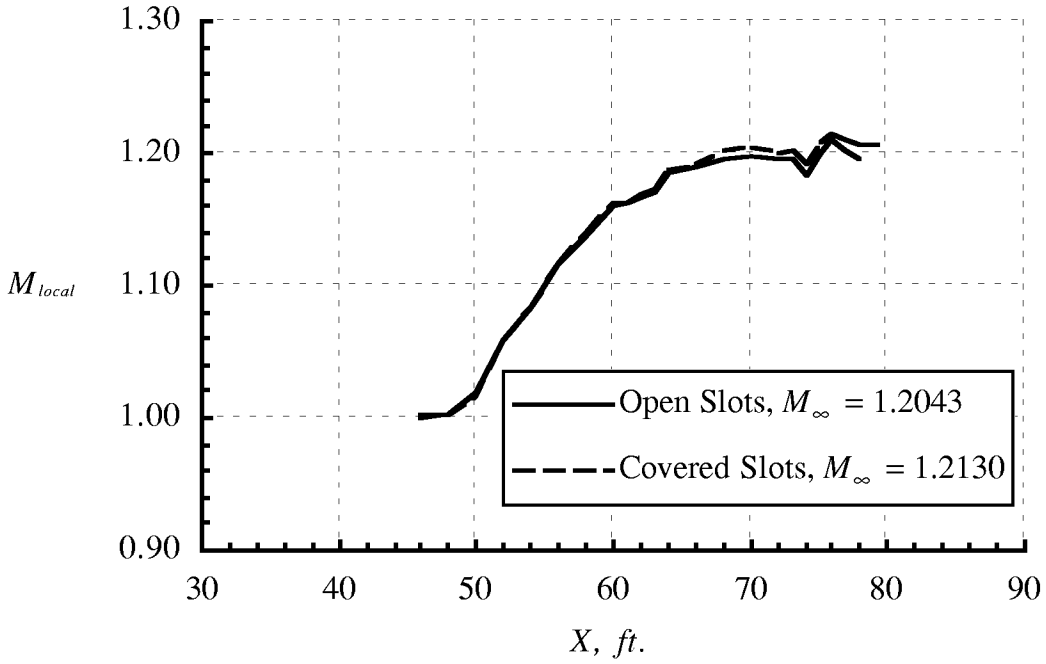

(c) Effect of sealing the east wall sidewall slots on ceiling Mach number distribution.
Figure 27. Continued.

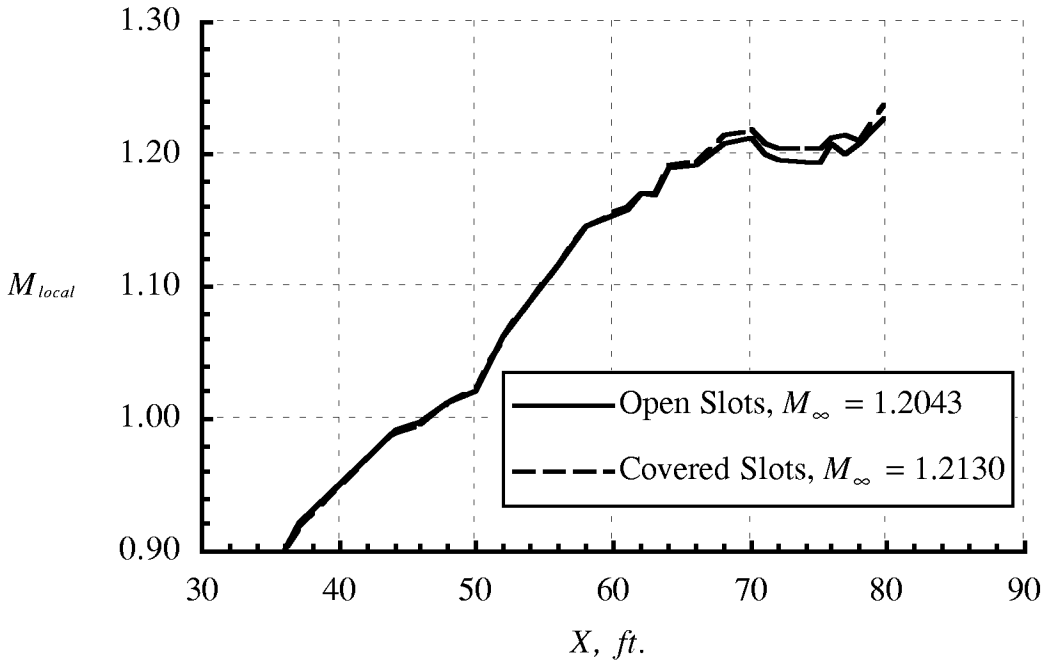

(d) Effect of sealing the east wall sidewall slots on floor Mach number distribution.
Figure 27. Concluded.

REPORT DOCUMENTATION PAGE

Form Approved
OMB No. 0704-0188

1. AGENCY USE ONLY (Leave blank)	2. REPORT DATE	3. REPORT TYPE AND DATES COVERED
	June 2001	Technical Memorandum

4. TITLE AND SUBTITLE
Sidewall Mach Number Distributions for the NASA Langley Transonic Dynamics Tunnel

5. FUNDING NUMBERS
WU 706-31-41-02

6. AUTHOR(S)
James R. Florance and José A. Rivera, Jr.

7. PERFORMING ORGANIZATION NAME(S) AND ADDRESS(ES)
NASA Langley Research Center
Hampton, VA 23681-2199

8. PERFORMING ORGANIZATION REPORT NUMBER
L-18085

9. SPONSORING/MONITORING AGENCY NAME(S) AND ADDRESS(ES)
National Aeronautics and Space Administration
Washington, DC 20546-0001

10. SPONSORING/MONITORING AGENCY REPORT NUMBER
NASA/TM-2001-211019

11. SUPPLEMENTARY NOTES

12a. DISTRIBUTION/AVAILABILITY STATEMENT
Unclassified-Unlimited
Subject Category 05 Distribution: Nonstandard
Availability: NASA CASI (301) 621-0390

12b. DISTRIBUTION CODE

13. ABSTRACT (Maximum 200 words)
The TDT was recalibrated due to the conversion of the heavy gas test medium from R-12 to R-134a. The objectives of the tests were to determine the relationship between the free-stream Mach number and the measured test section Mach number, and to quantify any necessary corrections. Other tests included the measurement of pressure distributions along the test-section walls, test-section centerline, at certain tunnel stations via a rake apparatus, and in the tunnel settling chamber. Wall boundary layer, turbulence, and flow angularity measurements were also performed. This paper discusses the determination of sidewall Mach number distributions.

14. SUBJECT TERMS
Aerodynamics; TDT; Mach number distributions; calibration

15. NUMBER OF PAGES
78

16. PRICE CODE
A05

17. SECURITY CLASSIFICATION OF REPORT	18. SECURITY CLASSIFICATION OF THIS PAGE	19. SECURITY CLASSIFICATION OF ABSTRACT	20. LIMITATION OF ABSTRACT
Unclassified	Unclassified	Unclassified	UL